Persistent legacy effects on soil microbiota facilitate plant adaptive responses to drought

Nichole A. Ginnan[1,2*], Valéria Custódio[3*], David Gopaulchan[3*], Natalie Ford[1,4], Isai Salas-González[5], Dylan H. Jones[3], Darren M. Wells[3], Ângela Moreno[6], Gabriel Castrillo[3#], Maggie R. Wagner[1,4#]

[1] Kansas Biological Survey and Center for Ecological Research, University of Kansas, Lawrence, KS, USA 66045
[2] One Health Microbiome Center, Huck Institutes of the Life Sciences, Penn State University, State College, PA, USA
[3] School of Biosciences, University of Nottingham, Sutton Bonington, UK
[4] Department of Ecology and Evolutionary Biology, University of Kansas, Lawrence, KS, USA 66045
[5] Centre for Genomics Sciences. Universidad Nacional Autónoma de México
[6] Ministério da Agricultura e Ambiente, Cabo Verde

[*]These authors contributed equally
[#]Corresponding authors (gabriel.castrillo@nottingham.ac.uk and maggie.r.wagner@ku.edu)

Abstract

Both chronic and acute drought alter the composition and physiology of the soil microbiota, favoring the selection of microbes with functional traits that preserve fitness in these challenging conditions[1]. This drought-adapted microbiota may influence water-use efficiency mechanisms in host plants. Currently, it is largely unknown how this soil microbial drought legacy manifests at the molecular and physiological levels and how it influences microbe-dependent plant responses to drought in diverse natural soils. Here, to infer how drought legacy affects soil microbiota composition and function, we collected soils spanning two distinct and geographically distant precipitation gradients. By controlling for variation in numerous other soil properties including porosity and elemental profiles, we identified a group of bacterial taxa that are highly sensitive to water availability and critical for the formation of soil drought memory. Next, by imposing an acute experimental drought we show that this microbial drought legacy is robust to short-term perturbations. Furthermore, we reveal that soil microbiota from historically dry climates buffered a wild grass species native to the precipitation gradient, but not the domesticated crop species

maize, from the negative effects of subsequent acute drought. In particular, microbiota with a legacy of chronic water limitation altered the expression of a small subset of host genes that mediate the effect of acute drought on transpiration and intrinsic water use efficiency. Our results reveal how long-term exposure to water stress alters soil microbial communities and demonstrate the resulting "legacy effects" on the drought responses of neighboring plants.

Main Text

Rapid global changes, such as escalating temperatures and changing precipitation patterns, intensify pressure on both natural and agricultural ecosystems. Among these changes, increasing frequency and intensity of droughts are particularly formidable challenges, with devastating consequences for plant health and survival. However, soil microbial communities, with their remarkable ability to quickly adapt to environmental shifts[2], may play a crucial role in bolstering the resilience of plants and ecosystems to drought stress[3]. Additionally, previous exposure to stress can shape the future trajectories of microbial communities and influence their responses to subsequent environmental disturbances, a phenomenon referred to as legacy effects or ecological memory[4]. Despite the growing recognition of microbial legacy effects, little is known about the mechanisms driving them, their long-term persistence, and whether their effects extend uniformly across different plant species. Furthermore, soil properties such as porosity or mineral nutrient content can also govern soil microbiomes[5], and vice versa, making it difficult to isolate the effects of precipitation on the microbiome.

Here, to investigate microbial drought legacy effects and isolate the drivers and impacts of microbial adaptations to water limitation, we (1) evaluate natural microbiome variation across two independent precipitation gradients, (2) test the ability of legacy effects to persist through experimental perturbation, and (3) evaluate the impacts of microbiome precipitation history on plant responses to acute drought at the molecular and physiological levels. Finally, we assess the

extent to which microbiome legacy effects are transferable across plant species. Our results demonstrate that legacy effects of historical exposure to dry conditions are particularly salient at the metatranscriptomic level and trigger transcriptional changes in plant roots that improve resistance to subsequent acute droughts, at least in some plant species.

Mineral nutrient accumulation and historical precipitation impact soil microbiota composition

To explore the relationship between free-living soil microbiota and water availability, we analysed microbiome compositional and functional traits in soils exposed to a gradient of water availability. First, we identified six never-irrigated remnant prairies along a steep precipitation gradient in Kansas, USA (Fig. 1a, b and Supplementary Table S1). We sequenced the metagenomes of these six soils to evaluate genetic variation within and among the bacterial communities along the precipitation gradient. In general, we did not observe significant differences in bacterial alpha diversity in the soils examined (Extended Data Fig.1a). In line with previous findings[6], Actinomycetota and Bacillota were enriched in historically drier soils, while Pseudomonadota and Acidobacteriota were more prevalent in wetter soils (Extended Data Fig. 1b). Supporting these findings, between-sample variation showed a strong biogeographic signature (PERMANOVA, $R^2 = 0.11$, $p = 0.001$) and site precipitation explained 5.3% of the variation (Fig. 1c). The first axis of principal coordinate analysis (PCoA) separated the bacterial communities of the two soils exposed to the highest precipitation levels (CWR, WEL) from the rest of soils (Fig. 1c).

To disentangle the influence of soil edaphic properties and precipitation history on the microbiota compositional changes detected across the gradient of soils, we examined 24 mineral nutrient and trace element profiles (K, Fe, Mg, Ca, Zn, etc.) across all soils using ICP-MS. Soil nutrients are known drivers of microbial taxonomic and functional composition, particularly bacterial communities[7,8]. Consistent with the pattern seen for microbial taxonomic composition, we

observed significant mineral nutrient differences, with site explaining 27.9% of the variation and precipitation explaining 28.6% (Extended Data Fig. 1c). The first principal coordinate axis of the soil mineral nutrient profiles separated the three low-precipitation sites (TRI, SVR, and HAY), from the three higher-precipitation sites (KNZ, CWR, and WEL) (Extended Data Fig. 1c). Concentrations of several individual mineral nutrients were correlated with mean annual precipitation (Extended Data Fig. 1d and e), and the overall mineral nutrient dissimilarities were correlated with the microbiota composition dissimilarities across the gradient of soils (Mantel, r = 0.384; *p*-value = 1e-04; Extended Data Fig. 1f). This suggests that the accumulation of mineral nutrients in these soils might be influenced by the precipitation patterns, and both may impact the composition of the microbiota in the soil collection.

Next, we used X-ray computed tomography to quantify soil porosity of undisturbed soil cores. Soil porosity, the percent of space or pores among soil aggregates, is directly related to soil hydraulic properties such as water retention and infiltration[9]. In general, lower porosity results in lower water retention and infiltration. Therefore, it is a good indicator for assessing the effect of precipitation on the actual water content in the soil. In all cases, soil porosity decreased with depth and increased with precipitation (Extended Data Fig. 2a-b). These results suggest that precipitation history might affect soil porosity in surface layers of soils[10], which could affect soil niche properties and, consequently, the abundance of specific microbiota members. Nevertheless, we found no correlation between the soil porosity dissimilarities and the microbiota composition dissimilarities in these soils (Extended Data Fig. 2c). This suggests that soil porosity is not a key element controlling the overall microbial community composition in these soils.

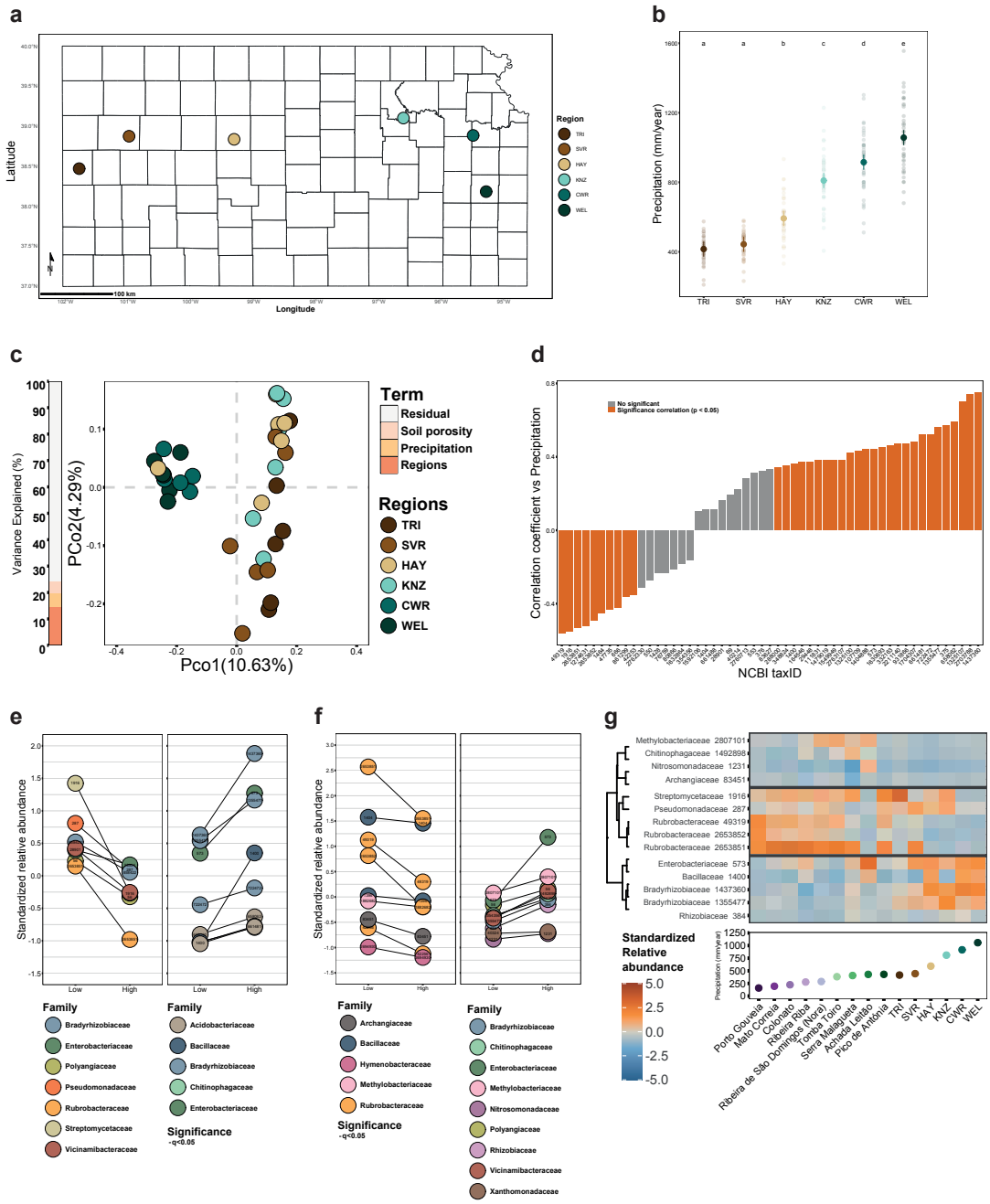

Fig. 1. Water-related soil memory traits are preserved across distant precipitation gradients. a. Map of Kansas, USA, showing the locations selected for collecting the soils used in this work. **b.** The graph shows the precipitation (mm/year) recorded for the Kansas soils over the period 1981 to 2021 in the NASA POWER database. Statistical significance between soils was determined via an ANOVA on a fit linear model and letters represent the compact letter display of a Tukey *post-hoc* test ($p < 0.05$). **c.** Principal coordinate analysis (PCoA) of the soil microbiota projection from Kansas soils representing a gradient of precipitation. Colors represent the individual soils. The bar on the left denotes the percentage of the variance explained by the different experimental variables. **d**. Bar graph showing the correlation coefficient calculated between each mineral nutrient abundance and the precipitation gradient across Kansas soils. Bars in orange are significant ($p < 0.05$). **e and f**. Comparative analysis of relative abundances of the water legacy bacterial markers identified in soils from Kansas (**e**) and Santiago Island (**f**) exposed to low or high

precipitation levels. Colored points represent the average value of standardized relative abundance for each bacterial taxon. The line connecting both points is the difference between low and high-precipitation soils. A black line indicates statistical significance ($q < 0.05$). **g**. Heatmap showing the standardized relative abundance of validated bacterial markers of water legacy across both collections of soils exposed to distinct precipitation levels (Bottom panel).

Soil bacterial taxonomic and functional enrichments suggest local adaptations to water availability

Next, to identify microbial biomarkers of precipitation legacy, we modelled the relative abundances of bacterial taxa in relation to precipitation levels while controlling for soil porosity and soil elemental composition. This analysis revealed distinct clusters of bacterial taxa at multiple taxonomic levels (NCBI taxID, species, and family) whose relative abundances varied significantly along the precipitation gradient (Extended Data Fig. 2d-f). Across the soils, 19 bacterial taxa (NCBI taxIDs) were positively correlated and nine were negatively correlated with precipitation (Fig. 1d). Taken together, these results indicate that water availability in the soil likely modulates the composition of soil bacterial communities, possibly through the selection of functions necessary to adapt to water availability in the soil.

We used assembled metagenomic contigs to explore the enrichment of bacterial biological processes in the soils spanning the precipitation gradient. To focus on functions that are associated with water availability rather than site-specific variation, we collapsed our six soils into two groups representing our sites with low-precipitation histories (TRI, SVR, HAY) and high-precipitation histories (KNZ, CWR, WEL). These groupings preserved the observed similarities in microbiome taxonomic composition, mineral nutrient content, and porosity (Fig. 1c and Extended Data Fig. 1c, 2a). We identified 62 Gene Ontology (GO) categories that were differentially abundant between these groups (Extended Data Fig. 2g). Biological processes typically associated with drought tolerance[11], such as nitrogen cycle metabolic processes, fatty acid (a major cell membrane structural component) biosynthesis, DNA repair, and glucan metabolism

151 were enriched in low-precipitation soils (Extended Data Fig. 2g)[12–14], while processes related to
152 ion transport, lipid catabolism, and cellular aldehyde and ketone metabolism were depleted
153 (Extended Data Fig. 2g). These results confirm that the bacterial communities from the low-
154 precipitation soils are functionally different from those associated with high-precipitation soils, and
155 even with multiple soil factors influencing these communities, there is still clear evidence of
156 adaptations to osmotic stress. From this, we can conclude that the bacterial communities across
157 the Kansas precipitation gradient are functionally adapted to local precipitation levels, making
158 them excellent candidates for exploring how precipitation legacy of the soil microbiome affects
159 drought tolerance in plants.
160
161 Lastly, to isolate bacterial biomarkers of water availability in soils, we fit the relative abundances
162 of the most abundant (>0.1%) and prevalent (>20%) taxa to five statistical models that
163 incorporated mean annual precipitation, soil mineral nutrient composition, and soil porosity as
164 predictors. This analysis revealed seven bacterial taxa (NCBI taxaIDs) belonging to
165 *Bradyrhizobiaceae*, *Enterobacteriaceae*, *Polyangiaceae*, *Pseudomonadaceae*,
166 *Rubrobacteraceae*, *Streptomycetaceae*, and *Vicinamibacteraceae* enriched in soils with low
167 precipitation history (Fig. 1e). We also identified 7 taxa from *Acidobacteriaceae*, *Bacillaceae*,
168 *Bradyrhizobiaceae*, *Chitinophagaceae*, and *Enterobacteriaceae* that were enriched in soils with
169 high precipitation history (Fig. 1e). Therefore, we postulated that these precipitation-sensitive
170 bacteria can serve as biomarkers of water availability and likely contribute to the formation of
171 drought memory in these soils.
172
173 **Distant natural precipitation gradients have conserved metagenomic properties**
174 To validate that these bacterial community changes are generally associated with precipitation
175 patterns, rather than being specific to Kansas, we repeated our analyses for nine never-irrigated
176 (rain-fed) natural soils from a second precipitation gradient in Santiago Island, Cabo Verde

177 (Extended data Fig. 3a). Compared to the steep Kansas macro-gradient, these soils represent a
178 stable micro-gradient of precipitation (Extended Data Fig. 3b). Like in Kansas, bacterial alpha
179 diversity was similar across all soil samples (Extended Data Fig. 1a and 3c), and Actinomycetota
180 was enriched, while Pseudomonadota was depleted in soils with the lowest precipitation
181 (Extended Data Fig. 3d). We observed small differences in bacterial beta diversity among the
182 soils, partially explained by their geographical location (Extended Data Fig. 3e). As expected due
183 to the smaller geographic area covered by these samples, a principal coordinates analysis
184 showed a reduced biogeographic signature in the bacterial community composition of Santiago
185 soils compared to Kansas soils (Fig. 1c and Extended Data Fig. 3e).
186
187 Unlike in the Kansas soils (Extended Data Fig. 1d–f), neither the mineral nutrient profiles
188 (Extended Data Fig. 3f and g) nor the porosity profiles (Extended Data Fig. 4a) of the Santiago
189 soils corresponded to high- and low-precipitation groups. However, several individual mineral
190 nutrients were correlated with precipitation (Extended Data Fig. 3h) and mineral nutrient
191 dissimilarities were correlated with microbiota dissimilarities in these soils (r = 0.541; *p*-value =
192 1e-04; Extended Data Fig. 3i).
193
194 Soil porosity was correlated with neither mean annual precipitation (Extended Data Fig. 4b) nor
195 mineral nutrient content in the soils (Extended Data Fig. 4c). Consistent with findings from Kansas
196 (Extended Data Fig. 2c), soil porosity dissimilarities were uncorrelated with microbiota
197 composition dissimilarities in the Santiago soils (Extended Data Fig. 4d). Despite the reduced
198 biogeographic signature in the Santiago soils (Extended Data Fig. 3e), we speculated that a
199 reduced set of bacterial biomarkers that are highly sensitive to minor but consistent differences in
200 water availability may be detectable.
201

202 To determine whether small variations in precipitation affect specific members of the bacterial
203 communities, we identified clusters of bacterial taxa with differential relative abundance in high-
204 precipitation *vs.* low-precipitation soils (Extended Data Fig. 4e). These differences were most
205 pronounced when comparing soils at the extremes of the precipitation micro-gradient (Extended
206 Data Fig. 4e) and were consistent across taxonomic levels (Extended Data Fig. 4e-g). We found
207 22 bacterial taxa that were positively correlated with mean annual precipitation, and 10 that were
208 negatively correlated (Extended Data Fig. 4h). The patterns of bacterial GO term
209 enrichment/depletion due to precipitation, such as ornithine metabolic processes and purine
210 nucleoside triphosphate metabolic processes (enriched in drier soils) and lipid catabolic process
211 and ionic homeostasis (important for maintaining cell turgor, enriched in wetter soils), were similar
212 to those observed in the Kansas gradient (Extended Fig. 2g and Extended Data Fig. 4i). This
213 indicates that the strategies used by soil bacteria to cope with water limitation are robust to
214 variation in other edaphic properties and are conserved across geographically distant regions.
215
216 By applying the same procedures used to identify biomarkers in the Kansas soils, we identified
217 19 bacterial taxa in Santiago soils whose relative abundances responded to mean annual
218 precipitation after controlling for soil mineral nutrient content and porosity. Nine taxa (from
219 *Archangiaceae*, *Bacillaceae*, *Hymenobacteraceae*, *Methylobacteriaceae*, and
220 *Rubrobacteraceae*) were enriched in low-precipitation soils while ten (from *Bradyrhizobiaceae*,
221 *Chitinophagaceae*, *Enterobacteriaceae*, *Methylobacteriaceae*, *Nitrosomonadaceae*,
222 *Polyangiaceae*, *Rhizobiaceae*, *Vicinamibacteraceae*, *Xanthomonadaceae*) were depleted in low-
223 precipitation soils (Fig 1f and Extended Data Fig. 3b). Notably, seven of these families—
224 *Bradyrhizobiaceae*, *Enterobacteriaceae*, *Polyangiaceae*, *Rubrobacteraceae*,
225 *Vicinamibacteraceae, Bacillaceae*, and *Chitinophagaceae*—were also identified as biomarkers of
226 soil precipitation legacy in the Kansas soils. To validate the consistency of these bacterial
227 biomarkers across different geographic regions, we examined whether the enrichment patterns

228 of the Kansas biomarkers were conserved in Santiago soils and vice versa (Extended Data Fig.
229 4j-k and Supplementary Table S2). We validated eight bacterial markers from Kansas and eleven
230 biomarkers from Santiago as showing the same pattern of enrichment across both precipitation
231 gradients (Extended Data Fig. 4j-k). In particular, three bacterial taxa (*Rubrobacteraceae*
232 2653851, *Bradyrhizobiaceae* 1355477, *Enterobacteriaceae* 573) were consistently identified in
233 both soil gradients, validating them as robust bacterial biomarkers of soil water legacy (Fig. 1g).
234 Thus, we conclude that the functional and taxonomic differences among our Kansas soils
235 accurately represent the legacy effects of chronic water limitation and are likely generalizable to
236 other water-limited soil microbiomes.
237
238 **Strain-level genetic analysis identifies candidate genes for bacterial drought tolerance**
239 Finally, we investigated whether there were genetic differences between bacterial lineages across
240 the precipitation gradient, focusing on the identified bacterial markers and other highly abundant
241 and prevalent taxa from both Kansas and Santiago soils. We mapped the shotgun metagenomic
242 sequence reads from each sample to reference genomes of the focal species, and subsequently
243 identified sequence variants across the genomes (Fig. 1e-g). Analysis of the genetic distances
244 showed variations in strain-level microbiome structure across both the Kansas and Santiago
245 precipitation gradients (Extended Data Fig. 5a), between precipitation levels (Extended Data Fig.
246 5b), and between geographical regions (Extended Data Fig. 5c).
247
248 Subsequently, we conducted a genotype-environment association analysis to identify genetic
249 variants associated with mean annual precipitation. Significant associations were found in the
250 genomes of the biomarkers *Luteitalea* (ID1855912), *Bradyrhizobium* (ID1355477),
251 *Bradyrhizobium* (ID1325100), *Edaphobacter* (ID2703788), *Candidatus* Solibacter (ID332163),
252 and *Microvirga* (ID2807101) (Extended Data Fig. 5d). All identified variants were located within
253 protein-coding regions, specifically the LuPra_RS24355 (DNA-directed RNA polymerase subunit

254 beta), Bdiaspc4_RS17620 (epoxide hydrolase family protein), XH93_RS32435 (response
255 regulator transcription factor), GWR55_RS00680 (NADP-dependent oxidoreductase),
256 GWR55_RS05605 (glucose-6-phosphate isomerase), HYX25_05330 (carbamoyl-phosphate
257 synthase large subunit), and JO965_13190 (IS630 family transposase) (Extended Data Fig. 5d).
258 These associations suggest candidate genes related to drought tolerance in free-living bacteria
259 (Extended Data Fig. 5d). These results indicate that in addition to the bacterial biomarkers of
260 precipitation history identified at species or higher taxonomic level (Supplementary Table S2),
261 precipitation legacy effects likely manifest through genetic differentiation of bacterial lineages
262 within taxa. These groups of water-sensitive taxa might be critical for the formation of soil memory
263 traits, and their study could reveal new ecological mechanisms by which soil drought legacy drives
264 responses to water stress in plants.
265
266 **Metagenomic and especially metatranscriptomic precipitation legacies are resilient to**
267 **short-term perturbations**
268 To assess the effects of short-term perturbations on soil microbiome legacy, we exposed the six
269 Kansas soils to a five-month-long conditioning phase in a growth chamber. Replicate pots of each
270 soil were either left unplanted or planted with a seedling of the grass species *Tripsacum*
271 *dactyloides* (eastern gamagrass, which is native to Kansas), and were either drought-challenged
272 or well-watered, in a factorial design (Extended Data Fig. 6a). To confirm that our experimental
273 acute drought applied had physiological consequences in our system, we quantified various
274 morphological and anatomical features of the eastern gamagrass plants (Fig. 2a and Extended
275 Data Fig. 6b-d). Compared to well-watered plants, the plants exposed to acute drought treatments
276 were shorter and had more root aerenchyma (Fig. 2a and Extended Data Fig. 6b-c), which are
277 both indicative of drought stress[15]. This indicates that our experimental drought was sufficient to
278 induce differential responses in the plants and, presumably, in the soil-dwelling microbes.
279

280 Next, we explored how precipitation legacy affected the responses of free-living (bulk soil) and
281 gamagrass-associated (rhizosphere) microbial communities when exposed to intermittent
282 drought and watering events. Congruent with the pattern seen across the natural precipitation
283 gradient, bacterial community alpha diversity was similar across treatment groups (Extended Data
284 Fig. 6e). There were also no major taxonomic profile shifts across treatments at the phylum level
285 (Extended Data Fig. 6f). However, canonical analysis of principal coordinates of metagenomic
286 sequences indicated that the conditioning water and host treatments impacted metagenome
287 content but only explained 4.3% and 1.1% of the variation in the data, respectively (Extended
288 Data Fig. 6g). In contrast, precipitation history explained 14.1% of the variation in bacterial
289 community composition, confirming that the conditioning treatments did not erase the ecological
290 memory of the soils (Fig. 2b). In fact, we still detected significant differences in bacterial
291 enrichment between the two soil groups with different precipitation legacies across taxonomic
292 levels, regardless of the treatment applied (Extended Data Fig. 6h). For instance,
293 *Ktedonosporobacteraceae* and *Rubrobacteraceae* were consistently depleted and enriched,
294 respectively, in all low-precipitation soils compared to high-precipitation soils across all treatments
295 (Extended Data Fig. 6h). Furthermore, the identified bacterial markers for drought legacy (Fig. 1d-
296 f) generally followed the expected enrichment and depletion patterns (Extended Data Fig. 6i),
297 which remained robust despite the applied treatments (Extended Data Fig. 6i). This resilience
298 was particularly evident in soils with low-precipitation legacies (Fig. 2c and Extended Data Fig.
299 6i).
300
301 To further validate the robustness of the water soil legacy to experimental perturbation, we
302 investigated patterns of strain-level genetic variation in the identified bacterial markers and other
303 prevalent species across the samples, as described previously (Fig. 1e-g). We aligned the
304 shotgun metagenomic sequence reads to the reference genomes of the focal species to identify
305 sequence variants, then conducted a principal coordinates analysis of standardized pairwise

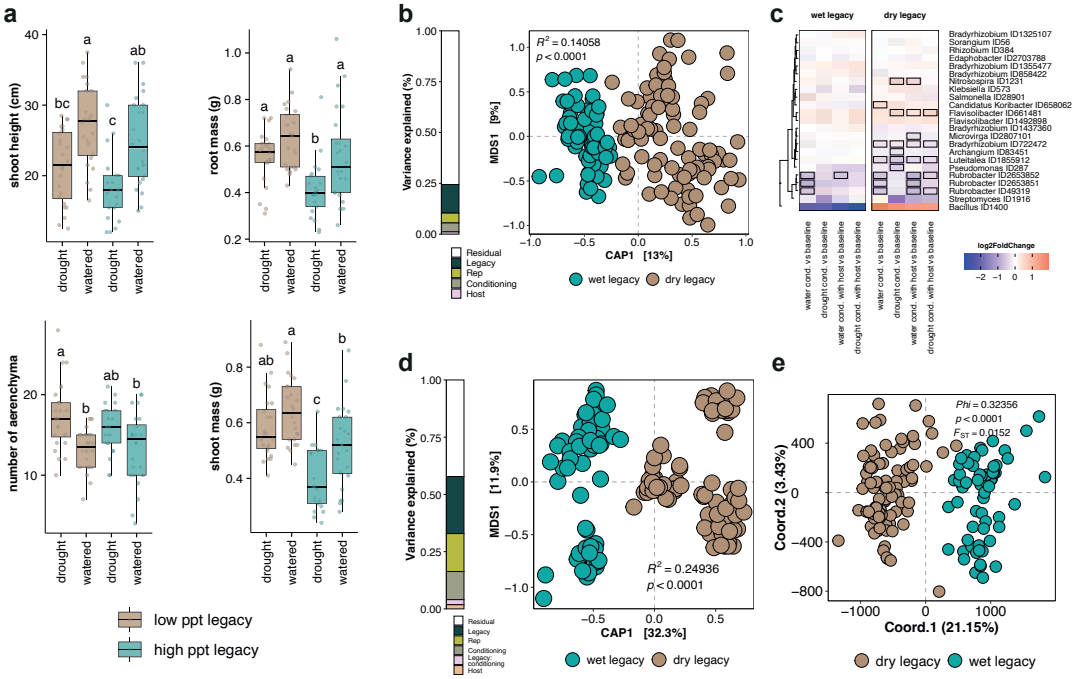

Fig. 2. Soil drought microbial legacy is resilient to short-term perturbations. a. Box plot showing the quantification of different *Tripsacum dactyloides* phenotypes in response to the treatments applied (drought conditions or regular watering) during the conditioning phase. In the graph, the data from soils with low precipitation legacy (low ppt legacy) is colored in brown while the data from soils with high precipitation legacy (high ppt legacy) is colored in blue (see also Data extended Fig. 6b). ANOVA was used to discern significant differences among groups and means were separated using Tukey's post hoc test. **b.** Canonical analysis of principal coordinate showing the projection of the microbiota of each soil with wet and dry legacy after the different treatments. Notice that the soil legacy separates the samples into two groups on the first axis and explains a significant proportion of the observed variance (left bar). **c**. Heatmaps showing the soil enrichment patterns (in relation to soil baseline (wet or dry legacy)) of different drought legacy markers across the collection of soils exposed to the different treatments. The tiles of the heatmaps are colored based on the log2 fold change estimated from a generalized linear model contrasting the abundance of each bacterial marker (y-axis) in a given soil (x-axis) against their corresponding soil baseline. The bacterial markers (y-axis) are clustered. Squares outlined in black represent bacterial markers significantly enriched (red) and depleted (blue) with respect to the corresponding soil baseline ($q < 0.1$). **d**. Canonical analysis of principal coordinates showing the projection of the metatranscriptome of each soil with wet and dry legacy after the different conditioning treatments. Notice that the soil legacy (wet and dry) separates the samples into two groups on the first axis and explains a significant proportion of the observed variance (left bar). **e**. Principal coordinate analysis based on standardized pairwise genetic distances showing the projected identified SNPs found in the genome of the drought legacy markers. Notice that despite the conditioning perturbations applied there is a clear separation of the samples on the first axis based on the soil water legacy (drought and precipitation).

genetic distances based on those variants. This revealed a clear separation of the samples in the first axis based on the soil water legacy (Fig. 2e) rather than the experimental treatments. Consistent with our previous findings (Fig. 2), our experimental perturbations did not affect allele

332 frequencies (Extended Data Fig. 7a,b). Additionally, a genome-wide association analysis showed
333 significant associations with genes from the bacterial markers *Luteitalea* (ID1855912) and
334 *Bradyrhizobium* (ID1355477), which had been previously identified across the precipitation
335 gradients (Extended Data Fig. 5d, 7c). Additional associations were also detected with the
336 biomarker *Bradyrhizobium*: ID1325107 (Extended Data Fig. 7c).
337
338 Next, to investigate the robustness of drought legacy effects on bacterial functions, we tested
339 whether enrichment of GO terms between low-precipitation and high-precipitation soils was
340 maintained after experimental perturbation (Extended Data Fig. 8a). Again, we found a consistent
341 enrichment of GO terms related to the nitrogen cycle metabolic process, including
342 purine−containing compound metabolic process and pyrimidine−containing compound metabolic
343 process, and a depletion of ion transport and amino acid catabolic process. Some of these GO
344 categories were also identified in the free-living communities from Kansas and Santiago soils
345 (Extended Fig. 2g, 4i, and 8a). These results show that the legacy effect of precipitation on the
346 functional content of soil metagenomes was robust to the perturbations applied during the
347 conditioning phase.
348
349 To further validate this conclusion, we analysed metatranscriptome data from the same samples
350 to confirm which biological processes were actually active across the different treatments and
351 soils. A canonical analysis of principal coordinates showed that precipitation history explained
352 24.9% of the variation in microbial gene expression while conditioning phase water treatment and
353 host treatment explained only 12.3% and 1.8% of the variation, respectively (Fig. 2d and Extended
354 Data Fig. 8b). Indeed, we confirmed that the conditioning phase treatments did not alter the
355 functional characteristics of the main bacterial phyla in these soils: even after five months of
356 experimental perturbation, functionally active Actinomycetota and Bacillota remained enriched in
357 all historically dry soils while Acidobacteriota, Planctomycetota, and Pseudomonadota remained

358 enriched in all historically wet soils (Extended Data Fig. 8c). Furthermore, in agreement with our
359 previous observations (Extended Data Fig. 6h), conserved patterns of functional activation within
360 multiple taxonomic groups were detected across both soil groups, regardless of the conditioning
361 treatments applied (Extended Data Fig. 8d-e). Also, the metatranscriptome analysis revealed GO
362 categories that remained enriched in low-precipitation soils after the applied conditioning
363 treatments, such as tetrapyrrole metabolic process, response to osmotic stress, liposaccharide
364 metabolic process, heme metabolic process, and trehalose catabolic process (Extended Data
365 Fig. 8f). Therefore, we confirmed that the long-term legacy of precipitation on soil bacterial
366 community function is robust to short-term (five months) perturbations, including acute drought
367 and the introduction of a host plant. This functional memory of the soil microbial community could
368 influence host responses to water changes in natural ecosystems, potentially providing protection
369 against subsequent acute drought.
370

371 **Microbiome precipitation legacy alters host plant responses to subsequent acute drought**
372 **despite taxonomic convergence of root microbiomes**

373 During the conditioning phase, we observed that the *T. dactyloides* plants grown in low-
374 precipitation-legacy soils had increased shoot height, root and shoot mass, and total aerenchyma
375 area under drought treatment compared to plants grown in high-precipitation-legacy soils (Fig. 2a
376 and Extended Data Fig. 6c). To confirm that these effects of soil precipitation legacy on plant
377 phenotype (Fig. 2a) were conferred by the microbiome rather than co-varying soil properties, we
378 extracted the experimentally-conditioned microbial communities and used them to inoculate a
379 new generation of *T. dactyloides* cv. “Pete”. These “test phase” plants were divided between
380 water-limited conditions (⅔ of all plants) and well-watered control conditions (⅓ of plants;
381 Extended Data Fig. 6a). We confirmed that our test phase drought treatment impaired plant
382 growth (Extended Data Fig. 9a). After five weeks we uprooted gamagrass plants for phenotyping
383 and sampled crown roots, which are highly active in water acquisition[16,17], for 16S rRNA gene

384 microbiome profiling and root gene expression analysis. Our focus only on bacteria was motivated
385 by past work showing that root-colonizing fungi from these soils were insensitive to drought[18] and
386 by our observation that >97% of all metagenomic reads in this study were bacterial. To capture
387 the effects of the precipitation gradient extremes, we measured plant gene expression only for
388 plants that received inocula derived from the two easternmost (wet-legacy) and two westernmost
389 (dry-legacy) soils.
390
391 We found that precipitation legacy did not affect the alpha diversity (Shannon diversity) or the
392 taxonomic composition of the gamagrass root bacterial community as measured by 16S rRNA
393 gene sequencing (Fig. 3a). The taxonomic composition of the crown root bacterial community
394 was only impacted by the test phase water treatment (Fig. 3b; ANOVA.CCA, $F_{1,139}$=2.57,
395 R^2=0.016, p = 0.004), not legacy (Fig. 3c), which only explained 1.6% of the variation in the data.
396 We further assessed root microbiome stability by calculating beta-dispersion, a measure of within-
397 group variability. Neither test phase water treatment, inoculum legacy, nor their interaction
398 impacted gamagrass root bacterial community beta-dispersion (Fig. 3d; ANOVA $F_{1,144}$=0.571, p =
399 0.45). Altogether, these results suggest that gamagrass exerts a strong homogenizing influence
400 during root microbiome formation, resulting in the assembly of a stable and drought-resistant
401 microbiota. The stability of the gamagrass root bacterial microbiome, even after receiving
402 compositionally different inocula, indicates a deterministic process (not stochastic) of community
403 assembly. Because eastern gamagrass (and the "Pete" cultivar in particular[19]) shares a long
404 evolutionary history with Kansas soil microbes, this result supports previous findings that co-
405 evolution promotes stable community assembly[20,21].
406
407
408
409
410
411
412

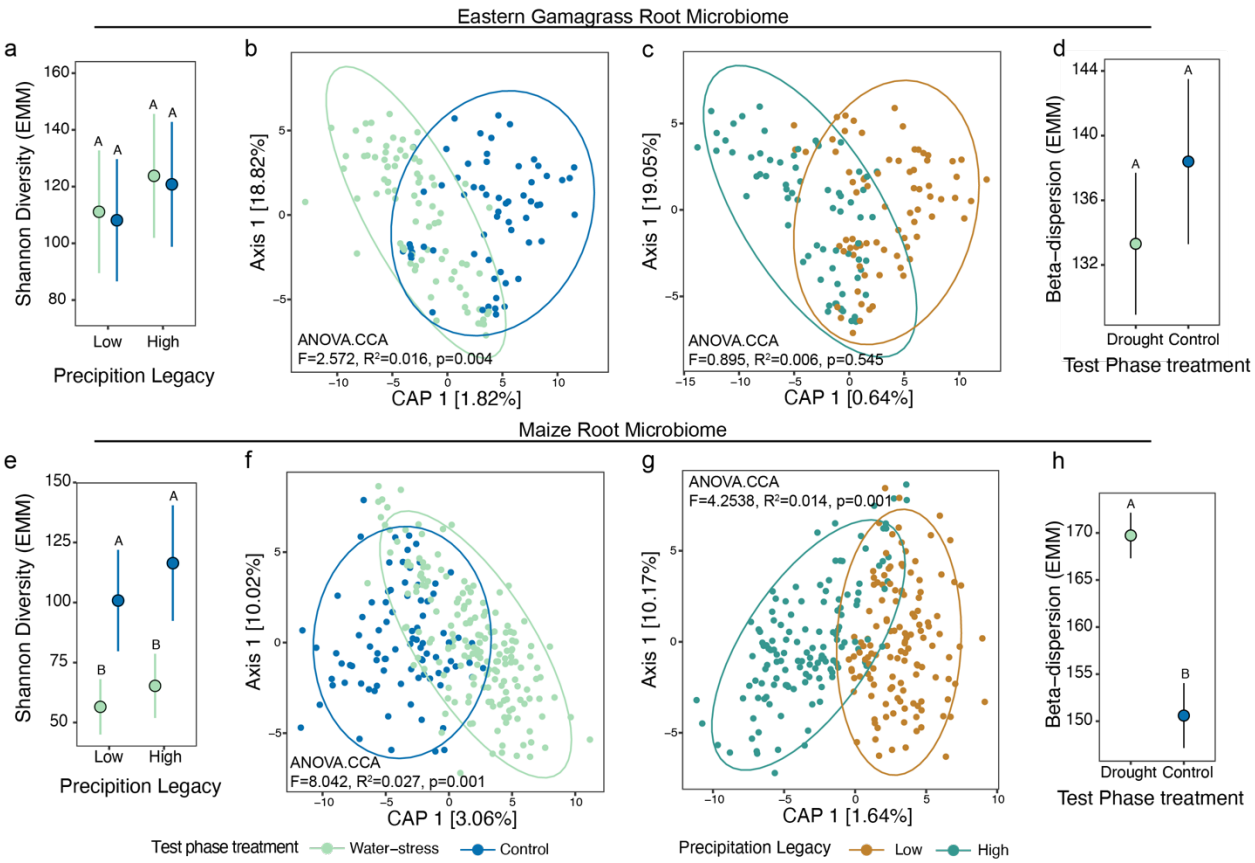

Fig. 3. Test phase gamagrass root microbiome is remarkably stable. **a.** Shannon diversity was not impacted by precipitation legacy or test phase water treatment. Points are EMMs and error bars represent the standard error. ANOVA was used to discern significant differences among groups and means were separated using Tukey's post hoc test. **b**. A canonical analysis of principal coordinates indicates that test phase water treatment, but not legacy (**c**) significantly impacted the gamagrass root bacterial microbiome composition. Ellipses represent the 95% confidence intervals. **d.** Drought treatment did not impact the root microbiome within group variation (beta-dispersion). Points are EMMs and error bars represent the standard error. **e**. Maize root microbiome Shannon diversity was significantly impacted by test phase water treatment, but not legacy. Points are EMMs and error bars represent the standard error. ANOVA was used to discern significant differences among groups and means were separated using Tukey's post hoc test. **f**. Legacy and Test phase water treatment (**g**) significantly impacted the maize root bacterial microbiome composition. Ellipses represent the 95% confidence intervals. **h.** Acute drought treatment also increased maize root microbiome within group variation. Points are EMMs and error bars represent the standard error.

Although precipitation legacy did not significantly shape 16S rRNA gene diversity within the *T. dactyloides* root microbiome, its clear effect on metagenome content and microbial gene expression (Fig. 2e, 2f, and 2g and Extended Data Fig. 8f) suggested high potential to influence plant phenotypes. Indeed, RNA-seq analysis confirmed that microbial inocula with contrasting precipitation legacies differentially influenced host gene expression in the crown roots. In addition

432 to 15 *T. dactyloides* genes that were differentially expressed depending on whether the inoculum
433 originated from a high-precipitation or low-precipitation region (Fig. 4a; Supplementary Table S3),
434 we observed that microbial legacy influenced the responses of 183 genes to acute drought (Fig.
435 4b). The majority of these (55%) were unresponsive to acute drought in plants grown with a dry-
436 legacy microbiota, but were significantly down-regulated or up-regulated in plants grown with a
437 wet-legacy microbiota (Fig. 4b, gene sets I and II, respectively; Supplementary Table S3). This
438 strongly suggests that the ecological memory of drought transmitted through soil microbiota
439 subdued the overall transcriptional response of gamagrass to acute drought. The 50 *T.*
440 *dactyloides* genes that decreased expression under acute drought only in the presence of a wet-
441 legacy microbiome (Fig. 4b gene set I) included five that are orthologous to maize genes predicted
442 to be involved in ethylene- or ABA-mediated signalling of water stress (Td00002ba004498,
443 Td00002ba024351, Td00002ba011993, Td00002ba005402, Td00002ba000033) and a heat
444 shock protein linked to temperature stress (Td00002ba042486) (Supplementary Data 1). Notably,
445 the latter three genes were not identified as drought-sensitive when averaging across inocula,
446 demonstrating that the microbial context is necessary for a complete understanding of molecular
447 plant drought responses. We note that these signatures of microbiota legacy on the plant
448 transcriptome were detectable even when averaging across all treatments applied during the
449 conditioning phase (Extended data Fig. 6a), again confirming that microbiome legacy effects with
450 implications for plant fitness are robust to short-term perturbations.
451
452 Next, we phenotyped the test phase plants to determine whether microbial precipitation legacy
453 altered host physiological and morphological responses to a subsequent acute drought. For each
454 of 63 traits, including mineral and nutrient content, mass and height, photosynthesis and gas
455 exchange rates, crown root anatomy, and root system architecture, we calculated a drought
456 susceptibility index (S-index) that measures the stability of a trait under drought relative to control
457 plants that received the same inoculum type (Supplementary Table S4). We used a random forest

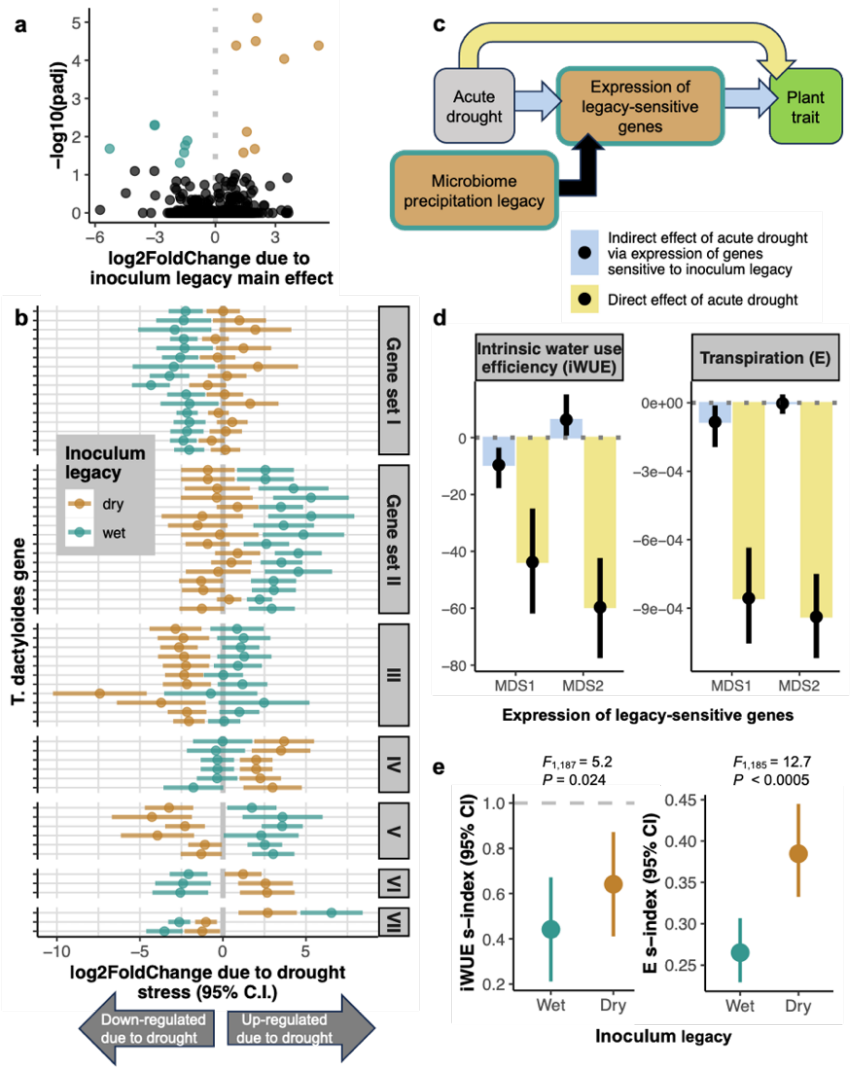

Fig. 4. Drought legacy of microbial inocula alters the response to drought in eastern gamagrass. a. 15 genes were up-regulated in plants inoculated with microbiota from a low-precipitation region, relative to plants inoculated with microbiota from a high-precipitation region. **b.** In total, 183 *T. dactyloides* genes responded to acute drought in a manner that was dependent on the drought legacy of the soil microbiota, regardless of the inoculum's treatment during the conditioning phase (Supplementary Data 1). Only genes with a drought response of ≥ 4-fold and with annotated maize ortholog(s) are shown here for illustration purposes. Each pair of points shows one gene; the relative position of the two points illustrates how the gene's expression changed in response to acute drought during the Test Phase, depending on whether the plant had been inoculated with microbiota derived from a low-precipitation or high-precipitation environment. Genes are grouped into sets according to the pattern of how inoculum legacy altered their drought responses. **c.** The model used for mediation analysis to test whether the expression of the 198 legacy-sensitive genes (see panels a-b) contributed to the overall effect of acute drought on plant phenotype. **d.** Mediation analysis confirmed that the expression of legacy-sensitive genes is part of the plant response to acute drought resulting in decreased intrinsic water-use efficiency (iWUE, units: µmol/mol) and transpiration (E, units: mol m^{-2} s^{-1}). Error bars indicate 95% confidence intervals. **e.** Microbiomes with a low-precipitation legacy caused increased iWUE and E during acute drought, relative to inocula derived from high-precipitation-legacy soils. The s-index describes trait values scaled by the mean value of well-watered control plants, such that an s-index of 1 indicates that droughted plants were phenotypically identical to non-droughted plants.

477 model to rank and identify the ten most important traits for describing the phenotypic effects of
478 microbiome precipitation legacy (Extended Data Fig. 10a,b). We then summarized the variation
479 in these top traits using constrained redundancy analysis, which revealed that microbiome
480 precipitation legacy explained 5% of the total variation in host phenotypic response to acute
481 drought (ANOVA.CCA, $F_{1,187} = 10.1$, $R^2 = 0.05$, $p = 0.001$) (Extended Data Fig. 11a). Microbiota
482 precipitation legacy significantly impacted six of the top eight non-correlated traits: transpiration,
483 leaf chlorophyll content, max root width, root total metaxylem area, median root diameter, Cu, K,
484 and intrinsic water use efficiency (iWUE) – an important plant drought response trait[22,23] (Extended
485 Data Fig. 11b-j).
486
487 To solidify the mechanisms linking microbiome legacy to plant phenotype, we used mediation
488 analysis to determine whether the 198 genes that were differentially expressed depending on
489 inoculum legacy (Fig. 4a-b) were causally involved in trait responses to acute drought (Fig. 4c).
490 Expression patterns of this subset of genes were summarized in two dimensions (MDS1 and
491 MDS2) using non-metric multidimensional scaling of Bray-Curtis dissimilarities among individual
492 plants. MDS1 mediated 18% of the total drought-induced decrease in iWUE ($p < 0.001$), and 8.9%
493 of the total decrease in transpiration ($p = 0.018$; Fig. 4d). In contrast, MDS2 mediated 11% of the
494 iWUE response to drought ($p = 0.03$), but in the opposite direction, meaning that the activity of
495 these genes counteracted the negative effects of acute drought on iWUE. Four of the top eight
496 genes with the strongest positive loadings on MDS2 were orthologs of the maize gene ZmNAS7,
497 which encodes the enzyme nicotianamine synthase; two of these were also in the top 5% of genes
498 with the strongest negative loadings on MDS1 (Extended Data Fig. 12), indicating that they have
499 a protective function that minimizes the drop in iWUE during acute drought. All four ZmNAS7
500 orthologs were up-regulated between 4-fold and 12-fold in response to drought, but only in plants
501 that were inoculated with dry-legacy microbiota (Fig. 4b, gene set IV), suggesting a possible
502 mechanism by which microbiota with a legacy of chronic water stress confer drought tolerance.

503 Consistent with this, salicylic acid–a key regulator of root microbiome assembly[24]–is reported to
504 induce expression of ZmNAS7[25]. Furthermore, although nicotianamine is best known for its role
505 in metal transport, the overexpression of NAS genes in rice conferred tolerance of acute drought,
506 including maintenance of photochemical efficiency at pre-drought levels[26]. Overall, these results
507 show that microbiomes with a history of water-stress improve the drought response of eastern
508 gamagrass, and that a complete understanding of plant drought response requires consideration
509 of the microbial environment, including legacy effects of water scarcity.
510
511 **Beneficial microbiome drought legacy effects do not extend to the crop species *Zea mays***
512 To explore whether the observed microbial legacy effects were transferable across hosts, we
513 simultaneously applied the same inocula to seedlings of the maize (*Zea mays* ssp. *mays*)
514 genotype B73. Maize is genetically closely related to gamagrass, making it a good candidate for
515 testing whether microbiome legacy effects are transferable to domesticated, non-native species.
516 Maize plants were four weeks old at the time of sampling, and the drought treatment was sufficient
517 to hinder maize growth (Extended Data Fig. 9b). Unlike in eastern gamagrass, the taxonomic
518 composition of bacterial communities in maize crown roots retained clear signatures of the
519 inoculum precipitation legacy (Fig. 3g., ANOVA.CCA, $F_{1,255} = 4.254$, $R^2 = 0.014$, $p = 0.001$), in
520 addition to being impacted by acute drought treatment (Fig. 3f). Also, unlike gamagrass, acute
521 drought significantly increased beta-dispersion compared to the well-watered control, indicating
522 that water deprivation gave rise to more variability in the maize microbiome (Fig. 3h; ANOVA $F_{1,262}$
523 $= 18.17$, $p < 0.001$). Like in eastern gamagrass, however, all inocula resulted in root communities
524 with a similar mean Shannon diversity, but drought treatment significantly decreased alpha
525 diversity (Fig. 3e). Next, we identified bacterial amplicon sequence variants (ASVs) that were
526 differentially abundant in droughted *vs.* control plants in a manner that depended on the
527 precipitation legacy of the microbiome. This included only two ASVs in gamagrass roots,
528 ASV1598 (*Azospirillum* sp.) and ASV2352 (*Enterobacteriaceae*) (Extended Data Fig. 13a;

529 Supplementary Table S5), but 100 ASVs in maize roots (Extended Data Fig. 13b; Supplementary
530 Table S5), again indicating that gamagrass root microbiomes are more stable than those of maize.
531 The maize ASV enrichments did not show a phylogenetic pattern. We speculated that these
532 drought-responsive ASVs could contribute to plant phenotypic responses to drought.
533
534 To validate this, we also characterized the transcriptional response of maize and found that 23
535 genes were up-regulated in plants inoculated with dry-legacy microbiota, relative to those that
536 received wet-legacy inocula (Extended Data Fig. 14a). These included six defense-related genes,
537 particularly those related to jasmonic acid signaling, suggesting that soil microbiota from low-
538 precipitation sites were perceived as pathogens by maize, but not eastern gamagrass. Other
539 notable functions that were up-regulated by the dry-legacy inocula in maize include root
540 development and iron acquisition (Supplementary Table S3). We also identified 109 maize genes
541 that responded to acute drought in a manner that was dependent on microbial precipitation
542 legacy, of which only 30 were identified as drought-responsive when averaging across inocula
543 (Extended Data Fig. 14b). Like in eastern gamagrass, most of these were drought-responsive
544 only in wet-legacy-inoculated or only in dry-legacy-inoculated plants, with relatively few genes
545 reversing the direction of their drought response depending on inoculum legacy (Extended Data
546 Fig. 14c). For example, 30 genes were up-regulated in response to drought only in plants grown
547 with wet-legacy microbiota (Extended Data Fig. 14c, gene set I). These genes included several
548 related to pathogen defense (Zm00001eb116230, Zm00001eb150050, Zm00001eb222540) and
549 one involved in the response to symbiotic fungi (Zm00001eb033580), suggesting that soils from
550 high-precipitation regions contain both harmful and beneficial microorganisms and that
551 interactions with both types are activated under water deprivation in maize (Supplementary Table
552 S3). Notably, one of the 18 genes that reversed its drought response depending on the inoculum
553 was TIP3, which encodes an aquaporin that regulates water storage in the vacuole[27]. In the
554 presence of wet-legacy microbiota, TIP3 expression increased 7-fold during acute drought,

555 whereas in the presence of dry-legacy microbiota TIP3 expression decreased nearly 3-fold
556 (Extended Data Fig. 14c, gene set VI). Averaged across the two inocula, however, TIP3 was not
557 differentially expressed between droughted and well-watered plants; thus, its role in drought
558 response was apparent only when accounting for microbiota legacy.
559
560 We identified four sets of orthologous genes that were sensitive to microbiota legacy in both host
561 species. Zm00001eb076200 encodes a peroxidase that reversed its drought response depending
562 on inoculum in maize; however, its *T. dactyloides* ortholog, Td00002ba025285, was up-regulated
563 4-fold due to drought but only in plants grown with wet-legacy inoculum. The gene
564 Zm00001eb077640, encoding L-allo-threonine aldolase, also reversed its drought response in
565 maize. In contrast, its ortholog Td00002ba026366 was consistently up-regulated in response to
566 drought, but more so in plants inoculated with dry-legacy biota. The maize pathogenesis-related
567 protein-like gene Zm00001eb150050, which has been linked to both biotic and abiotic stress
568 responses, was up-regulated 7-fold in response to drought only in plants inoculated with wet-
569 legacy microbiota; however, both of its *T. dactyloides* orthologs were down-regulated 8-fold in
570 plants inoculated with microbiota from low-precipitation sites, relative to inocula from high-
571 precipitation sites, regardless of water availability. Finally, Zm00001eb301540 encodes a
572 tryptophan synthase that was up-regulated 1.7-fold in the presence of wet-legacy but not dry-
573 legacy microbes; its ortholog Td00002ba012570, in contrast, was down-regulated in the presence
574 of wet-legacy microbes. Thus, none of these four sets of orthologous genes showed congruent
575 responses to drought in maize and eastern gamagrass.
576
577 Finally, we investigated whether the beneficial effects of microbiome legacy on *T. dactyloides*
578 physiological and morphological phenotypes (Fig. 4d-e) were also conferred on maize. Overall,
579 microbiome precipitation legacy explained only 2.0% of the phenotypic variation in maize
580 (Extended Data Fig. 15a., ANOVA.CCA, $F_{1,175} = 3.72$, $R^2 = 0.02$, $p = 0.001$), a weaker effect than

581 observed in eastern gamagrass. In fact, in general, we observed no significant phenotypic
582 differences attributable to microbiome legacy (Extended Data Fig. 15b,c). Thus, the capacity to
583 integrate the beneficial effect of soil drought legacy is host specific and it is related to the ability
584 of the host to maintain a stable microbiota in response to drought stress.
585
586 **Conclusions**
587 Microbially-mediated legacy effects of past water-limited conditions can affect plant performance
588 during subsequent droughts[28,29]. Our results reveal the importance of these stable signatures of
589 historical precipitation in microbiota composition and function not only for microbial adaptation,
590 but also for host survival under water-scarce conditions. We identified bacterial markers and
591 numerous microbial genes and functional pathways that are associated with mean annual
592 precipitation, including those suggesting an increased nitrogen-metabolizing and DNA repair
593 capacity in dry-legacy microbiota. We validated these findings by controlling for other soil
594 properties that influence microbial communities, namely soil porosity and mineral nutrient content.
595 Furthermore, we confirmed that these metagenomic patterns are shared by two independent
596 natural precipitation gradients separated by more than 7,000 km, suggesting that these signatures
597 of historic precipitation levels may generalize to soils across the globe. Thus, we provide evidence
598 for the ecological mechanisms involved in the formation of soil drought memory and demonstrate
599 its robustness to a five-month perturbation, which could mimic a particularly dry or wet season.
600
601 We have shown that these metagenomic precipitation legacies have significant implications for
602 plant response to drought. Inoculation with dry-legacy microbiota altered the transcription of key
603 genes controlling drought responses in the plant. In the prairie grass *Tripsacum dactyloides*, dry-
604 and wet-legacy soil microbiomes give rise to taxonomically similar root endosphere microbial
605 communities yet have strikingly different effects on plant gene expression and phenotypes during

606 a subsequent acute drought. This effect was less obvious in maize, which has a relatively unstable
607 root microbiome and reduced physiological and morphological sensitivity to soil microbiome
608 legacy during drought. Based on these findings, root microbiome stability appears to play a role
609 in adaptive plant responses to a subsequent acute drought. Importantly, differences in gamagrass
610 and maize responses to microbiome history indicate that crops may not reap the same benefits
611 as native plant species from potentially beneficial microbial communities. Therefore, our
612 discoveries significantly contribute to our mechanistic understanding of microbiome drought
613 legacy effects, their resistance to perturbation, and their role in plant drought responses, with
614 implications for agricultural and ecosystem management.
615

616 **Data availability**

617 The 16S rRNA amplicon sequencing and metagenomic data associated with this study have been
618 deposited in the NCBI Sequence Read Archive under the BioProject IDs PRJNA1186942 and
619 PRJNA1179931, respectively. The raw transcriptomic and metatranscriptomic data have been
620 deposited in the Gene Expression Omnibus under accession XXXXX and XXXX, respectively.
621 We deposited all scripts and additional data structures required to reproduce the results of this
622 study in the following Zenodo repository: doi: 10.5281/zenodo.13821006. Source data are
623 provided with this paper.
624

625 **Acknowledgements**

626 We thank Arun Seetharam, Matthew Hufford, and the PanAnd consortium for granting early
627 access to the *Tripsacum dactyloides* genome and annotation. We thank Dr. Mitch Greer, Michaela
628 VonLintel, Justin Roemer, Dr. Alan Schlegel, and the Nature Conservancy for granting access to
629 soil collection sites in Kansas, and Dr. Peter Balint-Kurti for providing maize seeds. We thank Dr
630 Craig J. Sturrock and Dr Brian S. Atkinson from the Hounsfield Facility at the University of
631 Nottingham for their assistance with the analysis of the CT images. We are grateful to the

632 undergraduate student researchers and technicians who helped to set up experiments and collect
633 data: Felicity Tso, Hannah Reid, and Carmen Rodriguez. Thank you to Dr. Joel Swift, Ceyda
634 Kural-Rendon, Dr. Ben Sikes (University of Kansas), Dr. Manuel Kleiner (North Carolina State
635 University), Dr Omri Finkel (The Hebrew University of Jerusalem, Israel), and Dr Nicholas Girkin
636 (University of Nottingham, UK) for critical reading of the manuscript. This work was supported by
637 a UKRI/BBSRC - NSF/BIO Lead Agency Opportunity, National Science Foundation award #IOS-
638 2016351 and BBSRC grant #BB/V011294/1. Maize root transcriptome library preps and
639 sequencing were performed in the RTSF Genomics Core at Michigan State University. *T.*
640 *dactyloides* library preps and RNA-seq were performed at the NC State University Genomic
641 Sciences Laboratory (Raleigh, NC, USA). Research reported in this publication was made
642 possible in part by the services of the KU Genome Sequencing Core. This lab is supported by the
643 National Institute of General Medical Sciences (NIGMS) of the National Institutes of Health under
644 award number P30GM145499. We thank the University of Kansas Medical Center – Genomics
645 Core for generating the 16S amplicon sequence data sets. The Genomics Core is supported by
646 the Kansas Intellectual and Developmental Disabilities Research Center (NIH U54 HD 090216),
647 the Molecular Regulation of Cell Development and Differentiation – COBRE (P30 GM122731),
648 The NIH S10 High End Instrumentation Grant (NIH S10OD021743) and the Frontiers CTSA Grant
649 (UL1TR002366).
650

651 **Author contributions**

652 Conceptualization: N.A.G., V.C., D.G., G.C., and M.R.W. Data curation: N.A.G., V.C., D.G., and
653 M.R.W.; Formal analysis: N.A.G., V.C., D.G., I.S.-G., and M.R.W.; Investigation: N.A.G., V.C.,
654 D.G., N.F., D.D.J., D.M.W., A.M., G.C., and M.R.W.; Methodology: G.C. and M.R.W.; Project
655 administration: G.C. and M.R.W.; Software: N.A.G., V.C., D.G., and M.R.W.; Supervision: G.C.

656 and M.R.W.; Visualization: N.A.G., V.C., D.G., and M.R.W.; Writing – original draft: N.A.G., G.C.,
657 and M.R.W.; Writing – review & editing: V.C. and D.G.
658
659 **Competing interests:** The authors declare no competing interests.
660
661 **References**

662 1. Schimel, J., Balser, T. C. & Wallenstein, M. Microbial stress-response physiology and its
663 implications for ecosystem function. *Ecology* **88**, 1386–1394 (2007).
664 2. Chase, A. B., Weihe, C. & Martiny, J. B. H. Adaptive differentiation and rapid evolution of a
665 soil bacterium along a climate gradient. *Proc. Natl. Acad. Sci. U. S. A.* **118**, (2021).
666 3. Lau, J. A. & Lennon, J. T. Rapid responses of soil microorganisms improve plant fitness in
667 novel environments. *Proc. Natl. Acad. Sci. U. S. A.* **109**, 14058–14062 (2012).
668 4. Canarini, A. *et al.* Ecological memory of recurrent drought modifies soil processes via
669 changes in soil microbial community. *Nat. Commun.* **12**, 5308 (2021).
670 5. Custódio, V. *et al.* Sculpting the soil microbiota. *Plant J.* **109**, 508–522 (2022).
671 6. Naylor, D., DeGraaf, S., Purdom, E. & Coleman-Derr, D. Drought and host selection
672 influence bacterial community dynamics in the grass root microbiome. *ISME J.* **11**, 2691–
673 2704 (2017).
674 7. Liu, Z. *et al.* Shifts in microbial communities and networks are correlated with the soil
675 ionome in a kiwifruit orchard under different fertilization regimes. *Appl. Soil Ecol.* **149**,
676 103517 (2020).
677 8. Dai, Z. *et al.* Metallic micronutrients are associated with the structure and function of the
678 soil microbiome. *Nat. Commun.* **14**, 8456 (2023).
679 9. Guellouz, L., Askri, B., Jaffré, J. & Bouhlila, R. Estimation of the soil hydraulic properties
680 from field data by solving an inverse problem. *Sci. Rep.* **10**, 9359 (2020).

681 10. Rousseva, S., Torri, D. & Pagliai, M. Effect of rain on the macroporosity at the soil surface.
682 *Eur. J. Soil Sci.* **53**, 83–93 (2002).
683 11. Naylor, D. & Coleman-Derr, D. Drought Stress and Root-Associated Bacterial
684 Communities. *Front. Plant Sci.* **8**, 2223 (2017).
685 12. Sun, Y., Wilkinson, B. J., Standiford, T. J., Akinbi, H. T. & O'Riordan, M. X. D. Fatty acids
686 regulate stress resistance and virulence factor production for Listeria monocytogenes. *J.*
687 *Bacteriol.* **194**, 5274–5284 (2012).
688 13. Woodcock, S. D. *et al.* Trehalose and α-glucan mediate distinct abiotic stress responses in
689 Pseudomonas aeruginosa. *PLoS Genet.* **17**, e1009524 (2021).
690 14. Gil-Quintana, E. *et al.* Local inhibition of nitrogen fixation and nodule metabolism in
691 drought-stressed soybean. *J. Exp. Bot.* **64**, 2171–2182 (2013).
692 15. Zhu, J., Brown, K. M. & Lynch, J. P. Root cortical aerenchyma improves the drought
693 tolerance of maize (*Zea mays* L.). *Plant Cell Environ.* **33**, 740–749 (2010).
694 16. Gao, Y. & Lynch, J. P. Reduced crown root number improves water acquisition under water
695 deficit stress in maize (Zea mays L.). *J. Exp. Bot.* **67**, 4545–4557 (2016).
696 17. Ahmed, M. A. *et al.* Root type matters: measurement of water uptake by seminal, crown,
697 and lateral roots in maize. *J. Exp. Bot.* **69**, 1199–1206 (2018).
698 18. Swift, J. F. *et al.* Drought stress homogenizes maize growth responses to diverse natural
699 soil microbiomes. *Plant Soil* (2024) doi:10.1007/s11104-024-06853-x.
700 19. Springer, T. L. & Dewald, C. L. Eastern gamagrass and other*Tripsacum*species. in *Warm-*
701 *Season (C4) Grasses* 955–973 (American Society of Agronomy, Crop Science Society of
702 America, Soil Science Society of America, Madison, WI, USA, 2016).
703 20. Batstone, R. T., O'Brien, A. M., Harrison, T. L. & Frederickson, M. E. Experimental
704 evolution makes microbes more cooperative with their local host genotype. *Science* **370**,
705 476–478 (2020).
706 21. Morella, N. M. *et al.* Successive passaging of a plant-associated microbiome reveals robust

habitat and host genotype-dependent selection. *Proceedings of the National Academy of Sciences* **117**, 1148–1159 (2020).

22. Hund, A., Ruta, N. & Liedgens, M. Rooting depth and water use efficiency of tropical maize inbred lines, differing in drought tolerance. *Plant Soil* **318**, 311–325 (2009).
23. Schulz, P. *et al.* Improving plant drought tolerance and growth under water limitation through combinatorial engineering of signalling networks. *Plant Biotechnol. J.* **19**, 74–86 (2021).
24. Lebeis, S. L. *et al.* PLANT MICROBIOME. Salicylic acid modulates colonization of the root microbiome by specific bacterial taxa. *Science* **349**, 860–864 (2015).
25. Zhou, M.-L. *et al.* Nicotianamine synthase gene family as central components in heavy metal and phytohormone response in maize. *Funct. Integr. Genomics* **13**, 229–239 (2013).
26. Lee, D.-K. *et al.* The rice OsNAC6 transcription factor orchestrates multiple molecular mechanisms involving root structural adaptions and nicotianamine biosynthesis for drought tolerance. *Plant Biotechnol. J.* **15**, 754–764 (2017).
27. Chaumont, F., Barrieu, F., Wojcik, E., Chrispeels, M. J. & Jung, R. Aquaporins constitute a large and highly divergent protein family in maize. *Plant Physiol.* **125**, 1206–1215 (2001).
28. de Vries, F., Lau, J., Hawkes, C. & Semchenko, M. Plant–soil feedback under drought: does history shape the future? *Trends Ecol. Evol.* **38**, 708–718 (2023).
29. Evans, S., Allison, S. & Hawkes, C. Microbes, memory and moisture: Predicting microbial moisture responses and their impact on carbon cycling. *Funct. Ecol.* (2022) doi:10.1111/1365-2435.14034.

Supplementary Materials for

Persistent legacy effects on soil microbiota facilitate plant adaptive responses to drought

Nichole A. Ginnan, Valéria Custódio, David Gopaulchan, Natalie Ford, Isai Salas-González, Dylan H. Jones, Darren M. Wells, Ângela Moreno, Gabriel Castrillo, Maggie R. Wagner.

This PDF file includes:

Materials and Methods

Extended Data Fig. 1-15

Supplementary Tables 1-5

References

Materials and Methods

No statistical methods were applied to predetermine sample size. The experiments were randomized, and investigators were blinded to allocation during experiments and outcome assessment.

1. Legacy phase: Characterization of soils across precipitation gradients

1.1 Region selection and soil collection

Soils exposed to the macrogradient of precipitation were sampled from six never-irrigated native prairies across Kansas, USA in October 2020. This selection includes eastern Kansas tallgrass prairies: Welda Prairie (WEL), Clinton Wildlife Reserve (CWR), and Konza Wildlife Reserve (KNZ), as well as western Kansas shortgrass prairies: Hays Prairie (HAY), Smoky Valley Ranch (SVR), and Kansas State University's Tribune Southwest Research Center (TRI). The GPS coordinates of each collection site are available in the Supplemental Table S1. For soil collection, each site was split into three subplots. In each subplot, the surface soil (≈10 cm) containing thick plant root masses was removed with a bleach-sterilized metal shovel. Then, approximately 2.5 L of soil was collected from each site and pooled into a clean plastic bag, for a total of ≈7.5 L of soil collected per geographical location. Soil was held at room temperature for transport back to the laboratory where it was then stored at 4˚C until use (~ 1 month).

Soils exposed to the microgradient of precipitation were selected from nine regions in Santiago Island, Cabo Verde in March 2022. These regions included Porto Gouveia, Mato Correia, Colonato, Ribeira Riba, Ribeira de São Domingos (Nora), Tomba Toiro, Serra Malagueta, Achada Leitão and Pico de Antónia. GPS coordinates are available in the Supplemental Table S1. For the soil collection, each site was divided into six equal parts (subplots). Within each subplot, six samples were collected following a typical zig-zag pattern with approximately 3 m of separation between the harvesting points and avoiding field edges, roads, and pathways. In each collection

point, the top 2 cm layer of soil was discarded using a handheld soil auger and pooled to produce a unique composite sample per subplot. Thus, for each region, we collected six composite samples. All tools used for the soil collection were previously disinfected with 70% ethanol, and the operators wore gloves the whole time. Soil samples were transported in clean plastic bags to the Instituto Nacional de Investigação e Desenvolvimento Agrário (INIDA).

For both Kansas and Cabo Verde soils, sub-samples for downstream metagenomic sequencing and nutrient mineral content analyses were air-dried in sterile plastic trays at room temperature for 1 week and then sieved using a 2 mm sieve to remove rocks, big soil particles, and vegetable debris. The Kansas sub-samples were shipped to the University of Nottingham for further processing, and all sub-samples were stored at 4 ºC until use.

1.2 Precipitation data collection

For all collection sites in Kansas and Santiago Island, precipitation values were retrieved from publicly available sources with global coverage. Briefly, for Kansas, daily precipitation from 1981 to 2021 was extracted from the NASA POWER database based on the latitude and longitude of each site[1]. For Santiago Island, we used three different approaches to compile rainfall data. First, we compiled data from the available literature[2–4]. Briefly, the files containing the precipitation data were downloaded directly from the supplemental material of each publication or were kindly provided by the authors of the publications. Then, we extracted the rainfall data from stations in Colonato, Ribeira de São Domingos, and Serra Malagueta. Next, for Porto Gouveia, Ribeira Riba, Achada Leitão, and Pico de Antónia, the methodology of the World Meteorological Organization was applied, which advises that on a small scale, we can consider reliable data collected from stations located 10 km or less from the study region[5]. Finally, for Mato Correia and Tomba Toiro we extracted the data from NASA POWER database based on the latitude and longitude[1]. The

dataset used in each case included the monthly precipitation average data from 1981 to 2021 for Kansas and from 1981 to 2009 for Santiago.

1.3 Soil elemental content analysis

The soil mineral nutrients and trace elements profiles were determined using inductively coupled plasma mass spectrometry (ICP-MS). The soil samples were dried using plastic weighing boats in the fume hood for approximately 72 h at ambient temperature. Five grams of soil were weighed in 50 mL conical tubes with a four-decimal balance, and treated with 20 mL of 1 M NH_4HCO_3, 5 mM diamine-triamine-penta-acetic acid (DTPA), and 5 mL 18.2 MΩcm Milli-Q Direct water (Merck Millipore), for 1 h at 150 r.p.m. in a rotary shaker (adapted from[6]) to extract available elements. Each treated sample was gravity-filtered through a quantitative filter paper (Whatman 42-WHA1442070) to obtain approximately 5 mL of filtrate. Prior to the digestion, 20 µg/L of Indium (In) was added to the nitric acid Primar Plus (Fisher Chemicals) as an internal standard for assessing error in dilution, variations in sample introduction and plasma stability in the ICP-MS instrument. Next, 0.5 mL of the soil filtrates were open-air digested in glass Pyrex tubes using 1 mL of concentrated trace metal grade nitric acid spiked indium internal standard for 2 h at 115 ºC in dry block heater (DigiPREP MS, SCP Science; QMX Laboratories, Essex, UK). After cooling, the digests were diluted to 10 mL with 18.2 MΩcm Milli-Q Direct water and elemental analysis was performed using an ICP-MS, PerkinElmer NexION 2000 equipped with Elemental Scientific Inc 4DXX FAST Dual Rinse autosampler, FAST valve and peristaltic pump. The instrument was fitted with PFA-ST3 MicroFlow nebulizer, baffled cyclonic C3 high sensitivity glass spray chamber cooled to 2ºC with PC3X Peltier heated/cooled inlet system, 2.0 mm i.d. quartz injector torch and a set of nickel cones. Twenty-three elements were monitored including following stable isotopes: ^{7}Li, ^{11}B, ^{23}Na, ^{24}Mg, ^{31}P, ^{34}S, ^{39}K, ^{43}Ca, ^{52}Cr, ^{55}Mn, ^{56}Fe, ^{59}Co, ^{60}Ni, ^{63}Cu, ^{66}Zn, ^{75}As, ^{82}Se, ^{85}Rb, ^{88}Sr, ^{98}Mo, ^{111}Cd, ^{208}Pb and ^{115}In. Helium was used as a collision gas in Kinetic Energy Discrimination mode (KED) at a flow rate of 4.5 mL/min while measuring Na, Mg, P, S, K, Ca, Cr,

109 Mn, Fe, Ni, Cu, Zn, As, Se and Pb to exclude possible polyatomic interferences. The remaining
110 elements were measured in the standard mode. Any isobaric interferences were automatically
111 corrected by the instrument Syngistix™ software for ICP-MS v.2.3 (Perkin Elmer). The ICP-MS
112 measurements were performed in peak hopping scan mode with dwell times ranging from 25 to
113 50 ms depending on the element, 20 sweeps per reading and three replicates. The ICP-MS
114 conditions were as follows: RF power – 1600 Watts, auxiliary gas flow rate 1.20 L/min. Torch
115 alignment, nebulizer gas flow and quadrupole ion deflector (QID) voltages (in standard and KED
116 mode) were optimized before analysis for highest intensities and lowest interferences (oxides and
117 doubly charged ions levels lower than 2.5%) with NexION Setup Solution containing 1 µg/L of
118 Be, Ce, Fe, In, Li, Mg, Pb and U in 1% nitric acid using a standard built-in software procedure. To
119 correct for variation between and within ICP-MS analysis runs, liquid reference material was
120 prepared using pooled digested samples, and run after the instrument calibration, and then after
121 every nine samples in all ICP-MS sample sets. Equipment calibration was performed at the
122 beginning of each analytical run using seven multi-element calibration standards (containing 2
123 µg/L In internal standard) prepared by diluting 1000 mg/L single element standards solutions
124 (Inorganic Ventures; Essex Scientific Laboratory Supplies Ltd) with 10% nitric acid. As a
125 calibration blank, 10% nitric acid containing 2 µg/L In internal standard was used and it was run
126 throughout the course of the analysis.
127
128 Sample concentrations were calculated using the external calibration method within the
129 instrument software. Further data processing, including the calculation of final elements
130 concentrations was performed in Microsoft Excel. First, sample sets run at different times were
131 connected as an extension of the single-run drift correction. Linear interpolation between each
132 pair of liquid reference material standards was used to generate a theoretical standard for each
133 sample that was then used to correct the drift by simple proportion to the first liquid reference
134 material standard analysed in the first run. Liquid reference material composed of pooled samples

135 was used instead of the CRM to match the chemical matrix of the samples as closely as possible,
136 thereby emulating the sample drift. Second, the blank concentrations were subtracted from the
137 sample concentrations and each final element concentration was obtained by multiplying by the
138 dilution factor and normalizing the element concentrations to the sample's dry weight.
139
140 *1.4 Soil porosity analysis*
141 To quantify soil porosity, we used X-ray computed tomography. First, soils were collected from
142 the selected locations in Kansas (October 2020) and Santiago (March 2022), according to
143 material and methods 1.1. Briefly, each site was divided into three and six subplots in the case of
144 Kansas and Santiago, respectively. Within each subplot the top layer of soil was removed (10 cm
145 in Kansas and 2 cm in Santiago), and the soil samples were collected using polyvinylchloride
146 (PVC) columns of 5 cm internal diameter and 7 cm (Kansas) or 5 cm (Santiago) length. After the
147 soil collection, the bottom of each column was sealed with tape to retain the soil in the column.
148 We collected six soil columns per location.
149
150 The undisturbed soil columns were non-destructively imaged using Phoenix v|tome|x MDT
151 (Waygate Technologies GmbH, Wunstorf, Germany) at The Hounsfield Facility, University of
152 Nottingham. Scans were acquired by collecting 2695 projection images at 180 kV X-ray energy,
153 200 µA current and 334 ms detector exposure time in fast mode (15 min total scan time per
154 column). Scan resolution was 55 µm for Kansas columns and 40 µm for Santiago columns.
155
156 *1.5 Metagenomic analysis of free-living soil microbiota - DNA extraction*
157 For metagenomic analysis, approximately 5 g of each soil sample was transferred into 50-mL
158 conical tubes containing 20 mL of sterile distilled water. To remove large plant debris and soil
159 particles, the samples were shaken thoroughly and filtered into new sterile 50-mL tubes using
160 100-µm nylon mesh cell strainers. The filtered soil solutions were centrifuged at high speed for

161 20 min in a centrifuge Eppendorf 5810R and most of the supernatants were discarded. The
162 remaining 1-2 mL of supernatants were used to dissolve the soil pellets. The resulting
163 suspensions were transferred to sterile 1.5-mL Eppendorf tubes. Samples were centrifuged again
164 at high speed in a benchtop centrifuge and the supernatants were discarded. The remaining
165 pellets were stored at - 80ºC for DNA extraction. For DNA isolation we used 96-well-format MoBio
166 PowerSoil Kit (MOBIO Laboratories; QIAGEN) following the manufacturer's instructions. Before
167 starting the extraction, all samples were manually randomized by placing them in a plastic bag
168 that was shaken several times. Samples were then taken individually from the bag and loaded in
169 the DNA extraction plates. This random distribution was maintained throughout library preparation
170 and sequencing.
171
172 *1.6 Metagenomic library preparation and sequencing*
173 DNA sequencing libraries were prepared using the Rapid PCR Barcoding Kit (SQK-RPB004) from
174 Oxford Nanopore Technologies, UK. In brief, 1 µL Fragmentation Mix (FRM) was added to 3 µL
175 DNA (2-10 ng/µL), and the reaction was mixed by gently finger-flicking. The DNA was fragmented
176 using the following conditions: 30°C for 1 min, then 80°C for 1 min in an Applied Biosystems Veriti
177 96-Well Thermal Cycler (Applied Biosystems, CA, USA). The fragmented DNA was cooled, then
178 barcoded and amplified in a PCR reaction containing 20 µL nuclease-free water, 25 µL LongAmp
179 Taq 2X master mix (New England Biolabs, MA, USA), 4 µL fragmented DNA, and 1 µL barcode
180 adaptor. The reaction was gently mixed and amplified using the following conditions: 95°C for 3
181 min, 20 cycles of denaturation at 95°C for 15 s, annealing at 56°C for 15 s and extension at 65°C
182 for 6 min, and a final extension of 65°C for 6 min. The resulting DNA library was purified using
183 0.6X Agencourt AMPure XP beads (Beckman Coulter, CA, USA) and eluted in 10 µL 10 mM Tris-
184 HCl pH 8.0, 50 mM NaCl. The library concentration was determined using a Qubit 4 Fluorometer
185 with the Qubit dsDNA HS Assay Kit (Thermo Fisher Scientific, USA). Equimolar quantities of
186 individual barcoded sample libraries were pooled and the volume was adjusted to 10 µL using 10

187 mM Tris-HCl pH 8.0, 50 mM NaCl. Subsequently, 1 µL rapid sequencing adapter (RAP) was
188 added to the pooled library and the tube was incubated at room temperature for five minutes.
189 Then, 34 µL Sequencing Buffer, 25.5 µL Loading Beads, and 4.5 µL nuclease-free water were
190 added to the tube, and the contents were mixed gently. The prepared pooled library was added
191 to a verified and primed FLO-MIN106 R9.4.1 flow cell (Oxford Nanopore Technologies, UK) in a
192 MinION (Oxford Nanopore Technologies, UK) following the manufacturer's instructions. DNA
193 sequencing was conducted with default parameters using a MinIT (Oxford Nanopore
194 Technologies, UK) with MinKNOW v2.1.12 (Oxford Nanopore Technologies, UK). Fast5 files were
195 base-called with Guppy v4.0.15 using the template_r9.4.1_450bps_hac.jsn high accuracy model
196 (Oxford Nanopore Technologies, UK).
197
198 *1.7 Metagenomic sequences processing*
199 The initial dataset underwent demultiplexing, and primer and barcode sequences were trimmed
200 using qcat v1.1.0 (Oxford Nanopore Technologies Ltd., UK). Reads with ambiguous barcode
201 assignments were excluded from further analysis. The reads were filtered with NanoFilt v2.8.0[7]
202 to discard low-quality sequences (Q-score < 9) and sequences < 100 bp. We used the Kraken
203 v2.1.2 pipeline[8] to classify the whole metagenome shotgun sequencing reads. The reads were
204 classified using the Kraken 2 archaea, bacteria, viral, plasmid, human, UniVec_Core, protozoa,
205 and fungi reference database (k2_pluspf_20220607). To estimate relative abundances, the
206 Bracken v2.7 pipeline[9] was applied to the classification results. Subsequently, Pavian v1.0[10] was
207 used to extract abundance and taxonomic tables.
208
209 *1.8 Data Analysis*
210 *1.8.1 Precipitation data analysis*
211 To determine the differences in precipitation levels across regions, we compared the mean annual
212 precipitation in each region by fitting a linear model with the following formula:

Mean annual precipitation ~ Region

Differences between regions were indicated using the confidence letter display derived from Tukey's *post hoc* test implemented in the package multcomp v.1.4.25[11]. We inspected the normality and variance homogeneity (here and elsewhere) using Q-Q plots and the Levene test, respectively. We visualized the results via a point range plot using the ggplot2 v3.5.1 R package[12].

1.8.2 Soil elemental content analysis

For the soil elemental profile, we created a matrix in which each cell contained the calculated element concentration in one sample. Then, we applied a z-score transformation to each ion across the samples in the matrix. Afterward, we applied a principal component analysis (PCA) using the Euclidean distance between samples and the z-score matrix as input to compare the elemental profiles of soils. Additionally, we estimated the variance explained by porosity, precipitation, region, and the interaction between them by performing a PERMANOVA via the function *adonis2* from the vegan v.2.6-4 R package[13]. The significant variables were visualized via a stacked bar plot using the *ggplot2* v3.5.1 R package.

To visualize the mineral content in each region, the z-score matrix created above was hierarchically clustered (method *ward.D*, function *hclust*), and we visualized the results using a heatmap. The rows in the heatmap were ordered according to the dendrogram order obtained from the clustered ions, and the regions were ordered according to the precipitation gradient (low precipitation to high). The heatmap was coloured based on the z-score.

To explore the relationship between ion concentrations and the precipitation gradient, we performed a correlation test using *cor* function from *stats* v.4.3.1 package in R[14] of the average z-

238 score measurement of each ion against the precipitation gradient. Afterward, we plotted the
239 correlation coefficient for each ion in a barplot.
240
241 *1.8.3 Soil porosity analysis*
242 The soil core images taken using x-ray computed tomography were analyzed using ImageJ
243 software[15]. First, XY slice projection images were filtered using a median function to remove any
244 noise from the raw data then an automatic threshold (Li method) was applied to produce binary
245 images. In the binary images pores and solid particles were represented by black and white pixels,
246 respectively. Afterwards, a region of interest (ROI) was defined in the central part of each
247 projection to remove any potential border effect, cropping to a 600x600 pixel area. From the ROI
248 defined in each image we extracted soil features, including particle area, perimeter, circularity,
249 roundness, solidity, compactness, percentage of pores and pore size using the *measurement*
250 function.
251
252 To remove the variability in the topsoil due to transportation and handling, we used two strategies.
253 Firstly, we plotted the pore average size (mm) and soil porosity (%) for each sample. Then, we
254 excluded from the analysis all projections having a value of soil porosity > 40% and considered
255 the topsoil of those samples as the first projections after the exclusion. The second strategy was
256 applied to samples with an irregular shape (e.g., mountain-like shape) at the topsoil level. We
257 discarded all the projections with an irregular shape until we found projections with a regular
258 distribution of soil layers. For each collection of soils defined in Kansas and Santiago, we created
259 a data frame with the projection number (or slice) and the soil depth (projection number multiplied
260 by the resolution). The soil porosity for each soil type was visualized via a point plot using ggplot2
261 v3.5.1 R package[12].
262

263 To compare the soil elemental profiles against soil porosity across the samples in Kansas and
264 Santiago, first, we applied a z-score transformation of each ion and soil porosity across the
265 samples. Then, we estimated the distance between samples using Euclidean distance.
266 Afterwards, we contrasted the dissimilarity matrices of each pair of datasets (soil elemental profile
267 vs. soil porosity) using the *mantel* test implemented in the vegan v.2.6-4 R package[13]. Finally, we
268 computed the significance of the correlation between matrices by permuting the matrices 10,000
269 times[11].
270
271 *1.8.4 Taxonomic data analysis*
272 To compare the alpha diversity across regions, we calculated the Shannon diversity index using
273 the diversity function from the vegan v.2.6-4 package in R[13]. We used an ANOVA to test the alpha
274 diversity differences between regions. Differences between regions were indicated using the
275 confidence letter display derived from Tukey's *post hoc* test implemented in the R package
276 multcomp v.1.4.25[11].
277
278 The beta diversity analysis (Principal Coordinates Analysis, PCo) was based on Bray-Curtis
279 dissimilarity matrices calculated using the rarefied relative abundance tables. Additionally, we
280 estimated the variance explained by soil porosity, precipitation, regions, and the interaction
281 between them by performing a PERMANOVA via the function adonis2 from the vegan v.2.6-4 R
282 package[13]. The significant variables were visualized via a stacked bar plot using ggplot2 v3.5.1 R
283 package[12].
284
285 The relative abundance of bacterial phyla was depicted using a stacked bar plot using ggplot2
286 v3.5.1 package.
287

288 To compare the microbiome composition against the elemental profiles and soil porosity, we
289 contrasted the dissimilarity matrices of each pair of datasets (soil microbiome vs. soil elemental
290 profile and soil microbiome vs. soil porosity) using the *mantel* test implemented in the vegan v.2.6-
291 4 R package[13]. Briefly, we calculate the microbiome dissimilarity matrix using Bray-Curtis
292 distance. Next, we applied a z-score transformation of each ion and soil porosity across the
293 samples. Afterward, we calculated the soil elemental dissimilarity matrix and soil porosity
294 dissimilarity matrix using Euclidean distance. Finally, we used the *mantel* test to compare and test
295 the significance of the correlation between matrices by permuting the matrices 10,000 times[11].
296
297 *1.8.5 Heatmap and enrichment analysis*
298 We used the R package DESeq2 v.1.40.2[16] to compute the bacterial enrichment profiles in the
299 soils across the precipitation gradient. For each taxID (NCBI's taxonomic identifier assigned to
300 the taxa) in the rarefied table, as well as at the species, and family levels, we estimated difference
301 in abundance compared to the wettest region in Kansas and Santiago using a generalized linear
302 model (GLM) with the following design:
303 Abundance ~ Region
304
305 We extracted the following comparisons from the fitted model CWR vs WEL, HAY vs WEL, KNZ
306 vs WEL, SVR vs WEL, TRI vs WEL for Kansas samples and Achada Leitão vs Pico de Antónia,
307 Colonato vs Pico de Antónia, Mato Correia vs Pico de Antónia, Porto Gouveia vs Pico de Antónia,
308 Nora vs Pico de Antónia, Ribeira Riba vs Pico de Antónia, Serra Malagueta vs Pico de Antónia,
309 Tomba Toiro vs Pico de Antónia for Santiago samples. A taxID, species, or family was considered
310 statistically significant if it had a p-value < 0.05. We visualized the results for the GLM using a
311 heatmap. The rows in the heatmap were ordering according to the dendrogram obtained from the
312 tax ID, species and family analysis. The relative abundance matrix was standardized across the

313 significant tax ID, species, and family by using the z-score and the heatmap was coloured based
314 on this value.
315
316 *1.8.6 Identification of marker taxa associated with precipitation gradients*
317 To identify the corresponding bacterial isolates considered as “biomarker” taxa associated with
318 precipitation gradients, we identified the principal components (PCs) that explain more than 80%
319 of the variance in the data. These identified PCs were used to control the effects of soil elemental
320 profile on the taxa abundances. Then, we fit five models: Poisson, negative binomial, two zero-
321 inflated, and a multiple regression model.
322 For Poisson and negative binomial models, we fitted the following design:
323 Abundance ~ precipitation + offset (porosity) + offset (soil elemental profile: six first PCs for
324 Kansas and seven first PCs for Santiago)
325
326 In parallel, we fitted the zero-inflated models using the following design:
327 Poisson: Abundance ~ precipitation + offset (porosity) | 1 + offset (soil elemental profile) | 1
328 Negative binomial: Abundance ~ precipitation + porosity | porosity + soil elemental profile | soil
329 elemental profile
330
331 Next, to assess the statistical significance, we applied ANOVA to the best-performing model for
332 each taxon according to the Akaike Information Criterion (AIC). Additionally, we applied a multiple
333 regression model with the following design:
334 Abundance ~ precipitation + porosity + soil elemental profile
335
336 Then, we applied ANOVA to find taxIDs with a significant partial regression coefficient for
337 precipitation.
338

339 A taxa ID was considered a “marker” if it had a relative abundance > 0.01 and a prevalence >
340 20%. We visualized the average standardized relative abundance (z-score) of the significant taxa
341 ID in a point plot using ggplot2 v3.5.1 package[12].
342
343 *1.8.7 Enrichment of bacteria biological functions associated with precipitation gradients*
344 To identify biological processes enriched within the microbial communities, the sequence reads
345 were assembled into contigs for each sample using metaFlye from the Flye v2.9 package[17] with
346 default mode. The contigs generated were then grouped and deduplicated using the dedupe.sh
347 tool in BBTools v38.76[18] to eliminate redundancies. Next, we determined the relative abundance
348 of the contigs by mapping the reads from the samples to the contigs using minimap2 v2.17[19], and
349 extracting the relative abundance counts using CoverM v0.6.1[20] in the ‘contig’ mode and
350 reads_per_base coverage method. Taxonomic classification of the contigs was performed using
351 the CAT v8.22 taxonomic classification pipeline[21]. Subsequently, the contigs were filtered to retain
352 only bacteria sequences. DESeq2 v1.40.0[16] was used to determine the contig enrichment profiles
353 by fitting a GLM with the following design:
354 Abundance ~ Legacy + Biological Replicate
355
356 The low-precipitation soil versus the high-precipitation soil contrast was extracted from the fitted
357 model. Contigs meeting the criteria of an FDR-adjusted *p*-value (*q*-value) <0.05 and a $\log_2$-
358 transformed fold change >2 were selected for further analysis. Open reading frames encoded
359 within the contigs were predicted using FragGeneScanRs v1.1.0[22] with default settings. This was
360 followed by functional annotation of the predicted proteins using the eggNOG-mapper v2.1.9[23]
361 pipeline with the eggNOG v5.0.2 database[24] with Diamond v2.0.11[25] and MMseqs2[26].The genes
362 annotated with Gene Ontology (GO) classifications were subsequently extracted, and a GO
363 enrichment analysis focusing on biological processes was conducted. This involved employing
364 adaptive GO clustering in conjunction with Mann–Whitney U testing, using the GO_MWU tool[27],

365 which evaluates the enrichment of each GO category based on whether genes linked to the GO
366 category are significantly clustered at either the top or bottom of a globally ranked gene list. First,
367 genes were ranked based on the signed log_2-transformed fold change values. For each gene,
368 any missing parental terms for specific GO categories were then automatically added. Next, fully
369 redundant categories (those containing identical sets of genes), were collapsed into the more
370 specific GO term. To further streamline the analysis, highly similar categories were grouped using
371 complete linkage clustering based on the fraction of shared genes. We used default settings,
372 where GO categories were merged if the most dissimilar pair within a group, shared more than
373 75% of the genes in the smaller category. The merged group was named after the largest
374 category. Significantly enriched and depleted GO categories were then determined by an adjusted
375 *p*-value of <0.05. This approach simplified the GO hierarchy and addressed multiple testing which
376 improved the statistical power of the GO enrichment analysis. The most prominent enriched and
377 depleted GO categories shared across comparisons were visualized in ggplot2 v3.4.2 and
378 coloured based on the square root transformed delta rank values (enrichment score) of the GO
379 categories. GO enrichment analysis was repeated on the Santiago soil samples using the same
380 methodology, and comparisons between the following geographical regions were extracted: Serra
381 Malagueta vs Pico de Antonia, Tomba Toiro vs Pico de Antonia, Mato Correia vs Pico de Antonia,
382 Colonato vs Pico de Antonia, Ribeira de Sao Domingos (Nora) vs Pico de Antonia, Porto Gouveia
383 vs Pico de Antonia, Ribeira Riba vs Pico de Antonia.
384
385 *1.8.8 Analysis of genetic variation among bacterial lineages along the precipitation gradient*
386 To assess genetic differences between bacteria lineages along the precipitation gradient, we
387 focused on 22 of the identified bacterial markers (1:Pseudomonas ID287, 2:Salmonella ID28901,
388 3:Rubrobacter ID49319, 4:Sorangium ID56, 6:Bradyrhizobium ID722472, 7:Luteitalea
389 ID1855912, 9:Bradyrhizobium ID1355477, 10:Flavisolibacter ID661481, 11:Bradyrhizobium
390 ID858422, 13:Rubrobacter ID2653851, 16:Bradyrhizobium ID1437360, 17:Candidatus Koribacter

391 ID658062, 18:Streptomyces ID1916, 19:Klebsiella ID573, 20:Bradyrhizobium ID1325107,
392 21:Edaphobacter ID2703788, 24:Flavisolibacter ID1492898, 27:Rhizobium ID384,
393 28:Rubrobacter ID2653852, 29:Microvirga ID2807101, 30:Archangium ID83451, 33:Nitrosospira
394 ID1231), as well as 11 additional abundant and prevalent species (5:Bacillus ID1428,
395 8:Bradyrhizobium ID1274631, 12:Priestia ID1404, 14:Lacibacter ID2760713, 15:Bradyrhizobium
396 ID1325100, 22:Candidatus Solibacter ID332163, 23:Burkholderia ID28450, 25:Bacillus ID1396,
397 26:Escherichia ID562, 31:Pseudomonas ID303, 32:Paenibacillus ID1464) across the samples, as
398 proxies for the broader bacterial communities. Together, these taxa were selected for their high
399 genome coverage across samples, enabling more precise allele frequency estimates. Reference
400 genomes for each bacterium was retrieved from the NCBI Genome database, and the filtered
401 shotgun metagenomic reads were aligned to these genomes using minimap2 v2.17-r941[19].
402 Alignments were sorted and indexed with SAMtools v1.18[28], followed by variant calling using
403 BCFtools v1.18[29]. This process identified 32,358,569 sequence variants, which were then filtered
404 using VCFtools v0.1.16[30], to retain only biallelic single nucleotide polymorphisms (SNPs) for
405 further analysis. SNP filtering criteria included a variant quality score >20, a minor allele frequency
406 (MAF) >0.01, less than 50% missing data, and a minimum sequencing depth of 10x in each
407 sample. After filtering, 15,365 high-quality biallelic SNPs were retained. Genetic distances were
408 computed using PLINK v1.90p[31], and reduced to two dimensions through classical
409 multidimensional scaling with the stats v4.3.0 package. PCoA plots were created with ggplot2
410 v3.4.2[12], colored by soil type, precipitation levels and geographical region.
411
412 To identify genes potentially under selection across the precipitation gradient, we conducted a
413 genetic-environment association (GEA) analysis. For this, SNPs were re-filtered using VCFtools
414 v0.1.16[30] with the same criteria, but allowing <70% missing data and a minimum sequencing
415 depth of 3x per sample. After filtering, 885,990 biallelic SNPs were retained. Subsequently, GEA
416 analysis was performed using a general linear model in the rMVP v1.1.1 package[32], with native

417 SNP data imputation, and average precipitation at each sampling location as the environmental
418 variable. The genetic structure in the data was corrected using the first 10 principal components
419 (PCs). Manhattan plots were generated using CMplot v4.5.1[33] and significant associations were
420 identified using the permutation method within the rMVP package.
421

422 **2. Soil drought legacy is resilient to short-term perturbations**

423 *2.1 Experimental design*

424 The six soils collected from across the Kansas precipitation gradient, as described in materials
425 and methods 1.1, were used in this experiment. The conditioning perturbations imposed in these
426 experiments took place over approximately 20 weeks at the University of Kansas from December
427 17th, 2020 to May 5th, 2021. Each of the six input soils remained independent throughout the
428 experiment. Mesocosms consisted of a 1:1 (v/v) mixture of field-collected soil to sterile turface
429 MVP (Turface Athletics, Buffalo Grove, IL). A total of 192 sterile 100 mL pots were filled with the
430 six soils and which were then randomly assigned to one of four conditions in a fully-factorial
431 design: with or without a host, and either water-stressed or well-watered. Half the pots were
432 planted with seedlings of the native prairie grass *T. dactyloides* (Eastern gamagrass, cultivar
433 "Pete"); the rest remained unplanted. Thus, the replication was *N*=8 per soil per treatment. All
434 mesocosms were allowed to adapt to their watering regimes in a growth chamber set to a 12-hour
435 day cycle, 27°C/23°C, and ambient humidity. Well-watered control pots were watered every 1-2
436 days and water-stressed plants were watered every 3-5 days when plants displayed drought
437 symptoms (e.g., leaf curling). All pots were fertilized with 35 mL of 1mL/L concentration of Bonide
438 10-10-10 plant food (Bonide Products LLC, Oriskany, NY) on week 8 and week 12.
439

440 *2.2 Sample collection*

441 To characterize the baseline microbial communities going into the conditioning treatments, we
442 sampled four replicates of each soil/treatment combination one week after beginning the

443 experiment. To collect the samples, the top centimeter of soil was discarded and the remaining
444 soil was homogenized to ensure even sampling of the top, middle, and bottom of the pot. Two
445 grams of this homogenized soil were placed in a 15mL tube, flash-frozen in liquid nitrogen, and
446 stored at -80°C for microbial DNA and RNA extraction. To characterize the effects of the four
447 treatments on the microbial communities, we sampled all remaining replicates at the end of the
448 20-week conditioning phase. Soil samples were collected as described for the baseline
449 communities, but an additional 6 g of homogenized soil was preserved at 4°C in 50 mL conical
450 tubes for use as inocula in a downstream experiment. Additionally, for the planted pots, we
451 measured *T. dactyloides* shoot height before uprooting the plants. We collected samples of a
452 crown root from each plant (3 cm long each, beginning 2 cm from the base of the plant) and stored
453 them in 50% ethanol at 4°C for downstream laser ablation tomography analysis. The remaining
454 roots and shoots were dried in an oven at 225°C for 12 hours and then weighed separately.
455
456 *2.3 Changes in bacterial community structure associated with drought and well-watered*
457 *conditioning with and without a host.*
458 *2.3.1 DNA extraction*
459 Total DNA was extracted from baseline and post-conditioning soil sub-samples using the DNA
460 Set for NucleoBond RNA Soil Kit (Macherey-Nagel, Düren, Germany) according to the
461 manufacturer's instructions.
462
463 *2.3.2 Library preparation and sequencing*
464 DNA sequencing libraries were prepared using the Rapid PCR Barcoding Kit (SQK-RPB004) from
465 Oxford Nanopore Technologies, UK, and sequenced on a FLO-MIN106 R9.4.1 flow cell (Oxford
466 Nanopore Technologies, UK) in a MinION (Oxford Nanopore Technologies, UK), with a MinIT
467 (Oxford Nanopore Technologies, UK) using MinKNOW v2.1.12[34] (Oxford Nanopore
468 Technologies, UK) as described in materials and methods section 1.6.

469

470 *2.3.3 Sequence processing*

471 Raw sequence data were demultiplexed and primer and barcode sequences were trimmed using
472 qcat v1.1.0 (Oxford Nanopore Technologies Ltd., UK). Reads with ambiguous barcode
473 assignments were excluded from further analysis. The reads were filtered with NanoFilt v2.8.0[7]
474 to discard low-quality sequences (Q-score <9) and sequences <100 bp. We used the Kraken
475 v2.1.2 pipeline[8] for classifying the whole metagenome shotgun sequencing reads. The reads were
476 classified using the Kraken 2 archaea, bacteria, viral, plasmid, human, UniVec_Core, protozoa
477 and fungi reference database (k2_pluspf_20220607). To estimate relative abundances, the
478 Bracken v2.7 pipeline[9] was applied to the classification results. Subsequently, Pavian v1.0[10]
479 facilitated the extraction of abundance and taxonomic tables. Functions in phyloseq v1.44.0[35] with
480 microbiome v1.22.0 and microbiomeutilities v1.0.17[36] were used to filter the dataset and remove
481 samples with low read depth (<1000 reads), remove unidentified taxa and singletons, transform
482 abundance values using rarefaction, subset and merge sample and taxonomic groups and
483 perform other data frame manipulations.

484

485 *2.4 Plant biomass*

486 Root and shoots were detached, dried in an oven at 225˚C for 12 hours, and then weighed.

487

488 *2.5 Root Laser Ablation Tomography (LAT) analysis*

489 We collected samples of a crown root from each plant (3 cm long each, beginning 2 cm from the
490 base of the plant) and stored them in 50% ethanol at 4°C. The samples were shipped to the
491 University of Nottingham for downstream LAT analysis. Briefly, root segments were dehydrated
492 in 100% methanol for 48 hours, transferred to 100% ethanol for 48 hours, then dried with an
493 automated critical point dryer (CPD, Leica EM CPD 300, Leica Microsystem). Root anatomical
494 images were acquired using a laser ablation tomograph (LATScan, Lasers for Innovative

495 Solutions LLC). This utilises a combination of precise positioning stages with a guided pulsed UV
496 (355 nm) laser, to thermally vaporise thin sections of the root, and then to illuminate the exposed
497 surface. The tomograph was retrofitted with a microscopic imaging system, using a machine
498 vision camera unit (Model Grasshopper3, FLIR) and infinity-corrected long working distance
499 magnifying objectives (Mitutoyo (UK) Ltd.)
500
501 *2.6 Changes in gamagrass morphological features under drought and well-water conditioning*
502 To identify morphological features in gamagrass that changed with the conditioning (drought and
503 well-watered) treatments, we used Image J to quantify the average area aerenchyma, number
504 aerenchyma, number metaxylem, cortical cell layers, total area metaxylem, average area
505 metaxylem, stele min. diameter, stele max. diameter, stele area, stele perimeter, total area
506 aerenchyma, adjusted cortex area, root min. diameter, cortex min. diameter, root max. diameter,
507 cortex max. diameter, total perimeter, cortex perimeter, root total area, and cortex area.
508 Additionally, we quantified the root-shoot ratio, number of leaves, number of green leaves, root
509 mass, shoot mass, and shoot height.
510
511 *2.7 Metatranscriptome analysis*
512 *2.7.1 RNA isolation*
513 Total RNA was extracted from baseline and post-conditioning soil sub-samples with the
514 NucleoBond RNA Soil Kit (Macherey-Nagel, Düren, Germany) using the manufacturer's
515 instructions. Isolated RNA was treated with Turbo DNA-free (Applied Biosystems, Waltham, MA,
516 USA) to remove contaminating DNA, following the manufacturer's instructions.
517
518 *2.7.2 Library preparation and sequencing*
519 RNA libraries were prepared using 1 µg of total RNA according to established protocols with
520 modifications. Briefly, poly(A)-tail-containing RNA was removed from the RNA samples using

521 Sera-mag oligo(dT) magnetic beads (GE Healthcare Life Sciences, Marlborough, MA, USA) and
522 then the samples were subjected to ribodepletion with the NEBNext rRNA Depletion Kit (New
523 England Biolabs, MA, USA), following the manufacturers' instructions. The purified RNA was
524 resuspended in a fragmentation mix consisting of 6.25 µL Milli-Q water, 5 µL 5x First strand buffer,
525 and 1.25 µL random primers (3 µg/µL) and fragmented at 94°C for 6 min. First-strand cDNA
526 synthesis was performed using a mixture of 0.8 µL reverse transcriptase, 2 µL 100 mM DTT, 0.4
527 µL 25 mM dNTP, 0.5 µL RNAseOUT (40U/µL), 10 µL RNA, and 6.3 µL Milli-Q water. The reactions
528 were incubated at 25°C for 10 min, 42°C for 50 min, and 70°C for 15 min. Second-strand cDNA
529 synthesis was performed by adding a master mix of 18.4 µL Milli-Q water, 5 µL 10X second strand
530 buffer, 1.2 µL 25 mM dNTP, 0.4 µL RNAse H (5U/µL), and 5 µL DNA Pol I (10U/µL) to the sample,
531 followed by incubation at 16°C for 1 h. The samples were then purified using Agencourt AMPure
532 XP beads. Subsequently, the libraries were end-repaired with a mixture of 30 µL sample, 2.5 µL
533 of 3 U/µL T4 DNA polymerase, 0.5 µL of 5 U/µL Klenow DNA polymerase, 2.5 µL of 10 U/µL T4
534 PNK, 5 µL of 10X T4 DNA ligase buffer with 10 mM ATP, 0.8 µL of 25 mM dNTP mix, and 8.7 µL
535 Milli-Q water, incubated at 20°C for 30 min, and purified again using Agencourt AMPure XP
536 beads. Following this, the RNA libraries were adenylated in a mix containing 34 µL of the end-
537 repaired sample, 3 µL of 5 U/µL Klenow exo-, 5 µL of 10X Enzymatics Blue Buffer, 1 µL of 10 mM
538 dATP, and 9 µL of Milli-Q water. The mixture was incubated at 37°C for 30 min, followed by 70°C
539 for 5 min, and then purified using Agencourt AMPure XP beads. Individual samples were indexed
540 through ligation using a mix of 10.25 µL sample, 1 µL of 600 U/µL T4 DNA ligase, 12.5 µL of 2x
541 Rapid Ligation Buffer, and 1.25 µL of 2.5 µM indexing adapter from the KAPA Dual-Indexed
542 Adapter Kit (Kapa Biosystems, MA, USA). The samples were incubated at 25°C for 15 min,
543 followed by the addition of 5 µL of 0.5 M EDTA pH 8. The libraries were purified twice with
544 Agencourt AMPure XP beads. The libraries were enriched in a reaction containing 20 µL sample,
545 25 µL of 2X KAPA HiFi HS Mix (Kapa Biosystems, MA, USA), 2.5 µL of 5 µM I5 primer, and 2.5
546 µL of 5 µM I7 primer. The reactions were initially heated to 98°C for 45 seconds, followed by 14

547 cycles of 98°C for 15 seconds, 60°C for 30 seconds, and 72°C for 30 seconds, with a final
548 extension at 72°C for 1 minute. The resulting RNA libraries were purified using Agencourt AMPure
549 XP beads, quantified on a Qubit 4 Fluorometer (Thermo Fisher Scientific, USA), and the library
550 size was assessed using High Sensitivity D1000 ScreenTape on the Agilent 4200 TapeStation
551 (Agilent Technologies, Santa Clara, CA). Equimolar quantities of individual barcoded RNA
552 libraries were pooled in a randomized manner and shipped on dry ice to Beijing Genomics Institute
553 (BGI, Shenzhen, China). Each library pool was sequenced on an MGI Tech MGISEQ-2000
554 sequencing platform to generate a minimum of 10 million 100 bp paired-end reads per sample.
555

556 *2.7.3 Taxonomic classification of transcripts*

557 Cutadapt v4.6[37] was used to remove primer and barcode sequences and low-quality sequences
558 from the paired-end reads of the sequenced RNA libraries. To identify taxa with enriched gene
559 expression activity, the reads were classified using the Kraken v2.1.2 pipeline[8] with the archaea,
560 bacteria, viral, plasmid, human, UniVec_Core, protozoa and fungi reference database
561 (k2_pluspf_20220607), and the Bracken v2.7 pipeline[9] was applied to the classification results to
562 estimate the relative abundances. The counts table was generated from Pavian v1.0[10]. Data
563 filtering and statistical analysis were then performed as before using phyloseq v1.44.0[35] with
564 microbiome v1.22.0[38] and microbiomeutilities v1.0.17[36].
565

566 *2.8 Data Analysis*

567 *2.8.1 Changes in bacterial community structure associated with drought and well-watered*
568 *conditioning with and without a host*

569 To assess the alpha diversity across the samples, we calculated the Shannon Diversity Index
570 using phyloseq v1.44.0[35]. We used ANOVA to test for significant differences in Shannon Diversity
571 indices between groups and means were separated using Tukey's honestly significant difference
572 (HSD) test from the agricolae v1.3.5 R package[39]. For beta diversity, Bray-Curtis dissimilarity

573 matrices were calculated using phyloseq v1.44.0 and the variance explained by legacy,
574 conditioning, and host were estimated by performing permutational multivariate analysis of
575 variance (PERMANOVA) using the adonis2 function in vegan v2.6.4 R package[13]. Constrained
576 ordination of beta-diversity was plotted using canonical analysis of principal coordinates (CAP)
577 based on Bray-Curtis dissimilarity matrices calculated with vegan v2.6.4. We visualized
578 differences with the CAP analysis, using the following models:

579 ~ legacy + Condition (conditioning + host + biological replicate)

580 ~ conditioning + Condition (legacy + host + biological replicate)

581 ~ host + Condition (legacy + conditioning + biological replicate)

582

583 The relative abundance of taxa was plotted as a stacked bar representation using phyloseq
584 v1.44.0. The tax_glom function in phyloseq v1.44.0 was used to agglomerate taxa, and the
585 aggregate_rare function in microbiome v1.22.0 was used to aggregate rare groups. We used
586 DESeq2 v1.40.0[16] to calculate the enrichment profiles by fitting a generalized linear model (GLM)
587 with the following design:

588 Abundance ~ Legacy + Conditioning + Biological Replicate

589

590 We extracted the following comparisons from the fitted model: wet soil legacy with watered
591 conditioning vs wet soil legacy (baseline), wet soil legacy with drought conditioning vs wet soil
592 legacy (baseline), dry soil legacy (baseline) vs wet soil legacy (baseline), dry soil legacy with
593 watered conditioning vs wet soil legacy (baseline), and dry soil legacy with drought conditioning
594 vs wet soil legacy (baseline). Taxa were considered significant if they had an FDR-adjusted *p*-
595 value (*q*-value) <0.05. The results of the GLM analysis were rendered in heatmaps, coloured
596 based on the $\log_2$-transformed fold change output by the GLM. Significant differences between
597 comparisons with a *q*-value <0.05 with $\log_2$-transformed fold change >2 were highlighted with
598 black squares.

599

600 Relative abundances of the taxonomic markers were extracted, and an ANOVA was performed
601 to assess significant differences between treatment groups. Tukey's Honest Significant Difference
602 (HSD) test, implemented using the agricolae v1.3.5 R package[39], was used for post-hoc pairwise
603 comparisons. To further explore the effects of watering and drought treatments, with and without
604 a host, on the relative abundances of the taxonomic markers, we subset the data and applied a
605 generalized linear model (GLM) using DESeq2 v1.40.0[16]. The model was structured as follows:

606 Abundance ~ Legacy + Conditioning + Host + Biological Replicate

607

608 We then extracted the following comparisons from the fitted model for each soil legacy: water
609 conditioning vs baseline, drought conditioning vs baseline, water conditioning with host vs
610 baseline, drought conditioning with host vs baseline. Markers were considered significant if the
611 FDR-adjusted p-value (q-value) was < 0.05. Results from the GLM analysis were visualized in a
612 heatmap, with colours representing log2-transformed fold changes. Comparisons showing
613 significant differences (q-value <0.05 and log2-transformed fold change >2) were highlighted with
614 black squares.

615

616 *2.8.2 Gene Ontology (GO) term enrichment analysis*

617 To identify enriched biological processes within the microbial communities, the sequence reads
618 from individual samples were assembled into contigs, their relative abundance counts
619 determined, and were subjected to taxonomic classification as described before. DESeq2
620 v1.40.0[16] was utilized to determine the bacterial contig enrichment profiles by fitting a generalized
621 linear model (GLM) with the following design:

622 Abundance ~ Legacy + Conditioning + Biological Replica

623

624 We extracted the following comparisons from the fitted model: wet soil legacy with watered
625 conditioning vs wet soil legacy (baseline), wet soil legacy with drought conditioning vs wet soil
626 legacy (baseline), dry soil legacy (baseline) vs wet soil legacy (baseline), dry soil legacy with
627 watered conditioning vs wet soil legacy (baseline), and dry soil legacy with drought conditioning
628 vs wet soil legacy (baseline). Contigs meeting the criteria of an FDR-adjusted *p*-value (*q*-value) <
629 0.05 and a $\log_2$-transformed fold change > 2 were selected. Open reading frames were predicted
630 and functionally annotated, and genes with GO classifications were subjected to GO enrichment
631 analysis with the GO_MWU tool[27].
632
633 *2.8.3 Changes in gamagrass morphological features under drought and well-water condition*
634 For each root feature identified, we used ANOVA to test for significant differences between groups
635 and means were separated using Tukey's honestly significant difference (HSD) test from the
636 agricolae v1.3.5 R package[39] Subsequently, the feature values were normalized using the rescale
637 function from the scales v1.2.1 R package. The mean normalized feature values were then
638 visually represented on a heatmap using ggplot2 v3.4.2. Subsequently, Pearson correlation
639 coefficients between these features and corresponding *p*-values were computed using the rcorr
640 function from the Hmisc v5.0.1 package[40]. The results of the correlation analysis were graphically
641 presented using ggplot2 v3.4.2, where the colour of the plots reflected the correlation coefficient
642 values. Significant correlations (p <0.05) were emphasized with black squares on the plots.
643 Furthermore, the coefficient of variation for the feature values was calculated and depicted using
644 ggplot2 v3.4.2. The three plots were integrated based on the hierarchical clustering of the Pearson
645 correlation coefficients of the features. The clustering employed the ward.D2 method within the
646 hclust function in R, utilizing Euclidean distances calculated using the dist function.
647

648 *2.8.4 Metatranscriptome sequence analysis*

649 To assess transcriptional differences in the activity of the bacterial community, Bray-Curtis
650 dissimilarity matrices were calculated. The variance explained by legacy, conditioning, and host
651 was estimated using permutational multivariate analysis of variance (PERMANOVA) with the
652 adonis2 function from the vegan v2.6.4 R package[13]. Beta-diversity patterns were visualized
653 through constrained ordination using canonical analysis of principal coordinates (CAP). We
654 applied CAP analysis to visualize differences using the following models:

655 ~ Legacy + Condition (conditioning + host + biological replicate)

656 ~ Conditioning + Condition (legacy + host + biological replicate)

657 ~ Host + Condition (legacy + conditioning + biological replicate)

658

659 Transcriptional activity among taxa was displayed as a stacked bar plot using phyloseq v1.44.0.
660 We employed DESeq2 v1.40.0[16] to calculate enrichment profiles by fitting a generalized linear
661 model (GLM) with the following design:

662 Abundance ~ Legacy + Conditioning + Biological Replicate

663

664 From the fitted model, we extracted the following comparisons: wet soil legacy with watered
665 conditioning vs wet soil legacy (baseline), wet soil legacy with drought conditioning vs wet soil
666 legacy (baseline), dry soil legacy (baseline) vs wet soil legacy (baseline), dry soil legacy with
667 watered conditioning vs wet soil legacy (baseline), and dry soil legacy with drought conditioning
668 vs wet soil legacy (baseline). Taxa were considered differentially abundant if the FDR-adjusted
669 *p*-value (*q*-value) was <0.05. Results from the GLM analysis were visualized in heatmaps, where
670 colours represent log2-transformed fold changes. Comparisons showing significant differences
671 (*q*-value <0.05 and log2-transformed fold change >2) were highlighted with black squares.

672

673 Additionally, high-quality filtered reads of the transcriptome were de novo assembled into a
674 reference metatranscriptome using Trinity v2.15.1[41] with default parameters. Open reading
675 frames in transcripts were predicted with TransDecoder v5.7.1 with default settings. Functional
676 annotation of the predicted proteins was performed using the eggNOG-mapper v2.1.9[23] pipeline,
677 utilising the eggNOG v5.0.2 database[24] with Diamond v2.0.11[25] and MMseqs2[26]. The taxonomic
678 classification of transcripts was conducted using the CAT v8.22 taxonomic classification
679 pipeline[21]. Sequence reads were further filtered using SortMeRNA v4.3.6[42] with the
680 smr_v4.3_default_db.fasta database to remove residual amplified rRNA sequences. Transcript
681 quantification analysis was performed using Salmon v1.10.0[43] in the mapping-based mode with
682 the de novo assembled reference metatranscriptome. Subsequently, the transcript-level
683 abundance estimates from salmon were extracted as transcripts per million (TPM) for the
684 identified transcripts using the R package tximport v1.28.0[44]. DESeq2 v1.40.0[16] was utilized to
685 determine the bacterial transcript enrichment profiles by fitting a generalised linear model (GLM)
686 as described before. Genes meeting the criteria of an FDR-adjusted *p*-value (*q*-value) <0.05, a
687 $\log_2$-transformed fold change >2, and had GO classifications, were subjected to GO enrichment
688 analysis with the GO_MWU tool[27].
689
690 *2.8.5 Analysis of genetic variation among bacterial lineages*
691 Filtered shotgun metagenomic reads were aligned to the reference genomes of 33 selected taxa,
692 including 22 identified bacterial markers and 11 additional abundant and prevalent species (see
693 Supplementary Materials and Methods 1.8.8), using Minimap2 v2.17-r941[19]. The resulting
694 alignments were sorted and indexed with SAMtools v1.18[28]. Variant calling was performed using
695 BCFtools v1.18[29], and variants were filtered with VCFtools v0.1.16[30]. Filtering criteria included a
696 variant quality score >20, a minor allele frequency (MAF) >0.01, <50% missing data, and a
697 minimum sequencing depth of 10x in each sample. After filtering, a total of 8,293 high-quality
698 biallelic SNPs were available for further analysis. To assess genetic variation within and between

699 groups, we analysed molecular variance (AMOVA) using poppr v2.9.6[45]. The significance of the
700 AMOVA results was determined with a permutation test using the randtest function in ade4
701 v1.7.22[46]. To determine the extent of genetic differentiation between groups, we calculated the
702 Fixation index (FST) values using the hierfstat v0.5.11[47] package. Principal coordinates analysis
703 (PCoA) plots were generated as previously described in Supplementary Materials and Methods
704 1.8.8, and coloured to reflect soil legacy, drought/ well-watered and host/ no-host treatments. To
705 identify genes associated with soil legacy, we conducted a genome-wide association study
706 (GWAS). SNPs were re-filtered using VCFtools v0.1.16[30], applying the same criteria but allowing
707 for up to 70% missing data and a minimum sequencing depth of 3x in each sample. GWAS was
708 conducted using a general linear model in the rMVP v1.1.1 package[32]. Associations were
709 identified by comparing bacterial lineages from dry legacy soil to those from wet legacy soil.
710 Genetic structure was accounted for by incorporating the first 10 principal components. Significant
711 associations were identified through permutation testing within the rMVP package, and Manhattan
712 plots were generated using CMplot v4.5.1[33].
713
714 **3. Effects of soil microbiome legacy on plant tolerance to drought**
715 *3.1 Experimental design and non-destructive phenotypic measurements*
716 At the end of the "Conditioning Phase", homogenized soil was collected from each pot by
717 discarding the top one centimeter of soil, mixing the soil in the pot with a clean plastic spatula,
718 and placing six grams in a sterile 50 mL conical tube. For rhizosphere samples (i.e., planted pots),
719 plants were gently pulled from the pots and the soil particles adhered to and within the root bundle
720 were shaken into a sterile 50 mL conical tube. The rhizosphere particles were homogenized with
721 a clean plastic spatula and particles were poured out of the tube until six grams remained. Soil
722 and rhizosphere samples were stored at 4˚C overnight.
723
724 Soil microbes were extracted from the 6 g soil or rhizosphere sample the following day by adding

725 25 mL of autoclaved 1X PBS with 0.0001% Tween-89 to the 50 mL tube containing the sample.
726 Tubes were vigorously shaken to mix and break up large soil aggregates. Large particles were
727 allowed to settle to the bottom of the tube; the supernatant was then filtered through autoclaved
728 Miracloth (Sigma-Aldrich) into a new sterile 50 mL conical tube. Filtered samples were then
729 centrifuged at 3600g for 25 min at 4˚C. The supernatant was discarded, and the microbial pellet
730 was resuspended in 6 mL of 1X PBS buffer using a vortex. The resuspended pellets were stored
731 at 4˚C until used for inoculations a few hours later.
732
733 The microbial extract from each of the 192 Conditioning Phase pots (as well as the 24
734 uninoculated control pots) was used to inoculate 4 pots for the "Test Phase": one pot per
735 combination of watering treatment (droughted or control) and host species (maize or gamagrass).
736 To create the inoculum, the resuspended pellet was inverted three times to mix and 1 mL of the
737 sample was added to 100 mL of sterile 0.5X MS liquid medium, for a microbial titer equivalent to
738 0.01 g soil per mL. The "mock inoculation" controls were created by substituting 1 mL of sterile
739 PBS for the resuspended microbial pellet. Finally, 25 mL of this suspension was inoculated onto
740 the soil surface of each Test Phase pot. Thus, each microbial community extracted from one of
741 the 192 conditioning phase pots was used to inoculate four plants in the Test Phase. To maintain
742 statistical independence of the experimental replicates from the conditioning phase, no pooling
743 was performed.
744
745 Before inoculation, pots were planted with 3-4-day old gamagrass or maize germinants.
746 Gamagrass seeds were soaked in 3% hydrogen peroxide for 24 hours and germinated in seed
747 trays filled with sterile clay. Maize seeds were soaked in 70% ethanol for 3 minutes, then soaked
748 in 5% NaClO on a rotator for 2 min, and then rinsed with sterile DI water three times. Treated
749 maize seeds were germinated on sterile damp paper towels inside sealed plastic bags.
750

751 Pots were fully randomized and, prior to inoculation, were filled with a homogenized 5:1 (w/w)
752 mixture of all-purpose sand (TechMix All-purpose 110241) and calcined clay (Pro's choice rapid
753 dry) that had been sterilized by autoclaving on a one-hour liquid cycle. Pots were autoclaved on
754 a 30 min liquid cycle and then filled with the sand:clay mixture, leaving one inch of room at the
755 top of the pot. To help keep the mixture from falling out of the drain holes in the bottom of the
756 pots, a sterile filter paper was shaped into a cone, pushed to the bottom of the pot, and a sterile
757 marble was used to weigh the paper down. This effectively blocked the substrate, but still allowed
758 water to exit the drainage holes. Plants were grown under 12-h days, 27°C/23°C (day/night), and
759 ambient humidity, with the light setting set to 1, which is equivalent to 312 μmol/m^2s. Three-day
760 old gamagrass and maize leaf photosynthetic rates and gas exchange were measured using the
761 LI-6800 (LI-COR, Lincoln, NE, USA), across 3 days for each host. The LI-6800 aperture was 2
762 cm, warmup tests were performed at the start of each measurement session, the Fluorometry
763 was set to “on”, the APD_Leaf to set to 1.5 kpa. The newest fully emerged leaf, which was most
764 commonly the 4th leaf, on each plant was clamped in the chamber and allowed to stabilize until
765 all measurements were stable for at least 30 secs before the measurements were recorded, which
766 took approximately five minutes per leaf. Similarly, the leaf chlorophyll content was also measured
767 using the MC-100 Chlorophyll Concentration Meter (apogee instruments, Logan, UT, USA).
768 Maize plants were sampled four weeks after planting and gamagrass was sampled five
769 weeks after planting. In total, we measured 286 *T. dactyloides* plants (192 droughted, 94 well-
770 watered) and 268 maize plants (182 droughted, 86 well-watered).
771
772 At the end of the Test Phase, uprooted plants were gently shaken to remove the soil attached to
773 roots, prior to the collection of phenotypic, transcriptomic, and microbiome data as described
774 below. One crown root was cut off with a ceramic blade and placed in a 1.7 mL tube on dry ice
775 for downstream DNA extraction for *16S rRNA* gene sequencing. Another crown root (0.15 - 0.2
776 g) was cut off with a ceramic blade, placed in a 1.7 mL tube, and flash frozen in liquid nitrogen for

777 downstream RNA extraction. In between plants, the ceramic blade, plastic tweezers, plastic
778 cutting board, and gloves were cleaned with 30% bleach. All samples were held on dry ice and
779 then transferred to a -80˚C freezer for storage. Next, the root and shoot were separated with a
780 ceramic blade. Three cm of crown root beginning ~2 cm from the base of the shoot was cut with
781 a ceramic blade and submerged in 50% EtOH for LAT analysis. The rest of the root system was
782 submerged in 70% EtOH in a 50 mL centrifuge tube for downstream root architecture scanning.
783 Shoot height and number of leaves were recorded. Shoots were placed in individual paper bags,
784 dried in an oven at 225˚C for 12 hours, and the shoot dry weight was recorded.
785
786 *3.2 Root system architecture and root biomass analyses*
787 A Perfection V600 flatbed scanner (Epson, Nagano, Japan) was used to scan intact maize and
788 gamagrass root systems collected from Test Phase plants. The scanner was set to professional
789 mode, reflective, document, black and white mode, 600 dpi, with a threshold of 55. A clear plastic
790 tray filled with clean water was placed on the scanning bed. Each root system was placed in the
791 tray with water and the tangled roots were gently pulled apart using plastic tweezers until they
792 were no longer overlapping. A small amount of fine fibrous roots that fell off during this process
793 were pushed to the corner of the tray and not included in the root cluster scan. The scanned root
794 images were then analyzed using Rhizovision Explorer software[48] in “whole root” mode and
795 converted to 600 dpi. The region of interest tool was used to outline the main root bundle before
796 pressing play to collect feature measurements. Finally, after collection of root system architecture
797 data, the roots were dried in an oven at 225˚C for 12 hours and then weighed.
798
799 *3.3 Root Laser Ablation Tomography (LAT) analysis*
800 We collected one crown root from each plant (3 cm long each, beginning 2 cm from the base of
801 the plant) and stored them in 50% ethanol at 4°C. These samples were shipped to the University
802 of Nottingham for LAT analysis. Briefly, root segments were dried with an automated critical point

803 dryer (CPD, Leica EM CPD 300, Leica Microsystem). Then, samples were ablated by a laser
804 beam (Avia 7000, 355 nm pulsed laser) to vaporize the root tissue at the camera focal plane
805 ahead of an imaging stage and cross-sectional images were taken using a Canon T3i camera
806 with a 5×micro-lens (MP-E 65 mm) on the laser-illuminated surface. ImageJ software[15] was used
807 to measure root anatomical traits captured in the high-quality LAT images.
808
809 *3.4 Leaf ionome and shoot biomass analyses*
810 The elemental profiles of the shoots were measured using Inductively Coupled Plasma Mass
811 Spectrometry (ICP-MS). The shoot biomass from all uprooted plants was dried in an oven at
812 225°C for 12 h and then weighed. The dried biomass samples were cut into small pieces using a
813 clean ceramic scalpel and placed in 5 mL Eppendorf tubes with 3 zirconium oxide beads. Shoots
814 were pulverized using a Tissue Lyzer II (Qiagen) using 2 cycles of 60 seconds at the frequency
815 of 30 s^{-1}. Next, 5-10 mg of pulverized shoot samples were weighted on a Mettler five-decimal
816 analytical scale, and 1-3 mL (depending on the sample dry weight) of concentrated trace metal
817 grade nitric acid Primar Plus (Fisher Chemicals) was added to each tube. Prior to the digestion,
818 20 µg/L of Indium (In) was added to the nitric acid as an internal standard to assess putative errors
819 in dilution or variations in sample introduction and plasma stability in the ICP-MS instrument. The
820 samples were then digested in DigiPREP MS dry block heaters (SCP Science; QMX Laboratories)
821 for 4 h at 115°C. After cooling down, the digested samples were diluted to 10-30 mL (depending
822 on the volume of the nitric acid added) with 18.2 MΩcm Milli-Q Direct water. The elemental
823 analysis was performed using an ICP-MS, PerkinElmer NexION 2000 equipped with Elemental
824 Scientific Inc 4DXX FAST Dual Rinse autosampler, FAST valve and peristaltic pump. The
825 instrument was fitted with a PFA-ST3 MicroFlow nebulizer, baffled cyclonic C3 high sensitivity
826 glass spray chamber cooled to 2 ºC with PC3X Peltier heated/cooled inlet system, 2.0 mm i.d.
827 quartz injector torch and a set of nickel cones. Twenty-four elements were monitored including
828 the following stable isotopes: ^{7}Li, ^{11}B, ^{23}Na, ^{24}Mg, ^{31}P, ^{34}S, ^{39}K, ^{43}Ca, ^{48}Ti, ^{52}Cr, ^{55}Mn, ^{56}Fe, ^{59}Co,

829 ^{60}Ni, ^{63}Cu, ^{66}Zn, ^{75}As, ^{82}Se, ^{85}Rb, ^{88}Sr, ^{98}Mo, ^{111}Cd, ^{208}Pb and ^{115}In. Helium was used as a collision
830 gas in Kinetic Energy Discrimination mode (KED) at a flow rate of 4.5 mL/min while measuring
831 Na, Mg, P, S, K, Ca, Ti, Cr, Mn, Fe, Ni, Cu, Zn, As, Se and Pb to exclude possible polyatomic
832 interferences.
833
834 The remaining elements were measured in the standard mode. The instrument Syngistix™
835 software for ICP-MS v.2.3 (Perkin Elmer) automatically corrected any isobaric interferences. The
836 ICP-MS measurements were performed in peak hopping scan mode with dwell times ranging
837 from 25 to 50 ms depending on the element, 20 sweeps per reading and three replicates. The
838 ICP-MS conditions were adjusted to an RF power of 1600 Watts and an auxiliary gas flow rate of
839 1.20 L/min. Torch alignment, nebuliser gas flow and quadrupole ion deflector (QID) voltages (in
840 standard and KED mode) were optimized before analysis for highest intensities and lowest
841 interferences (oxides and doubly charged ions levels lower than 2.5%) with NexION Setup
842 Solution containing 1 µg/L of Be, Ce, Fe, In, Li, Mg, Pb and U in 1% nitric acid using a standard
843 built-in software procedure. To correct for variation between and within ICP-MS analysis runs,
844 liquid reference material was prepared using pooled digested samples and run after the
845 instrument calibration and then after every nine samples in all ICP-MS sample sets. Equipment
846 calibration was performed at the beginning of each analytical run using seven multi-element
847 calibration standards (containing 2 µg/L In internal standard) prepared by diluting 1000 mg/L
848 single-element standards solutions (Inorganic Ventures; Essex Scientific Laboratory Supplies Ltd)
849 with 10% nitric acid. As a calibration blank, 10% nitric acid containing 2 µg/L In internal standard
850 was used, and it was run throughout the analysis. Sample concentrations were calculated using
851 the external calibration method within the instrument software. Further data processing, including
852 the calculation of final element concentrations, was performed in Microsoft Excel.
853
854 *3.5 Crown root transcriptomics*

855 *3.5.1 RNA extraction and sequencing*

856 For RNA extractions and sequencing, flash-frozen crown roots were freeze-dried for 48 hours and
857 finely ground with pellet pestles. The RNA extraction protocol was carried out according to the
858 NucleoSpin RNA Plant kit (Macherey-Nagel, Düren, Germany).

859

860 For the 132 maize samples, remnant DNA was removed from purified RNA using the DNA-Free
861 kit (Invitrogen, Carlsbad, CA, USA). RNA-seq libraries were prepared using the QuantSeq 3'
862 mRNA-Seq V2 kit with unique dual sequences and the unique molecular identifier (UMI) module
863 (Lexogen, Vienna, Austria) following the manufacturer's recommendations. Libraries were pooled
864 at equimolar concentrations and then sequenced (2x150bp, but reverse reads were not used) on
865 a NovaSeq S4 flow cell (Illumina, San Diego, CA, USA) along with a 25% PhiX spike-in. Maize
866 RNA-seq library preparations and sequencing were performed by the RTSF Genomics Core at
867 Michigan State University. For the 132 *T. dactyloides* samples, RNA-seq libraries were prepared
868 using the NEBNext Ultra II Directional Library Kit with the oligo-dT magnetic isolation module
869 (New England Biolabs, Ipswich, MA, USA) and sequenced on the Illumina NovaSeq 6000
870 platform at the Genomic Sciences Laboratory at North Carolina State University to generate a
871 minimum of 40M read pairs (2x150bp) per sample.

872

873 *3.5.2 Sequence processing*

874 For the maize sequence reads, UMIs were removed from all sequences and added to the read
875 headers using UMI-tools[49]. Next, cutadapt version 4.2[37] was used to remove the first four bases
876 of each read, remove poly-A tails (if present), remove spurious poly-G runs using the --nextseq-
877 trim=10 parameter, and remove adapter sequences. Reads that were <10 bp long or that aligned
878 to maize rRNA gene sequences were removed; the remaining reads were aligned to the maize
879 reference genome B73 RefGen_v5[50] using HISAT2 version 2.2.1[51]. Aligned reads were converted
880 to BAM format, sorted, and indexed using samtools version 1.9[28]. We then used UMI-tools[49] to

881 de-duplicate reads that both shared a UMI and had identical mapping coordinates. Finally, we
882 used the FeatureCounts function of the subread package version 2.0.5[52] with the maize genome
883 annotation version Zm00001eb.1 and parameters -O --fraction -M --primary -g ID -t gene to
884 generate a table of gene expression estimates.
885
886 For the *T. dactyloides* sequence reads, we first used cutadapt to remove NEBNext adapter
887 sequences, poly-A tails, spurious poly-G runs, and low-quality tails using the -q 20,20 parameter
888 and other default parameters. The cleaned reads were aligned to the *T. dactyloides* reference
889 genome (Td-KS_B6_1-REFERENCE-PanAnd-2.0a[28] using HISAT2. The alignments were name-
890 sorted so that mate-pairs could be fixed using the fixmate function of samtools[28], and then re-
891 sorted based on coordinates, de-duplicated, and converted to indexed BAM files using the same
892 software. Finally, a table of transcript expression estimates was generated using the
893 FeatureCounts function of the subread package with parameters -p -O --fraction -M --primary -g
894 ID -t gene and the *T. dactyloides* genome annotation version Td-KS_B6_1-REFERENCE-
895 PanAnd-2.0a_Td00002ba.2.
896
897 *3.5.3 Statistical analyses*
898 Because the maize and *T. dactyloides* RNA-seq datasets were generated using different
899 approaches (3' tag sequencing *vs.* full-length sequencing, respectively) we analyzed them in
900 parallel rather than comparing them directly. For each species, we used DESeq2[16] to identify
901 genes that were differentially expressed between plants inoculated with microbiomes from a low-
902 precipitation climate ("dry legacy") *vs.* those inoculated with microbiomes from a high-precipitation
903 climate ("wet legacy"). A single negative binomial model with default parameters was used to
904 estimate $\log_2$-fold changes in gene expression due to inoculum legacy, while also controlling for
905 the other experimental factors, using the model:
906 Counts ~ Legacy + ConditioningPhaseWater + ConditioningPhaseHost + TestPhaseWater

907

908 Statistical support was obtained using the Wald test with Benjamini-Hochberg FDR correction. All
909 available samples were included in each analysis; thus, these results should be interpreted as
910 the gene expression response to microbiome precipitation legacy, averaged across all levels of
911 the other experimental factors.

912

913 In addition, we investigated whether plants' gene expression responses to limited *vs.* ample water
914 during the Test Phase were affected by inoculum precipitation legacy. To do so, we used DESeq2
915 to fit a model with the formula:

916 Counts ~TestPhaseWater*Legacy

917

918 Then, we extracted the estimated $\log_2$-fold changes due to acute drought (relative to well-watered
919 conditions) for both dry-legacy-inoculated and wet-legacy-inoculated plants. We inferred a
920 meaningful interaction between these variables when the 95% confidence intervals of the two
921 drought-induced $\log_2$-fold changes did not overlap at all. These interacting genes are candidates
922 for linking real-time plant drought response to the microbiome's historical environmental
923 conditions.

924

925 Finally, we conducted a mediation analysis to determine whether the *T. dactyloides* genes that
926 were sensitive to inoculum legacy were implicated in phenotypic responses to subsequent acute
927 drought. A gene was considered legacy-sensitive if its expression was significantly affected by
928 the main effect of inoculum legacy, or if it was affected by the interaction between inoculum legacy
929 and test phase drought treatment, as described above. We summarized expression patterns of
930 this subset of genes (normalized as transcripts per million, calculated using the full set of
931 expressed genes) using non-metric multidimensional scaling of the Bray-Curtis distances among
932 all *T. dactyloides* plants, which resulted in two axes of variation: MDS1 and MDS2. Next, we used

933 the mediation package in R[53] to compare the direct effects of test phase drought treatment on
934 each focal plant trait (see section *3.7.1. Plant trait feature selection*) to the indirect effects of the
935 drought treatment mediated through MDS1 and MDS2. Each mediation analysis used the linear
936 models:

937 Trait value ~ MDS + Test phase drought treatment

938 MDS ~ Test phase drought treatment

939 where MDS represents the "site score" of each individual plant on either MDS1 or MDS2.
940 Separate models were fit to test the potential roles of MDS1 and MDS2 as mediator variables;
941 however, a follow-up analysis using both MDS1 and MDS2 as simultaneous mediators,
942 implemented in lavaan[54], yielded equivalent conclusions.
943

944 *3.5.4 Gene annotation*

945 We downloaded maize and eastern gamagrass genome assemblies and annotations from
946 MaizeGDB[50,55]. Functional information for maize genes was taken from the *Zea mays* genome
947 annotation version Zm-B73-REFERENCE-NAM-5.0_Zm00001eb.1 and accessed using
948 MaizeGDB's MaizeMine tool[50,55–57]. For *Tripsacum dactyloides* genes, we relied on DNA
949 sequence homology with annotated maize genes to infer function. We used BEDtools[58] to extract
950 gene coordinates and protein-coding sequences from the *T. dactyloides* reference genome Td-
951 KS_B6_1-REFERENCE-PanAnd-2.0a, and then used OrthoFinder[59] to compare coding
952 sequences from the two species. OrthoFinder identified 32,785 *T. dactyloides* genes (71.5% of
953 the total) as homologs of maize genes, grouping them into 21,658 distinct orthogroups. All
954 differential gene expression analyses, however, considered the entire set of expressed genes;
955 those without maize orthologs, or with unannotated maize orthologs, were considered to be of
956 unknown function.
957

958 *3.6 16S rRNA amplicon sequencing*

959 *3.6.1 DNA extractions and library preparation*

960 One crown root from each plant was cut off with a ceramic blade and placed in a 1.7 mL tube and
961 flash frozen in liquid nitrogen for downstream amplicon library preparation. After collection, root
962 sub-samples were kept on dry ice and ceramic tweezers were used to transfer the whole root to
963 1.1 mL cluster tubes (USA Scientific, Ocala, FL, USA). Tweezers were sterilized with 80% EtOH
964 between samples. Roots were selected at random for placement in cluster tubes and were stored
965 at -80ºC until DNA extraction, at which time roots were freeze-dried for 48 hours in a FreeZone
966 lyophilizer (Labconco, Kansas City, MO, USA). After freeze-drying, roots were flash frozen in
967 liquid nitrogen. To break apart thick roots, sterile forceps and a dissecting needle were used
968 before placing the rack of cluster tubes in an HT Lysing Homogenizer (OHAUS, Parsippany, NJ,
969 USA) with two clean 5/32" steel balls in each tube. Samples were homogenized at 25 Hz for 1
970 min. Root material was then transferred to 2 mL bead-beating 96-well plates containing sterile 1
971 mm garnet beads with 850 µL of lysis buffer (1M Tris, pH = 8.0; 100 mM NaCl; 10 mM EDTA).
972

973 A positive (ZymoBiomics Microbial Community Standard) and negative control, (800 µL of lysis
974 buffer) were included on each plate. Bead-beating plates were stored at -20ºC until extraction.
975 After thawing, 10 µL of 20% sodium dodecyl sulfate (SDS) was added to each well before
976 homogenizing for a total of 20 min at 20 Hz. Plates were incubated in a water bath (55ºC for 90
977 min) and centrifuged (6 min at 4500 x g). 400 µL of the resulting supernatant was transferred to
978 new 1 mL 96-well plates containing 120 µL of 5 M potassium acetate in each well and incubated
979 overnight at -20ºC. After thawing the plates, they were centrifuged (6 min at 4500 x g) and 400
980 µL of the supernatant was transferred to a new 1 mL 96-well plate containing 600 µL of diluted
981 SPRI-bead solution (protocol derived from[60]). These plates were mixed thoroughly for 5 min at
982 1000 r.p.m. on an orbital plate shaker. Samples were allowed to incubate for 10 min so DNA could
983 bind to beads, after which the plate was centrifuged (6 min at 4500 x g) and placed on a magnet
984 rack for 10 min. The supernatant was removed, and the beads were washed twice with 900 µL of

985 80% EtOH. After washing, the supernatant was decanted and the beads were air-dried. DNA was
986 eluted in 75 µL of pre-heated 1x TE (pH = 7.5; 37ºC) and transferred to clean 0.45 mL plates and
987 stored at -20ºC.
988
989 16S-v4 rRNA gene amplification was performed using paired 515f/806r primers[61,62]. PCR
990 reactions contained DreamTaq Master Mix (Thermo Fisher Scientific, Waltham, MA, USA), 10
991 mg/µL bovine serum albumin (BSA), 100 µM peptide nucleic acid (PNA), and PCR-grade water.
992 BSA was used to enhance PCR amplification while PNA was used to suppress primer binding
993 and subsequent amplification of mitochondrial and chloroplast 16S regions[63]. The PCR included
994 an initial denaturation step at 95ºC for 2 min, followed by 27 cycles of an additional denaturation
995 at 95ºC for 20 s, PNA annealing at 78ºC for 5 s, primer annealing at 52ºC for 20 s, and extension
996 at 72ºC for 50 s. This was followed by a final extension step for 10 min at 72ºC. PCR products
997 were purified by incubating at 37ºC for 20 min and then 15 min at 80ºC after mixing with 0.78 µL
998 of PCR-grade water, 0.02 µL of 10 U/µL exonuclease I (Applied Biosystems), and 0.2 µL of 1U/µL
999 shrimp alkaline phosphatase (Applied Biosystems) per 10 µL PCR product. Two µL of the purified
1000 amplicons were used as template DNA in an indexing PCR to attach barcoded P5 and P7 Illumina
1001 adaptors. The 10 µL reaction included 5 µM each of P5 and P7 adaptors, 1x DreamTaq Master
1002 Mix (Thermo Fisher Scientific), 10 mg/mL BSA, 100 µM PNA, and PCR-grade water. An initial
1003 denaturation step was performed at 95ºC for 2 min. For 8 cycles, an additional denaturation was
1004 carried out at 95ºC for 20 s, PNA annealing at 78ºC for 5 s, primer annealing at 52ºC for 20 s,
1005 and extension at 72ºC for 50 s. A final extension step was performed at 72ºC for 10 min. PCR
1006 products were verified via 2% agarose gel electrophoresis and then pooled by 96-well plate using
1007 the “Just-a-Plate” PCR cleanup and normalization kit (Charm Biotech, St. Louis, MO, USA). Pools
1008 were size selected and combined in equimolar concentrations before being sequenced on an
1009 Illumina SP flow cell on the NovaSeq 6000 platform (2x250bp reads).
1010

1011 *3.6.2 Amplicon data processing*

1012 We removed primer sequences from raw 16S-v4 Illumina reads using cutadapt[37], requiring at
1013 least 5 nucleotides of overlap. Additional quality control and processing was performed with the
1014 DADA2 software[64]. Forward reads were discarded if they had more than 6 expected errors,
1015 otherwise they were truncated at 200 nucleotides; for reverse reads the parameters were 7
1016 expected errors and 170 nucleotides. Error rates were estimated separately for forward and
1017 reverse reads based on a sample of $1x10^8$ bases, then used to denoise and dereplicate reads
1018 using the standard DADA2 functions. Chimeric sequences were detected and removed using the
1019 "consensus" procedure in DADA2. Each individual sample was processed in parallel, after which
1020 all of the resulting amplicon sequence variant (ASV) tables were merged. Finally, taxonomy of
1021 each ASV was assigned by comparison to the RDP database[65].

1022

1023 *3.6.3 Root bacterial community diversity analysis*

1024 All statistical analyses were performed using R (v4.4.0). The cleaned and prepared microbiome
1025 data, as phyloseq objects, were loaded into R[35]. The phyloseq object sample data table was
1026 replaced with an updated metadata file. The "mock" samples were removed from the dataset and
1027 the data was subset by the test phase host, maize and gamagrass using
1028 phyloseq::subset_samples (v1.48.0). Maize and gamagrass root bacterial microbiome Shannon
1029 Diversity was fit to a mixed-effects model using the lme4 (v1.1-35.4) package[66] and lmer()
1030 function, using the following model:

1031 expShannon~TestWater+Legacy + (1|DNAplate)

1032

1033 A type III ANOVA was performed using stats::anova()[67] to test for significance, followed by
1034 pairwise comparisons and significance tests using emmeans (v1.10.2) package[68] with false
1035 discovery rate adjustments. Data visualizations were generated using ggplot2 (v3.5.1)[12], the error

1036 bars represent standard error and the points are estimated marginal means. All plots were saved
1037 in PDF format. Composite figures were created in Adobe Illustrator.
1038
1039 Bacterial community beta diversity was accessed with a Constrained Analysis of Principal
1040 Coordinates, using phyloseq::ordinate, method="CAP", and distance="Euclidean" with the
1041 following formulas:

1042 ~Legacy+Condition(DNAplate)+Condition(CondHost)+
1043 Condition(CondWater)+Condition(TestWater)
1044
1045 ~TestWater+Condition(DNAplate)+Condition(CondHost)+
1046 Condition(CondWater)+Condition(Legacy)
1047
1048 An ANOVA-like permutation test was used to test for model significance using the
1049 vegan::anova.cca() function[13]. CAP1 and MDS1 axes were plotted using ggplot2, including 95%
1050 confidence interval ellipse (stat_ellipse()). To evaluate treatment group beta-dispersion,
1051 Euclidean distances were calculated for the centered-log ratio transformed counts using
1052 phyloseq::distance(). Both "Legacy" and "TestWater" terms were tested for beta-dispersion
1053 differences using the Euclidean distances matrix and vegan::betadisper() and vegan::permutest()
1054 to test for significance[13]. Distances were then extracted from the results output and fit to a linear
1055 model. Estimated marginal means were calculated and plotted using the same methods as above.
1056 The error bars represent standard errors.
1057
1058 Then, an ASV differential abundance analysis was performed on gamagrass- and maize-
1059 associated ASVs separately. Centered-log ratio transformed counts of ASVs were each fit to a
1060 linear model using an iterative for-loop. Each ASV was subset using phyloseq:subset_taxa and

1061 the phyloseq::psmelt() function was used to reformat the phyloseq object into a data frame. Then
1062 the ASV abundance was fit to the following model:

1063 $$\text{Abundance} \sim \text{Legacy*TestWater}$$

1064

1065 Then, stats::anova() was used to test for significance, followed by an FDR p-value adjustment
1066 using stats::p.adjust(). ASVs with significant (≤0.05) adjusted p-values for the Legacy*TestWater
1067 interaction terms were extracted and z-scores of the center-log ration transformed counts were
1068 plotted in a heatmap using pheatmap::pheatmap()[69] with clustering_method="complete".

1069

1070 *3.7 Plant trait data analyses*

1071 *3.7.1 Plant trait feature selection*

1072 All plant data was loaded into RStudio. The intrinsic water use efficiency (iWUE) was calculated
1073 using the ratio of photosynthetic rate (A) and stomatal conductance (gs) or A/gs ((μmol m^{-2}
1074 s^{-1})/(mol m^{-2} s^{-1})). Data was subset by Test Phase host treatment groups (gamagrass and maize).
1075 For the feature selection, the "mock" treatment was removed. The 67 features that were selected
1076 for testing were subset into a data frame. Three sample rows were removed from the dataset
1077 because they had missing data. The drought susceptibility index (S-index) was calculated for
1078 each of these features using the following formula:

1079 $$S=\text{Trait}_{\text{drought}}/\text{mean}(\text{Trait}_{\text{control}})$$

1080

1081 Then, for each host, a random forest model was used to select the top 10 most important features
1082 from the 67 total s-index measurements using randomForest()[70], with "Legacy" as the predictor.
1083 Correlations (stats::cor()) were estimated for the top ten traits and if any two of the top 10 traits
1084 were highly correlated ($r \geq 0.7$), the trait that ranked lower in the random forest model was
1085 removed. Non-correlative top features from the test water treatment groups (drought vs. watered

control) were combined for each test phase host (maize and gamagrass). Vegan:rda() was used to perform a redundancy analysis on the top features using the following formula:

Top_features~ Legacy + Condition(CondGroup), scale=TRUE

3.7.2 Feature analyses

An ANOVA-like permutation test was used to test for model significance using the vegan::anova.cca() function. A biplot was created using ggplot2 plotting RDA1 and PC1 axes, as well as the species scores (represented by arrows), and stat_ellipse was used to plot 95% confidence intervals of the site scores.

Finally, s-indices for each of the top features and iWUE were fit to mixed-effects models, when possible, or a fixed-effects model if overfitting of the mixed effects model occurred. Each feature or trait was visually assessed for outliers, which were removed. Removing the outliers did not impact the interpretation of any of the results. Formulas used for the mixed effects or linear model, respectively, include:

lmer(s-index ~ Legacy + (1|CondGroup))

lm(s-index ~ Legacy + CondGroup)

The fit of the model was accessed and if needed, the s-index was transformed using sqrt(), exp(), or log() to improve the fit. ANOVA was used to assess significance and estimated marginal means were calculated and plotted as described above.

REFERENCES

1. Stackhouse, P. Nasa power. https://power.larc.nasa.gov/.
2. Neves, D. J. D., Silva, V. de P. R., Almeida, R. S. R., Sousa, F. de A. S. de & Silva, B. B.

da. General aspects of the climate in the Cabo verde archipelago. *Rev. Ambiência* **13**, (2017).

3. Varela-Lopes, G. E. & Molion, L. C. B. Precipitation patterns in Cape Verde islands: Santiago island case study. *Atmos. Clim. Sci.* **04**, 854–865 (2014).

4. Moreno, Â., Ramos, T. B., Gonçalves, M. C. & Pereira, L. S. Estimating soil hydraulic properties from limited data to improve irrigation management in agricultural soils of Santiago island, Cape Verde: Soil hydraulic properties in Cape Verde soils. *Irrig. Drain.* **63**, 405–415 (2014).

5. Unknown, (:unkn). Guide to Meteorological Instruments and Methods of Observation: (CIMO guide). 2014 edition, updated in 2017.[SUPERSEDED]. Preprint at https://doi.org/10.25607/OBP-432 (2017).

6. Soltanpour, P. N. & Schwab, A. P. A new soil test for simultaneous extraction of macro- and micro-nutrients in alkaline soils. *Commun. Soil Sci. Plant Anal.* **8**, 195–207 (1977).

7. De Coster, W., D'Hert, S., Schultz, D. T., Cruts, M. & Van Broeckhoven, C. NanoPack: visualizing and processing long-read sequencing data. *Bioinformatics* **34**, 2666–2669 (2018).

8. Wood, D. E., Lu, J. & Langmead, B. Improved metagenomic analysis with Kraken 2. (2019) doi:10.1101/762302.

9. Lu, J., Breitwieser, F. P., Thielen, P. & Salzberg, S. L. Bracken: estimating species abundance in metagenomics data. *PeerJ Comput. Sci.* **3**, e104 (2017).

10. Breitwieser, F. P. & Salzberg, S. L. Pavian: interactive analysis of metagenomics data for microbiome studies and pathogen identification. *Bioinformatics* **36**, 1303–1304 (2020).

11. Hothorn, T., Bretz, F. & Westfall, P. Simultaneous inference in general parametric models. *Biom. J.* **50**, 346–363 (2008).

12. Wickham, H. *Ggplot2: Elegant Graphics for Data Analysis*. (Springer, Berlin,

1137 Germany, 2016).
1138 13. Oksanen, J. *et al.* vegan : Community Ecology Package. R package version 1.8-
1139 5. (2007).
1140 14. The R Project for Statistical Computing. http://www.R-project.org/.
1141 15. Schneider, C. A., Rasband, W. S. & Eliceiri, K. W. NIH Image to ImageJ: 25
1142 years of image analysis. *Nat. Methods* **9**, 671–675 (2012).
1143 16. Love, M. I., Huber, W. & Anders, S. Moderated estimation of fold change and
1144 dispersion for RNA-seq data with DESeq2. *Genome Biol.* **15**, 550 (2014).
1145 17. Kolmogorov, M. *et al.* metaFlye: scalable long-read metagenome assembly using
1146 repeat graphs. *Nat. Methods* **17**, 1103–1110 (2020).
1147 18. BBTools. *DOE Joint Genome Institute* https://jgi.doe.gov/data-and-tools/bbtools/
1148 (2016).
1149 19. Li, H. Minimap2: pairwise alignment for nucleotide sequences. *Bioinformatics* **34**,
1150 3094–3100 (2018).
1151 20. Woodcroft, B. J. *CoverM: Read Coverage Calculator for Metagenomics*. (Github).
1152 21. von Meijenfeldt, F. A. B., Arkhipova, K., Cambuy, D. D., Coutinho, F. H. & Dutilh,
1153 B. E. Robust taxonomic classification of uncharted microbial sequences and bins with CAT
1154 and BAT. *Genome Biol.* **20**, 217 (2019).
1155 22. Van der Jeugt, F., Dawyndt, P. & Mesuere, B. FragGeneScanRs: faster gene
1156 prediction for short reads. *BMC Bioinformatics* **23**, 198 (2022).
1157 23. Cantalapiedra, C. P., Hernández-Plaza, A., Letunic, I., Bork, P. & Huerta-Cepas,
1158 J. eggNOG-mapper v2: Functional Annotation, Orthology Assignments, and Domain
1159 Prediction at the Metagenomic Scale. *Mol. Biol. Evol.* **38**, 5825–5829 (2021).
1160 24. Huerta-Cepas, J. *et al.* eggNOG 5.0: a hierarchical, functionally and
1161 phylogenetically annotated orthology resource based on 5090 organisms and 2502 viruses.
1162 *Nucleic Acids Res.* **47**, D309–D314 (2019).

1163 25. Buchfink, B., Reuter, K. & Drost, H.-G. Sensitive protein alignments at tree-of-life
1164 scale using DIAMOND. *Nat. Methods* **18**, 366–368 (2021).
1165 26. Steinegger, M. & Söding, J. MMseqs2 enables sensitive protein sequence
1166 searching for the analysis of massive data sets. *Nat. Biotechnol.* **35**, 1026–1028 (2017).
1167 27. Wright, R. M., Aglyamova, G. V., Meyer, E. & Matz, M. V. Gene expression
1168 associated with white syndromes in a reef building coral, Acropora hyacinthus. *BMC*
1169 *Genomics* **16**, 371 (2015).
1170 28. Li, H. *et al.* The Sequence Alignment/Map format and SAMtools. *Bioinformatics*
1171 **25**, 2078–2079 (2009).
1172 29. Danecek, P. *et al.* Twelve years of SAMtools and BCFtools. *Gigascience* **10**,
1173 (2021).
1174 30. Danecek, P. *et al.* The variant call format and VCFtools. *Bioinformatics* **27**, 2156–
1175 2158 (2011).
1176 31. Chang, C. C. *et al.* Second-generation PLINK: rising to the challenge of larger
1177 and richer datasets. *Gigascience* **4**, 7 (2015).
1178 32. Yin, L. *et al.* RMVP: A memory-efficient, visualization-enhanced, and parallel-
1179 accelerated tool for genome-wide association study. *Genomics Proteomics Bioinformatics*
1180 **19**, 619–628 (2021).
1181 33. LiLin-Yin. CMplot: Circle Manhattan Plot. *CRAN: Contributed Packages* The R
1182 Foundation https://doi.org/10.32614/cran.package.cmplot (2015).
1183 34. Faisal, M., Silander, O. & Freed, N. Starting a MinION sequencing run using
1184 MinKNOW v1. (2020) doi:10.17504/protocols.io.bfwqjpdw.
1185 35. McMurdie, P. J. & Holmes, S. phyloseq: an R package for reproducible
1186 interactive analysis and graphics of microbiome census data. *PLoS One* **8**, e61217 (2013).
1187 36. Shetty, S. Lahti L. microbiomeutilities: microbiomeutilities: Utilities for Microbiome
1188 Analytics. 2022. Preprint at (2023).

1189 37. Martin, M. Cutadapt removes adapter sequences from high-throughput
1190 sequencing reads. *EMBnet.journal* **17**, 10–12 (2011).
1191 38. Shetty, S. A. & Lahti, L. Microbiome data science. *J. Biosci.* **44**, (2019).
1192 39. De Mendiburu, F. & Simon, R. Agricolae - Ten years of an open source statistical
1193 tool for experiments in breeding, agriculture and biology. *PeerJ* (2015)
1194 doi:10.7287/peerj.preprints.1404.
1195 40. The Hmisc and rms Packages. in *Biostatistics and Computer-based Analysis of*
1196 *Health Data using R* 173–186 (Elsevier, 2016).
1197 41. Grabherr, M. G. *et al.* Full-length transcriptome assembly from RNA-Seq data
1198 without a reference genome. *Nat. Biotechnol.* **29**, 644–652 (2011).
1199 42. Kopylova, E., Noé, L. & Touzet, H. SortMeRNA: fast and accurate filtering of
1200 ribosomal RNAs in metatranscriptomic data. *Bioinformatics* **28**, 3211–3217 (2012).
1201 43. Patro, R., Duggal, G., Love, M. I., Irizarry, R. A. & Kingsford, C. Salmon provides
1202 fast and bias-aware quantification of transcript expression. *Nat. Methods* **14**, 417–419
1203 (2017).
1204 44. Soneson, C., Love, M. I. & Robinson, M. D. Differential analyses for RNA-seq:
1205 transcript-level estimates improve gene-level inferences. *F1000Res.* **4**, 1521 (2015).
1206 45. Kamvar, Z. N., Tabima, J. F. & Grünwald, N. J. Poppr: an R package for genetic
1207 analysis of populations with clonal, partially clonal, and/or sexual reproduction. *PeerJ* **2**,
1208 e281 (2014).
1209 46. Thioulouse, J. *et al. Multivariate Analysis of Ecological Data with ade4*. (Springer,
1210 New York, NY, 2019).
1211 47. Goudet, J. hierfstat, a package for r to compute and test hierarchical *F*-statistics.
1212 *Mol. Ecol. Notes* **5**, 184–186 (2005).
1213 48. Seethepalli, A. *et al.* RhizoVision Explorer: open-source software for root image
1214 analysis and measurement standardization. *AoB Plants* **13**, lab056 (2021).

1215 49. Smith, T., Heger, A. & Sudbery, I. UMI-tools: modeling sequencing errors in
1216 Unique Molecular Identifiers to improve quantification accuracy. *Genome Res.* **27**, 491–499
1217 (2017).
1218 50. Hufford, M. B. *et al.* De novo assembly, annotation, and comparative analysis of
1219 26 diverse maize genomes. *Science* **373**, 655–662 (2021).
1220 51. Guo, J., Gao, J. & Liu, Z. HISAT2 parallelization method based on Spark cluster.
1221 *J. Phys. Conf. Ser.* **2179**, 012038 (2022).
1222 52. Liao, Y., Smyth, G. K. & Shi, W. featureCounts: an efficient general purpose
1223 program for assigning sequence reads to genomic features. *Bioinformatics* **30**, 923–930
1224 (2014).
1225 53. Yimer, B. B., Lunt, M., Beasley, M., Macfarlane, G. J. & McBeth, J. BayesGmed:
1226 An R-package for Bayesian causal mediation analysis. *PLoS One* **18**, e0287037 (2023).
1227 54. Rosseel, Y. lavaan: An R Package for Structural Equation Modeling. *J. Stat.*
1228 *Softw.* **48**, 1–36 (2012).
1229 55. Portwood, J. L., 2nd *et al.* MaizeGDB 2018: the maize multi-genome genetics
1230 and genomics database. *Nucleic Acids Res.* **47**, D1146–D1154 (2019).
1231 56. Woodhouse, M. R. *et al.* A pan-genomic approach to genome databases using
1232 maize as a model system. *BMC Plant Biol.* **21**, 385 (2021).
1233 57. Shamimuzzaman, M. *et al.* MaizeMine: A Data Mining Warehouse for the Maize
1234 Genetics and Genomics Database. *Front. Plant Sci.* **11**, 592730 (2020).
1235 58. Quinlan, A. R. BEDTools: The Swiss-Army Tool for Genome Feature Analysis.
1236 *Curr. Protoc. Bioinformatics* **47**, 11.12.1–34 (2014).
1237 59. Emms, D. M. & Kelly, S. OrthoFinder: phylogenetic orthology inference for
1238 comparative genomics. *Genome Biol.* **20**, 238 (2019).
1239 60. Rohland, N. & Reich, D. Cost-effective, high-throughput DNA sequencing
1240 libraries for multiplexed target capture. *Genome Res.* **22**, 939–946 (2012).

1241 61. Apprill, A., McNally, S., Parsons, R. & Weber, L. Minor revision to V4 region SSU
1242 rRNA 806R gene primer greatly increases detection of SAR11 bacterioplankton. *Aquat.*
1243 *Microb. Ecol.* **75**, 129–137 (2015).
1244 62. Parada, A. E., Needham, D. M. & Fuhrman, J. A. Every base matters: assessing
1245 small subunit rRNA primers for marine microbiomes with mock communities, time series
1246 and global field samples. *Environ. Microbiol.* **18**, 1403–1414 (2016).
1247 63. Lundberg, D. S., Yourstone, S., Mieczkowski, P., Jones, C. D. & Dangl, J. L.
1248 Practical innovations for high-throughput amplicon sequencing. *Nat. Methods* **10**, 999–1002
1249 (2013).
1250 64. Callahan, B. J. *et al.* DADA2: High-resolution sample inference from Illumina
1251 amplicon data. *Nat. Methods* **13**, 581–583 (2016).
1252 65. Cole, J. R. *et al.* Ribosomal Database Project: data and tools for high throughput
1253 rRNA analysis. *Nucleic Acids Res.* **42**, D633–42 (2014).
1254 66. Bates, D., Mächler, M., Bolker, B. & Walker, S. Fitting linear mixed-effects
1255 models Usinglme4. *J. Stat. Softw.* **67**, (2015).
1256 67. *R: A Language and Environment for Statistical Computing : Reference Index*.
1257 (2010).
1258 68. https://CRAN.R-project.org/package=emmeans.
1259 69. pheatmap: Pretty Heatmaps. *Comprehensive R Archive Network (CRAN)*
1260 https://CRAN.R-project.org/package=pheatmap.
1261 70. CRAN: R News. https://CRAN.R-project.org/doc/Rnews/.

1262

1263

1264
1265
1266
1267

Figures

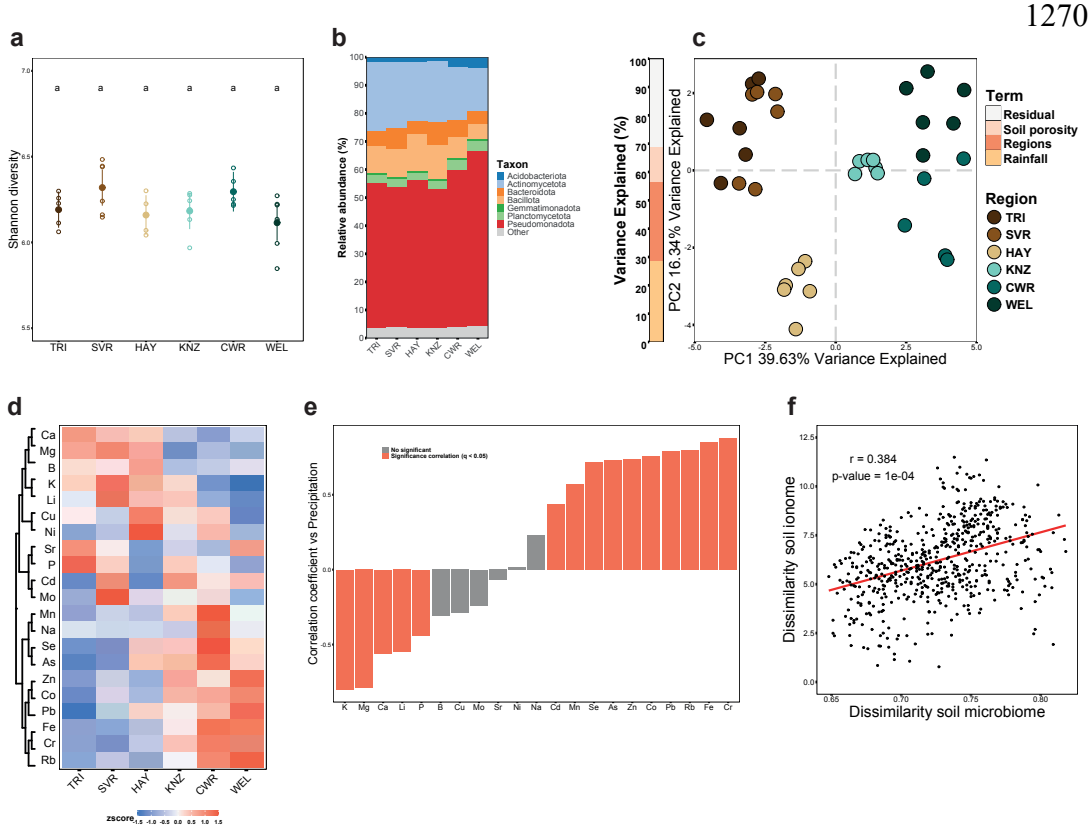

Extended Data Fig. 1. Precipitation level and mineral nutrient content in Kansas soils correlate with soil microbiota composition. a. Alpha diversity (estimated using the Shannon diversity index) did not differ across soil samples. Soils are ordered according to the gradient of precipitation (Fig 1a). **b**. Phylogram showing the relative abundance profiles of the main bacterial phyla across soils exposed to different precipitation levels. **c**. Principal component analysis showing the projected ionomic profiles among the different soils exposed to the gradient of precipitation. The bar on the left denotes the percentage of the variance explained by the different experimental variables. **d**. Heatmap showing the standardized concentration (z-score) of each mineral nutrient (rows) in the collection of soil exposed to different precipitation levels. The values were clustered according to the ion concentration and the region was ordered according to the precipitation gradient (lower to high). **e**. Bar graph showing the Pearson correlation coefficient between each mineral nutrient abundance and the level of precipitation across the collection of soils used. Coloured bars are significant ($q < 0.05$). **f**. Pairwise correlation analysis between soil mineral nutrient dissimilarities and soil microbiome composition dissimilarities in soils representing a gradient of precipitation. Panel shows the Mantel *r* statistic and its *p*-value.

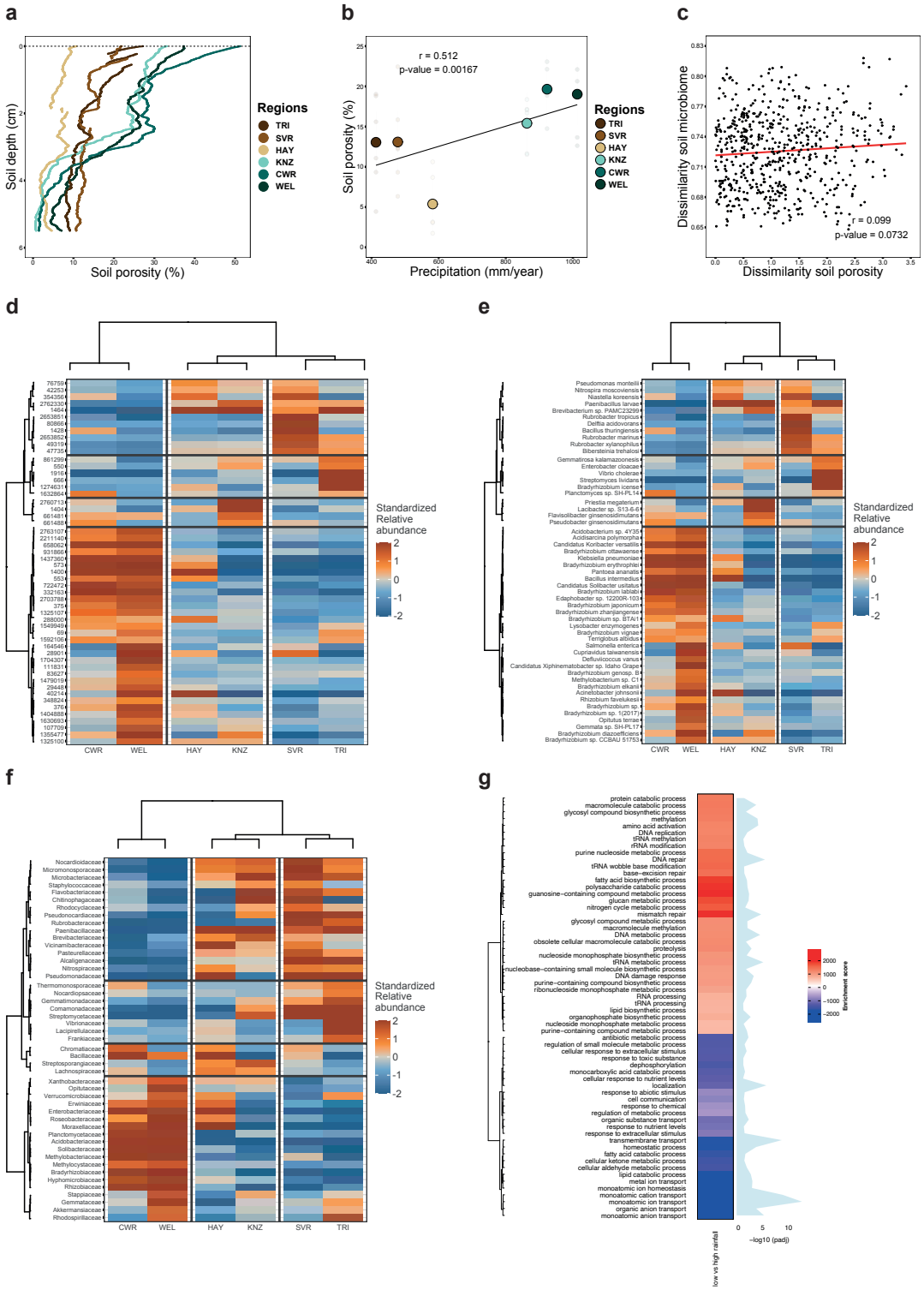

Extended Data Fig. 2. Precipitation levels, but not soil porosity, explain microbiota composition across the Kansas soil collection. a. Percent soil porosity changes with depth in soils exposed to the precipitation gradient. The data were obtained from soil images generated by X-ray computed tomography. **b**. Pearson correlation analysis between the soil porosity and the precipitation gradient. The correlation coefficient r and its *p*-value are shown. **c**. Pairwise correlation analysis between soil microbiota dissimilarities and soil porosity dissimilarities. The

panel show the Mantel *r* statistic and its *p*-value. **d-f**. Heatmaps showing changes in the relative abundance of bacterial taxa (d), species (e), and family (f) that were found to be significantly different from the wetter region in the Kansas soil collection. In all cases, the values have been clustered according to taxonomic categories and soils. Note that this soil collection represents a precipitation gradient. **g.** The heatmap illustrates the enriched or depleted biological processes between soils from three wet regions (high precipitation: WEL, CWR, and KNZ) and three dry regions (low precipitation: TRI, SVR, and HAY). Gene enrichment analysis was conducted using a generalized linear model, followed by Gene Ontology (GO) classification. Significantly enriched and depleted GO categories were identified based on an adjusted *p*-value threshold of < 0.05. The colours (red and blue) represent the enrichment score, calculated using square root-transformed delta rank values of the GO categories. The line graph on the right displays the -log10 adjusted *p*-value of the enriched or depleted GO categories in the comparison.

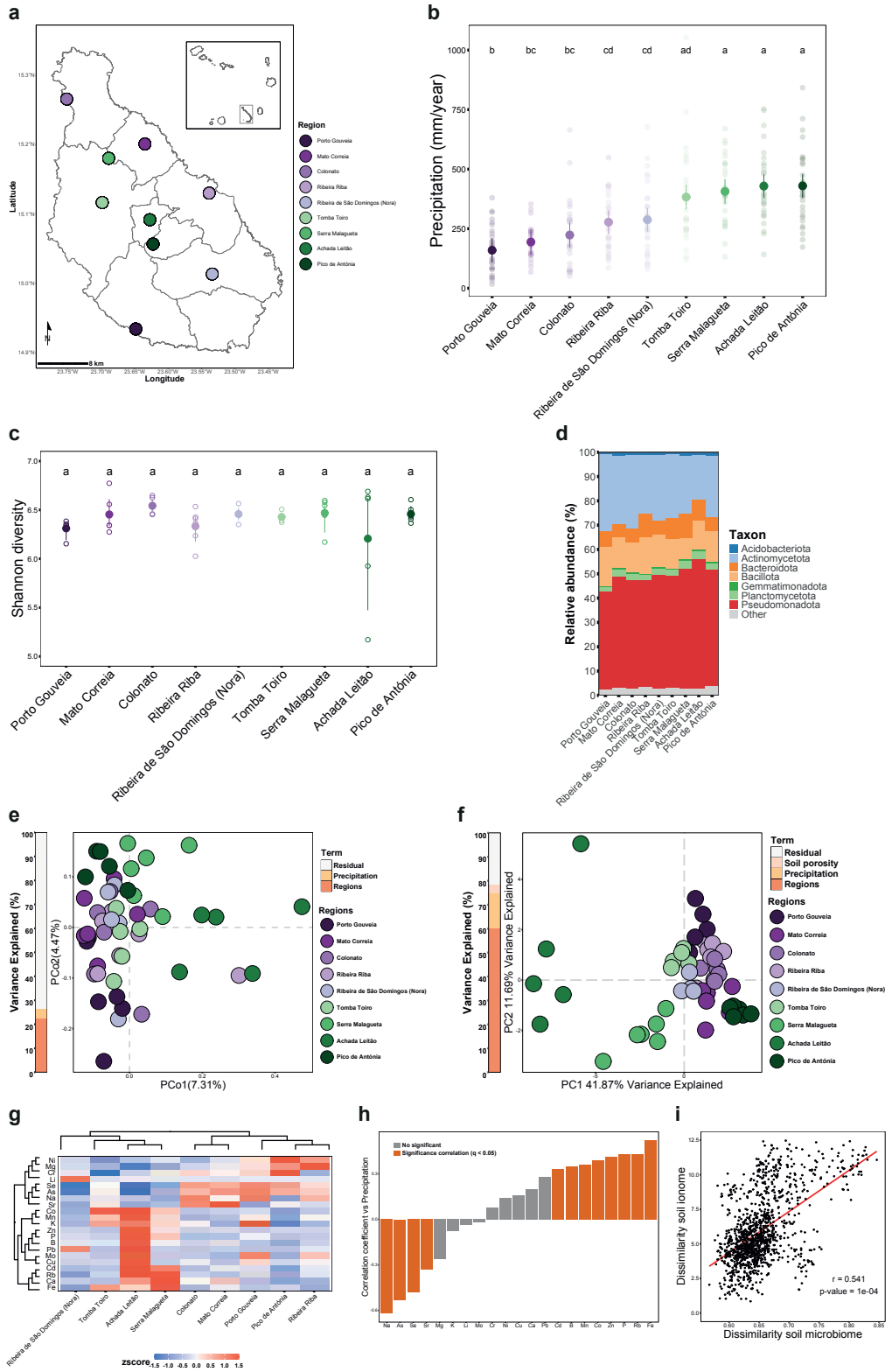

Extended Data Fig. 3. The microgradient of precipitation identified in Santiago island and the soil mineral content influence the general soil microbiota structure. a. Map of Santiago island, Cabo Verde, showing the locations selected for collecting the soils used in this work. **b.**

The graph shows the precipitation (mm/year) recorded or estimated for the Santiago soils over the period 1981 to 2009 across diverse databases. Statistical significance between soils was determined via linear modelling and letters represent the compact letter display of a Tukey *post-hoc* test. **c**. Alpha diversity, measured using the Shannon diversity index, did not differ across soil samples. Soils are ordered according to the gradient of precipitation (panel b)**.** **d**. Phylogram showing the relative abundance profiles of the most abundant bacterial phyla across Santiago soils. **e**. Principal component analysis showing the projected microbiota composition among the different soils (colours). The bar on the left denotes the percentage of the variance explained by the different experimental variables. **f**. Principal component analysis showing the projected mineral nutrient profiles among the different soils (colours). The bar on the left denotes the percentage of the variance explained by the different experimental variables. **g**. Heatmap showing the standardized concentration (z-score) of each mineral nutrient (rows) in the collection of Santiago soils. The values have been clustered according to the ion concentration and the region **h**. Bar graph showing the Pearson correlation coefficient between each mineral nutrient abundance and the level of precipitation across the collection of soils. Coloured bars are statistically significant ($q < 0.05$). **i**. Pairwise correlation analysis between soil mineral nutrient content dissimilarities and soil microbiota composition dissimilarities. Panel shows the Mantel r statistic and its p-value.

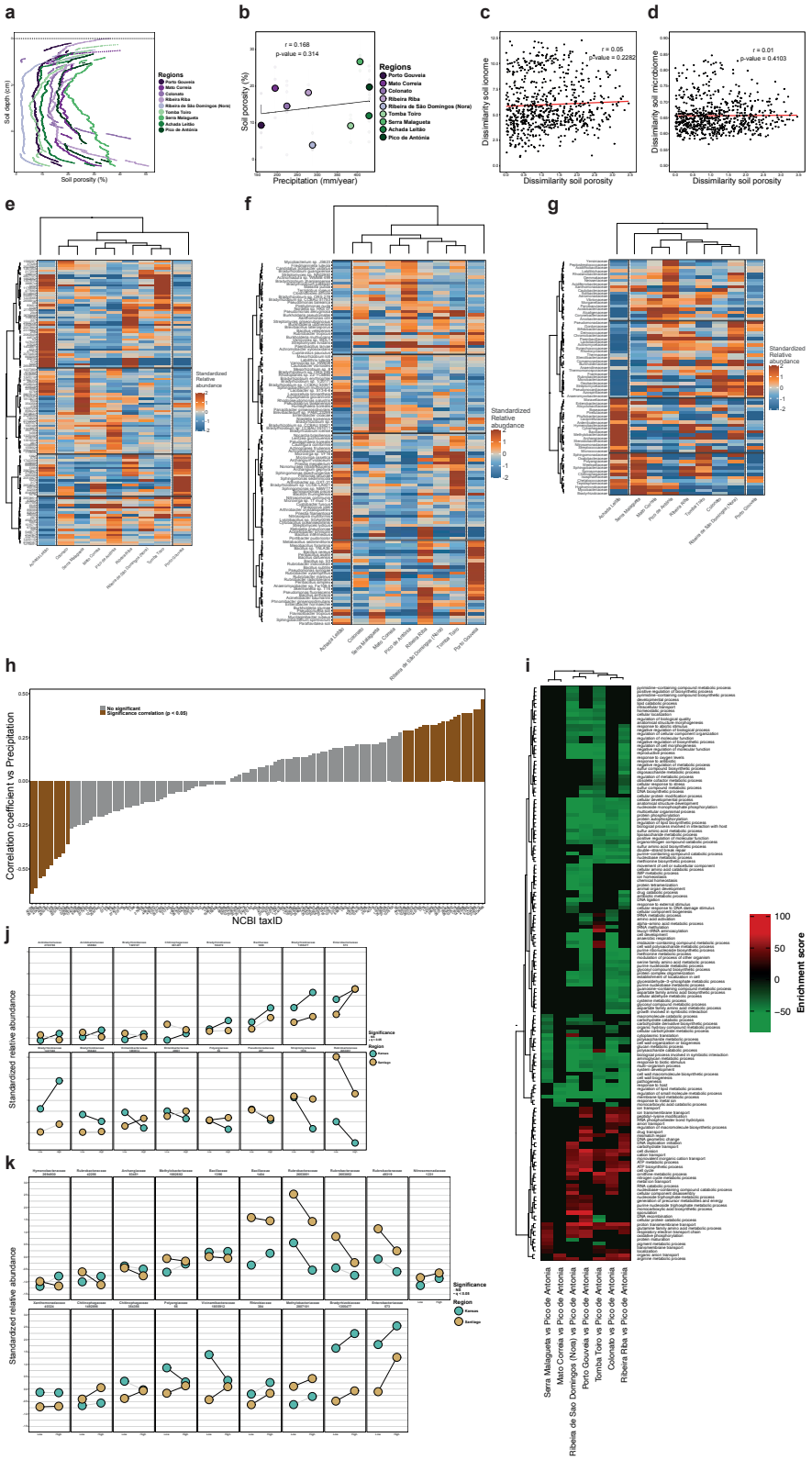

Extended Data Fig. 4. The microgradient of precipitation identified in Santiago explains the soil microbiota composition. a. Percentage of soil porosity changes with the soil depth in soils

across the precipitation microgradient. The data were obtained from soil images generated by X-ray computed tomography. The colours represent different soils. **b**. Pearson correlation analysis between the soil porosity and the precipitation microgradient. The correlation coefficient r and its *p*-value are shown. **c.** Pairwise correlation analysis between soil porosity dissimilarities and soil mineral nutrient content (ionome) dissimilarities. **d.** Pairwise correlation analysis between soil porosity dissimilarities and soil microbiota composition dissimilarities. In both panels, c and d, the Mantel *r* statistic and its *p*-value are shown. **e-g.** Heatmaps showing changes in relative abundance of **(e)** bacterial taxa**, (f)** species and **(g)** families across the soil collection. Only bacterial taxa with a significantly different relative abundance from the wetter region in the rainfall microgradient were used for this analysis. In all cases, values have been grouped by taxonomic categories and soils**. h.** Bar graph showing the Pearson correlation coefficient between the relative abundance of each bacterial taxa and the level of precipitation. Coloured bars are significant ($q < 0.05$). **i.** The heatmap depicts enriched or depleted biological processes between soils from the region with high annual precipitation (Pico de Antónia) and the remaining soils (Achada Leitão, Serra Malagueta, Mato Correia, Ribeira de São Domingos (Nora), Porto Gouveia, Tomba Toiro, Colonato, and Ribeira Riba). Gene enrichment analysis was performed using a generalized linear model, followed by Gene Ontology (GO) classification. Significantly enriched and depleted GO categories were identified based on an adjusted *p*-value threshold of < 0.05. Enriched (red) and depleted (green) GO terms represent the enrichment score, calculated using square root-transformed delta rank values of the GO categories. **j-k.** Comparative analysis of the relative abundances of bacterial markers identified in soils from (**j**) Kansas and (**k**) Santiago Island in the corresponding pool of soils with high or low levels of precipitation. Coloured points represent the average value of standardized relative abundance for each region (Kansas and Santiago). The line connecting both points is the difference between low and high precipitation soils. A black line indicates statistical significance ($q < 0.05$).

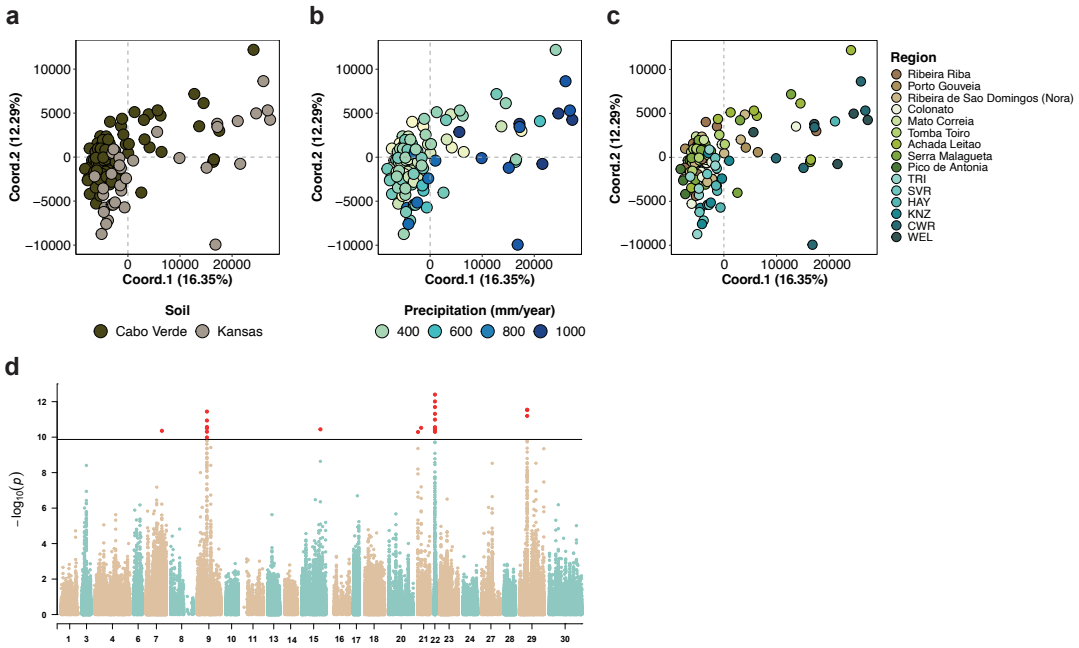

Extended Data Fig. 5. Genetic variation among bacterial lineages along the Kansas and Santiago precipitation gradients. To assess genetic differences between bacteria lineages along the precipitation gradient, we selected 33 bacterial species (22 of the identified bacterial markers and 11 additional abundant and prevalent taxa) that exhibited high genome coverage in the soil samples from Kansas, USA and Santiago Island, Cabo Verde, as proxies for the broader bacterial communities. Reference genomes for each species were retrieved from the NCBI Genome database, and filtered shotgun metagenomic reads were mapped to these genomes to identify high-quality biallelic single nucleotide polymorphisms (SNPs). Genetic distances between the bacterial lineages were calculated based on the identified SNPs and PCoA plots were generated and coloured by **a**. soil type, **b**. precipitation levels and **c**. geographical regions of Kansas (Kansas State University's Tribune Southwest Research Center (TRI), Smoky Valley Ranch (SVR), Hays Prairie (HAY), Konza Wildlife Reserve (KNZ), Clinton Wildlife Reserve (CWR), Welda Prairie (WEL)) and Santiago Island (Ribeira Riba, Porto Gouveia, Ribeira de São Domingos (Nora), Colonato, Mato Correia, Tomba Toiro, Achada Leitão, Serra Malagueta, Pico de Antónia). The variance explained by each axis is indicated. Manhattan plot **d**. illustrates significant SNPs linked to the precipitation gradient, derived from the genetic-environment association (GEA) analysis. The GEA analysis was conducted using a general linear model, with average precipitation at each sampling location as the environmental variable. Significant associations were identified using the permutation method. The x-axis of the plot represents the SNP positions along the genomes of the selected bacterial species, while the y-axis displays the -$\log_{10}$ *p*-values from the association model. The horizontal line indicates the statistical significance threshold, as determined by the permutation test. SNPs above this threshold, highlighted in red, were significantly associated with the precipitation gradient. Bacterial taxa with fewer than 1,000 high-quality biallelic SNPs after filtering, and with no significant SNPs detected from the GEA analysis, are not shown in the plot.

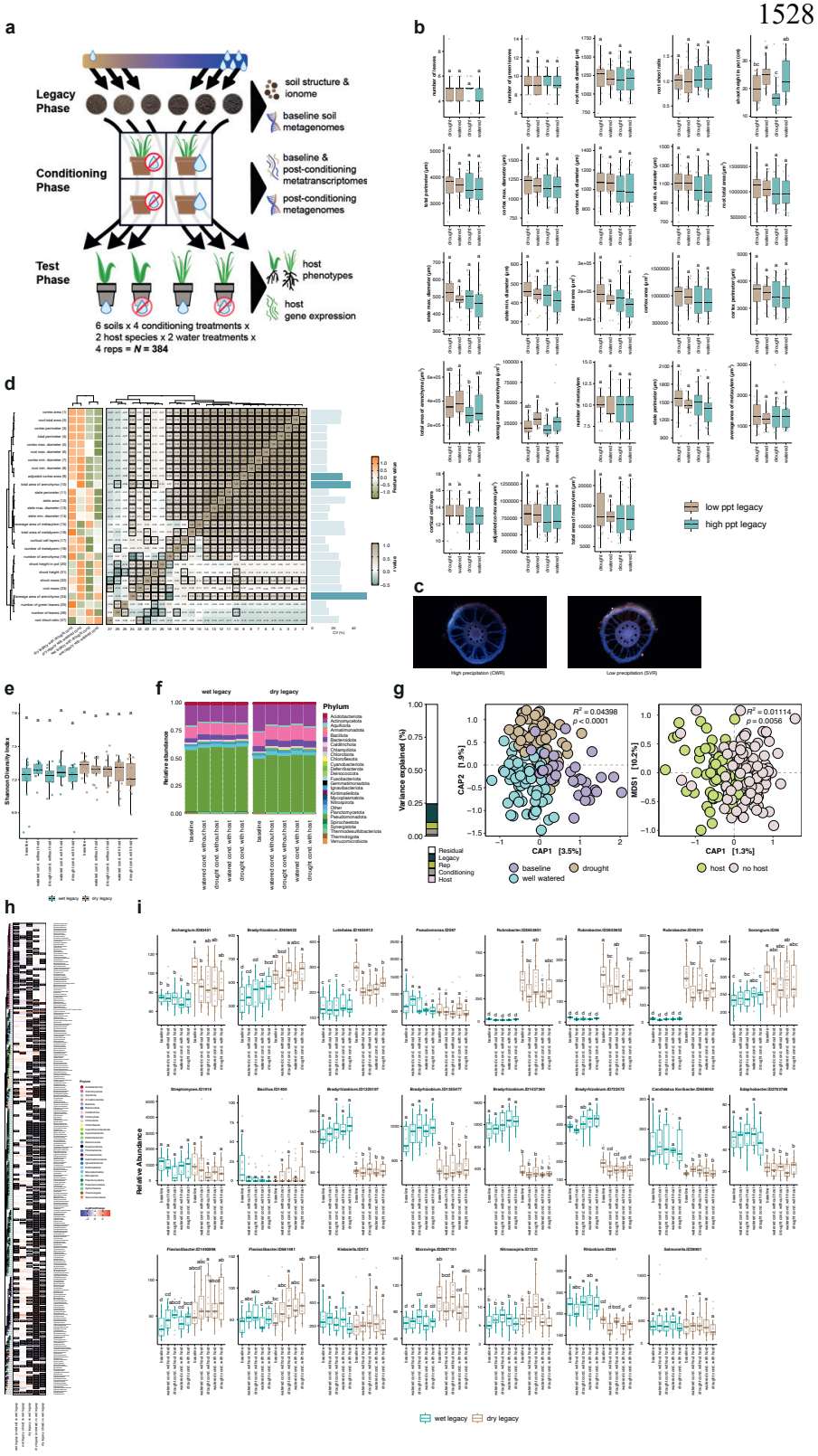

Extended Data Fig. 6. Soil water legacy is resilient to short-term water- and host-related perturbations. a. Schematic representation of the experimental pipeline used to evaluate the

resilience of the soil water legacy to perturbations and their functional importance to plant drought response. The six soils from Kansas, representing a gradient of precipitation with clear ecological memory of water availability (Legacy phase), were either left unplanted or planted with seedlings of the native grass species *Tripsacum dactyloides* (eastern gamagrass), and then subjected to either drought conditions or regular watering in a factorial design (Conditioning phase). To evaluate the functional effects of soil precipitation legacy on plants, and to isolate the role of the microbiota from possible roles of non-microbial soil properties, we then used the experimentally-conditioned microbial communities to inoculate a new generation of *T. dactyloides* and *Z. mays* plants. These "Test Phase" plants were divided between water-limited conditions and well-watered control conditions. **b**. Box plot showing the quantification of different *Tripsacum dactyloides* phenotypes in response to the treatments applied (drought conditions or regular watering) during the conditioning phase. ANOVA was used to discern significant differences among groups and estimated marginal means were compared using Tukey's post hoc test. **c**. Exemplary pictures taken by laser ablation tomography (LAT) of crown roots of *Tripsacum dactyloides* grown in soils with a high-precipitation (CWR) and low-precipitation (SVR) history after exposure to acute drought during. Note that the number of aerenchyma in the root, important for the drought response, in plants exposed to a low precipitation legacy (SVR) is higher compared to that found in plants grown in soils with high precipitation history (CWR). **d.** Phenotypic traits of *Tripsacum dactyloides* in response to the conditioning phase treatments (drought or regular watering). The heatmap on the left depicts key features extracted from the plant, colored based on mean normalised values. Pearson correlation coefficients (r) between these features are presented in the centre heatmap, with significant correlations ($p < 0.05$) highlighted by black squares. The bar plot on the right indicates the coefficient of variation of the feature values, with highly variable features highlighted in blue. The heatmaps are clustered based on Pearson correlation coefficient values. **e**. Alpha diversity of bacterial communities, measured using the Shannon diversity index, was not affected by the different conditioning treatments (drought or well-watered, with or without host). **f**. Phylograms show that the different conditioning treatments (drought or well-watered, with or without host) did not impact the relative abundance profiles of main bacterial phyla. **g**. Canonical analysis of principal coordinates (CAP) showing the effects of conditioning phase treatments on microbiome assembly: (left) soil legacy (baseline), well-watered, drought, and (right) host or no host. PERMANOVA R^2 and *p*-value are shown within the CAP plot. The bar on the left describes the percentage of the variance explained by the experimental variables. **h**. The heatmap displays the enrichment of bacterial families across soils with wet and dry legacies, exposed to either drought or well-watered treatments, in comparison to soils with a wet legacy. Colors in the heatmap represent $\log_2$ fold changes, calculated using a generalized linear model that contrasts the abundance of each bacterial family in the respective treatments with that of the wet soil legacy. Tiles outlined in black denote statistically significant enrichment (red) or depletion (blue) ($q < 0.05$) with a $\log_2$ fold change > ±2 with respect to the soils with wet legacy. The heatmap was clustered based on taxonomic classification (represented by the dendrogram on the left). **i**. Boxplots showing the relative abundance of bacterial markers of water legacy across soils with dry or wet legacy (baseline) after exposure to conditioning phase treatments (drought or well-watered, with or without host). ANOVA was performed to detect significant differences among the groups, with Tukey's post hoc test used to compare the estimated marginal means. Notice that in most cases the conditioning treatments did not affect the relative abundance of bacterial markers compared to the baseline soils.

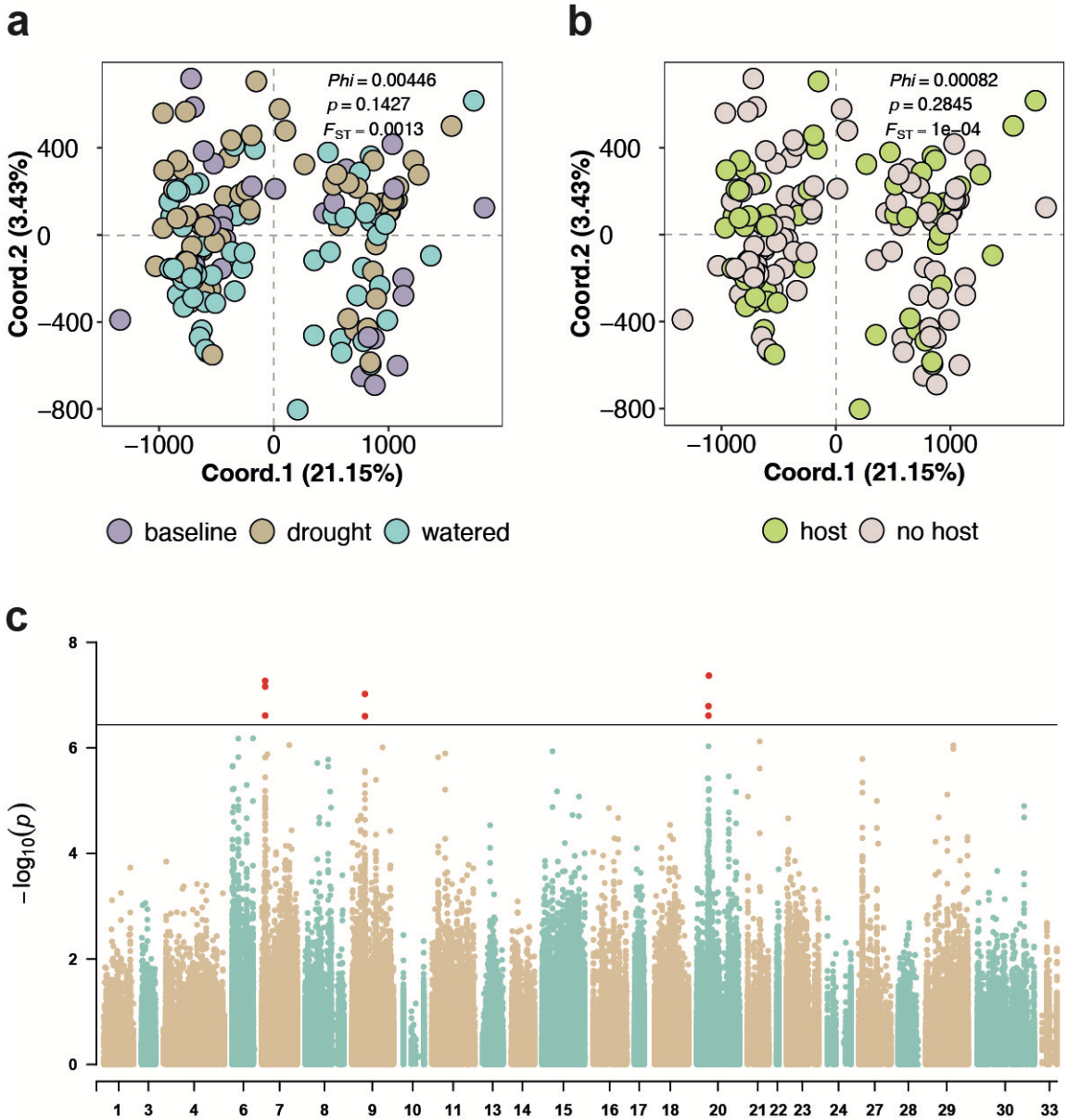

Extended Data Fig. 7. Genetic variation among bacterial lineages driven by long-term water legacy remains stable despite acute drought/water perturbations and host conditioning. Filtered shotgun metagenomic reads were aligned to the reference genomes of 33 selected taxa, including 22 identified bacterial markers and 11 additional abundant and prevalent taxa. Genetic distances between these bacterial lineages were calculated based on identified single nucleotide polymorphisms (SNPs). Principal Coordinate Analysis (PCoA) plots were generated and color to depict **a.** acute drought and well-watered treatments, and **b.** host and no-host conditioning perturbations. Phi values, derived from Analysis of Molecular Variance (AMOVA), indicate the genetic variance between groups, while the *p*-value reflects the significance of the AMOVA results based on permutation testing. Fixation Index (F_{ST}) values were used to measure the degree of genetic differentiation between groups. The variance explained by each axis is displayed on the PCoA plots. **c.** A Manhattan plot illustrated significant SNPs linked to the wet and dry soil legacies, derived from the genetic-environment association (GEA) analysis. This analysis was conducted using a general linear model and significant associations were identified using the permutation method. In the Manhattan plot, the x-axis represents the SNP positions along the genomes of the

selected bacterial species, while the y-axis displays the -log10 *p*-values from the association model. A horizontal line represents the statistical significance threshold, determined by the permutation test. SNPs exceeding this threshold (highlighted in red) were significantly associated with soil legacy effects. Bacterial taxa with fewer than 1,000 high-quality biallelic SNPs after filtering, or with no significant SNPs detected from the GEA analysis, are excluded from the plot.

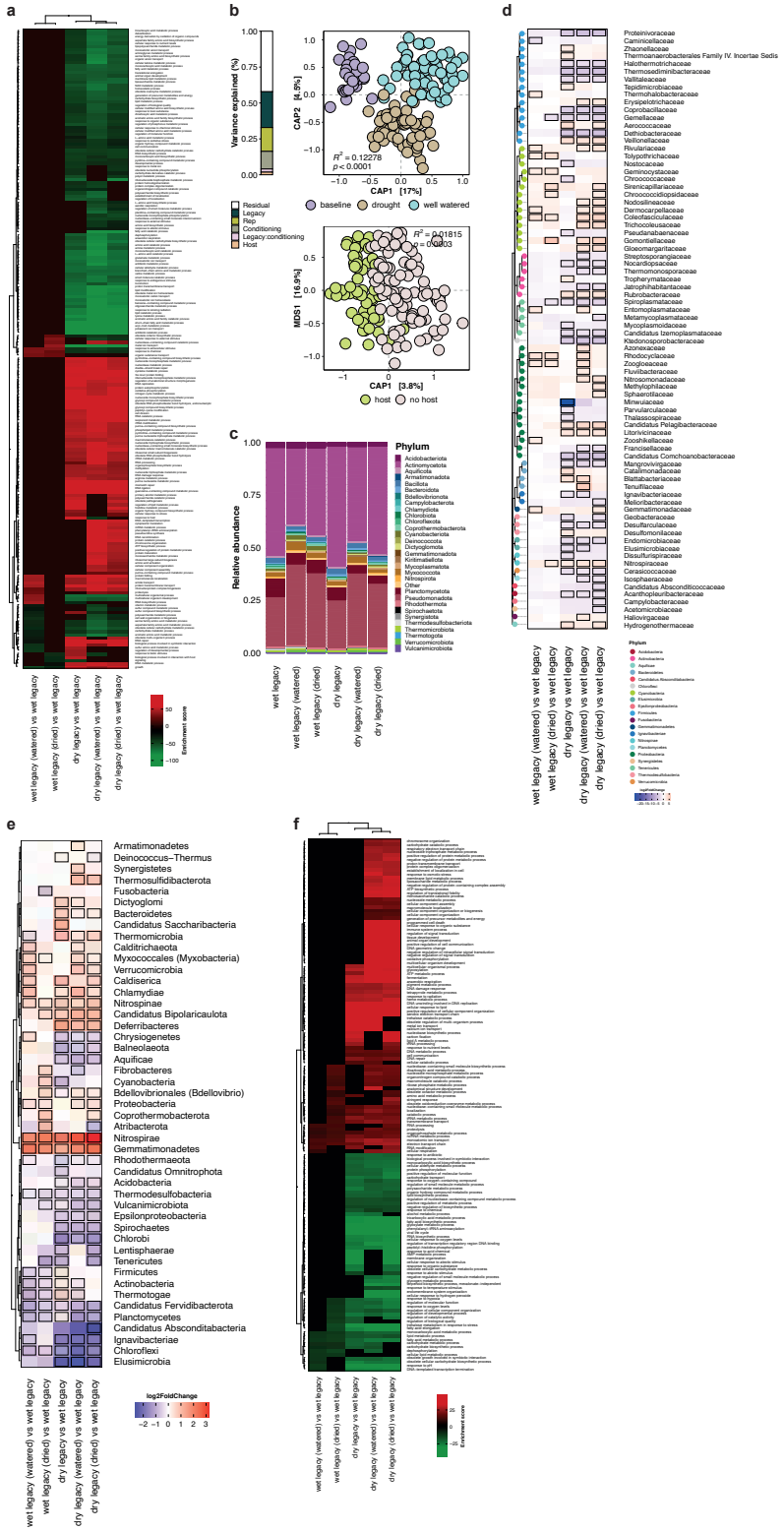

Extended Data Fig. 8. Precipitation legacy effects on microbial community function are robust to short-term (five months) acute perturbations. a. The heatmap illustrates enriched or depleted Gene Ontology (GO) categories in soils with wet or dry legacies, subjected to drought

or well-watered treatments, in comparison to soils with a wet legacy (baseline). Gene enrichment analysis was conducted using a generalized linear model, followed by GO classification. Significantly enriched and depleted GO categories were identified using an adjusted *p*-value threshold of < 0.05. Colors (red for enrichment, green for depletion) represent enrichment scores, calculated based on square root-transformed delta rank values of the GO categories. The heatmap is clustered by soil treatments and GO terms. **b**. Canonical analysis of principal coordinates (CAP) showing the projected metatranscriptome differences across the conditioning treatments: (top) baseline soil legacy, baseline exposed to well-watered or drought treatment, and (bottom) host or no host treatment. The bar on the left describes the percentage of the variance explained by the experimental variables. **c**. Phylogram showing the main bacterial phyla functionally active across soils with different water legacy subjected to drought or well-watered treatments. **d-e**. Heatmaps showing enrichment in functionally active bacterial (**d**) families and (**e**) phyla across soils with different water legacy and exposed to drought or well-watered treatments compared to soils with wet legacy. Heatmaps were colored based on $\log_2$ fold changes derived from a generalised linear model contrasting the abundance of each family in a given treatment against soils with wet legacy. Tiles outlined in black denote statistically significant enrichment (red) or depletion (blue) ($q < 0.05$) with a $\log_2$ fold change > ±2 with respect to the soils with wet legacy. Heatmaps were clustered based on taxonomic classification (tree on the left). **f**. The heatmap displays biological processes that are enriched or depleted based on metatranscriptomic analysis of soils with wet or dry legacies, subjected to drought or well-watered treatments, compared to soils with a wet legacy (baseline). Gene enrichment analysis was performed using a generalized linear model, followed by GO classification. Significantly enriched and depleted Gene Ontology (GO) categories were identified with an adjusted *p*-value threshold of < 0.05. Colors (red for enrichment and green for depletion) indicate enrichment scores, calculated from square root-transformed delta rank values of the GO categories. The heatmap is clustered by soil treatments and GO terms.

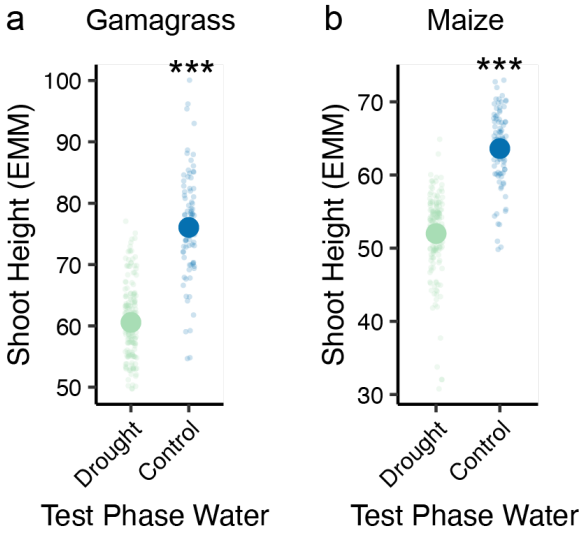

Extended Data Figure 9. Test phase gamagrass and maize drought treatments effectively reduce plant growth. Test phase drought treatment significantly reduced gamagrass shoot height (cm) (**a**) and maize shoot height (cm) (**b**).

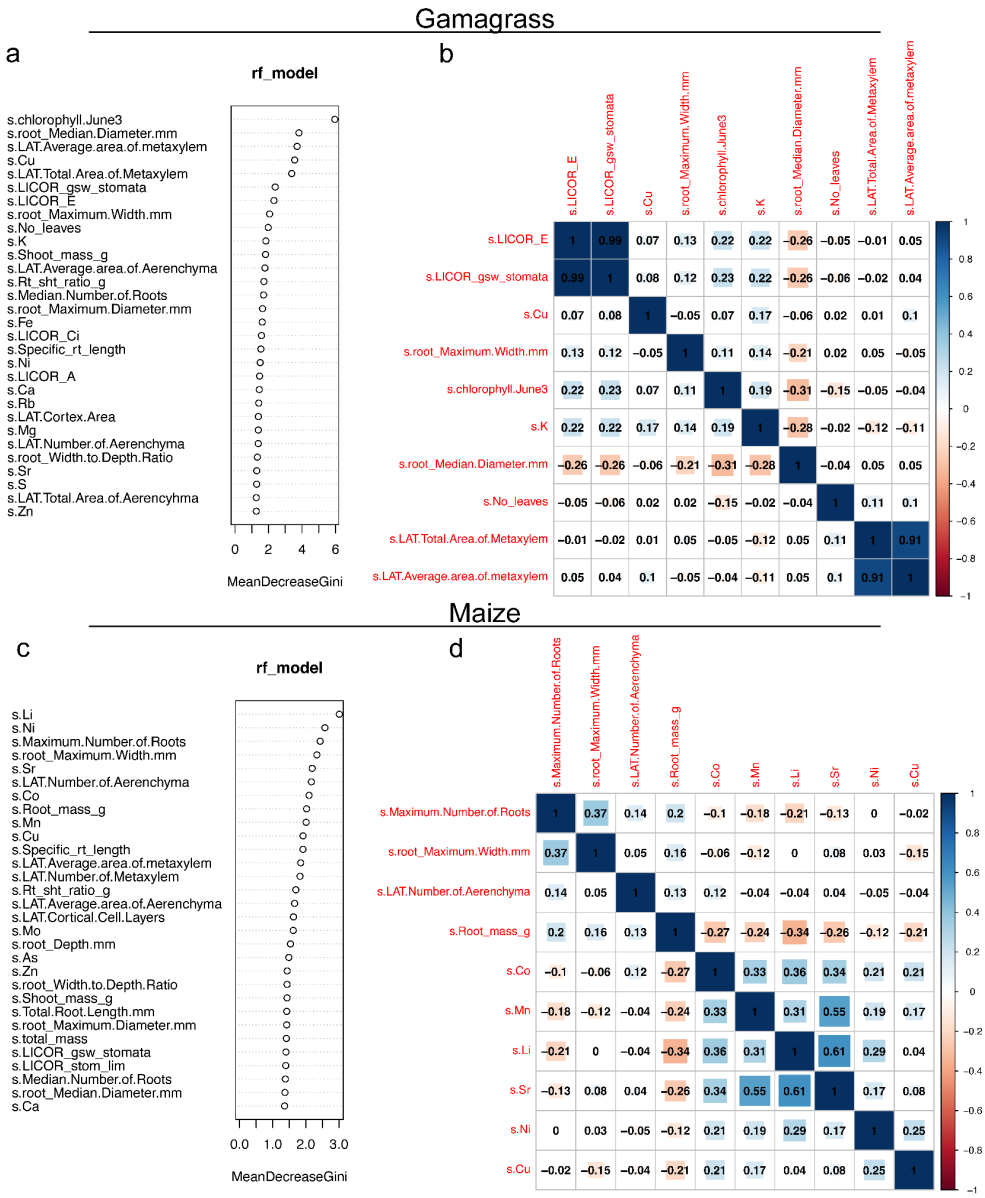

Extended Data Figure 10. Plant trait feature selection. a-b. Gamagrass and **c-d.** maize traits important in explaining legacy effects were ranked using a random forest model. The top ten traits were tested for significant correlations (≥ 0.7).

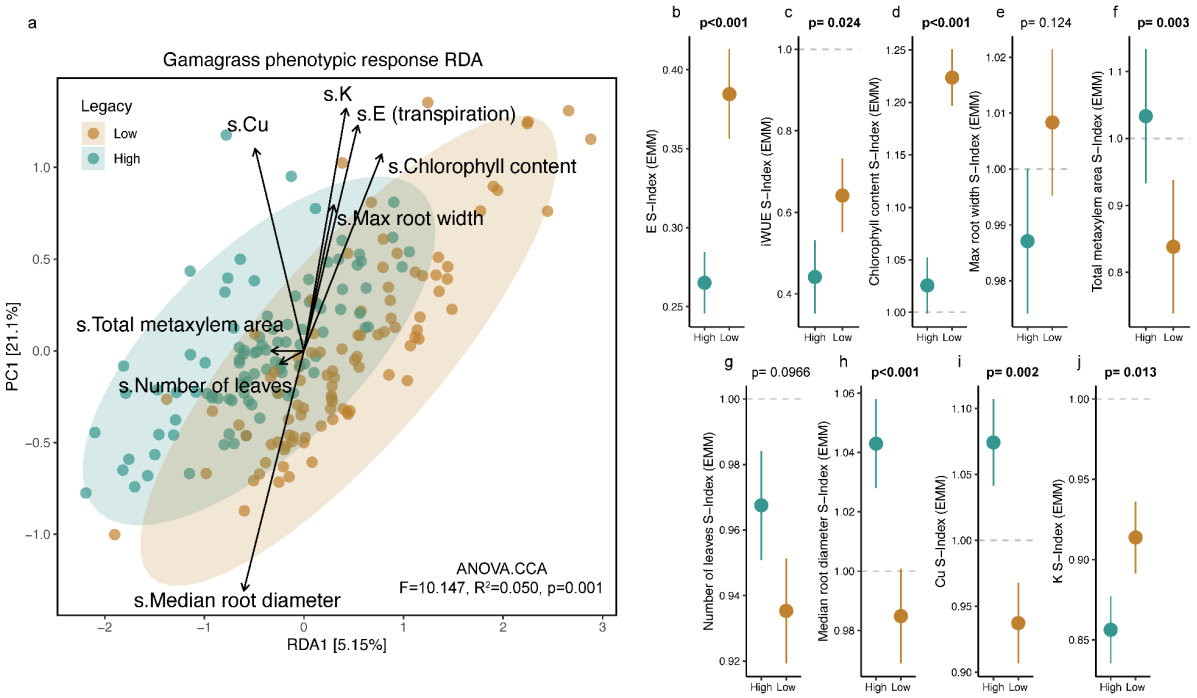

Extended Data Figure 11. Microbiome legacy impacts gamagrass phenotypic drought response. a. A constrained redundancy analysis on the top non-correlated traits found that legacy explains 5.0% of gamagrass phenotypic response to acute drought. **b-j**. Assessment of individual traits indicates that microbiome drought legacy significantly improved gamagrass performance under drought. Points are EMMs and error bars represent the standard error, and significant p-values (≤0.05) are bolded.

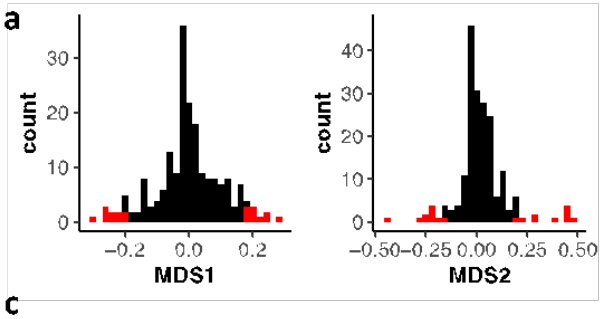

Top 5% of genes with strongest positive loadings on MDS1

Td_gene	MDS1	MDS2	Gene_set	Zm_orthologs	Zm_gene_symbol
Td00002ba000754	0.282	0.182	I	Zm00001eb057770	
Td00002ba018910	0.246	0.141	VII	Zm00001eb112460	cl31479_3
Td00002ba037703	0.241	-0.057	%	Zm00001eb237740	
Td00002ba002499	0.217	0.059	I	NA	
Td00002ba014047	0.21	0.021	I	Zm00001eb381580	
Td00002ba022717	0.208	0.065	III	Zm00001eb055100	
Td00002ba044330	0.205	0.103	VI	Zm00001eb199260	
Td00002ba019383	0.19	0.148	I	Zm00001eb115970	ms33
Td00002ba011993	0.181	0.078	I	Zm00001eb307550	ereb177
Td00002ba024147	0.178	0.057	I	Zm00001eb248540	umc2600a

Top 5% of genes with strongest positive loadings on MDS2

Td_gene	MDS1	MDS2	Gene_set	Zm_orthologs	Zm_gene_symbol
Td00002ba015526	-0.266	0.486	IV	Zm00001eb396120	nas7
Td00002ba015525	-0.259	0.46	IV	Zm00001eb396120	nas7
Td00002ba039891	-0.238	0.451	III	NA	
Td00002ba001144	0.168	0.447	VI	Zm00001eb053700	
Td00002ba001146	0.16	0.44	VI	Zm00001eb053700	
Td00002ba041411	-0.173	0.389	IV	NA	
Td00002ba015516	-0.141	0.272	IV	Zm00001eb396120	nas7
Td00002ba015515	-0.141	0.272	IV	Zm00001eb396120	nas7
Td00002ba033830	-0.15	0.218	V	Zm00001eb039280	ga20ox7
Td00002ba019393	-0.154	0.199	III	Zm00001eb286420	mads58

Top 5% of genes with strongest negative loadings on MDS1

Td_gene	MDS1	MDS2	Gene_set	Zm_orthologs	Zm_gene_symbol
Td00002ba046162	-0.203	0.116	V	Zm00001eb199320	
Td00002ba046161	-0.206	0.112	II	Zm00001eb199320	
Td00002ba036367	-0.222	0.138	II	Zm00001eb199320	
Td00002ba036368	-0.224	0.132	II	Zm00001eb199320	
Td00002ba019546	-0.236	-0.222	II	Zm00001eb147080	
Td00002ba039891	-0.238	0.451	III	NA	
Td00002ba007195	-0.257	0.113	II	Zm00001eb161990	
Td00002ba015525	-0.259	0.46	IV	Zm00001eb396120	nas7
Td00002ba015526	-0.266	0.486	IV	Zm00001eb396120	nas7
Td00002ba002239	-0.304	0.188	III	Zm00001eb048620	

% downregulated due to main effect of dry-legacy inoculum (no interaction with acute drought)

Top 5% of genes with strongest negative loadings on MDS2

Td_gene	MDS1	MDS2	Gene_set	Zm_orthologs	Zm_gene_symbol
Td00002ba023452	-0.061	-0.166	V	Zm00001eb027750	pat3
Td00002ba021901	0.012	-0.19	V	NA	
Td00002ba019546	-0.236	-0.222	II	Zm00001eb147080	
Td00002ba019177	0.023	-0.222	III	Zm00001eb180130	
Td00002ba009640	-0.077	-0.222	II	Zm00001eb210740	AY110625
Td00002ba008826	-0.138	-0.224	II	Zm00001eb125560	umc1742
Td00002ba045645	-0.019	-0.24	*	NA	
Td00002ba015343	0.124	-0.267	II	NA	
Td00002ba006731	-0.084	-0.272	II	Zm00001eb210740	AY110625
Td00002ba006546	-0.029	-0.435	VIII	Zm00001eb211300, Zm00001eb211310, Zm00001eb155430, Zm00001eb055690	pco095801, AY106518, GRMZM2G0249 58

* upregulated due to main effect of dry-legacy inoculum (no interaction with acute drought)

Extended Data Figure 12. Contributions of legacy-sensitive *Tripsacum dactyloides* genes to NMDS axes that mediate drought responses. **a**. Histograms showing the distributions of gene loadings onto both axes. The top 5% of genes with the strongest positive and negative loadings onto each axis are in red. **b**. Breakdown of the number of genes with positive/negative loadings onto each axis. **c**. Lists of genes comprising the 5% tails of the distributions in **a**. Detailed information about the expression responses of these genes is available in Supplementary Table S3. 'Gene_set' corresponds to the patterns of response to microbiome legacy presented in Figure 4a-b.

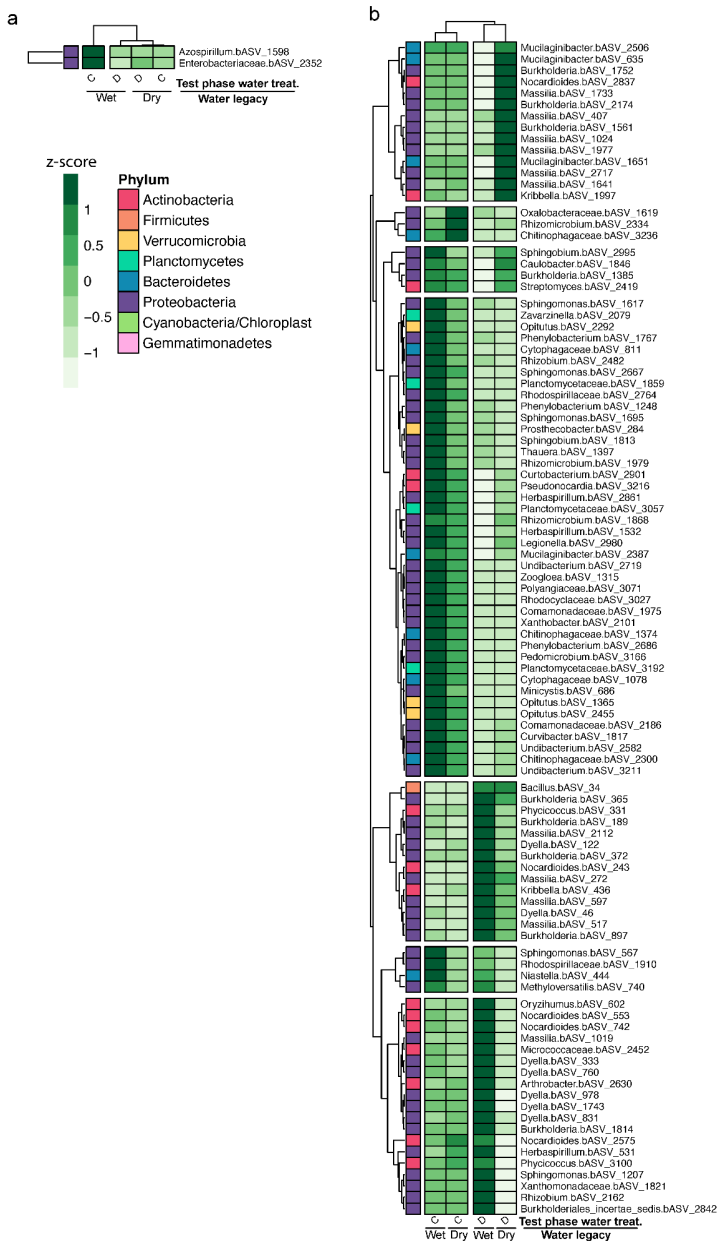

Extended Data Figure 13. Test phase water and legacy have a large impact on ASV abundances in maize, but not gamagrass. a. Gamagrass root bacterial and **b.** maize root bacterial centered-log ratio transformed ASV counts were individually fit to a linear model to identify ASVs that were differentially abundant across test phase water treatments in the context of precipitation legacy. Dark green represents ASV enrichment and light green to white represents depletion. Multi-colored squares indicate phylum-level taxonomic assignments, which do not have an obvious phylogenetic pattern.

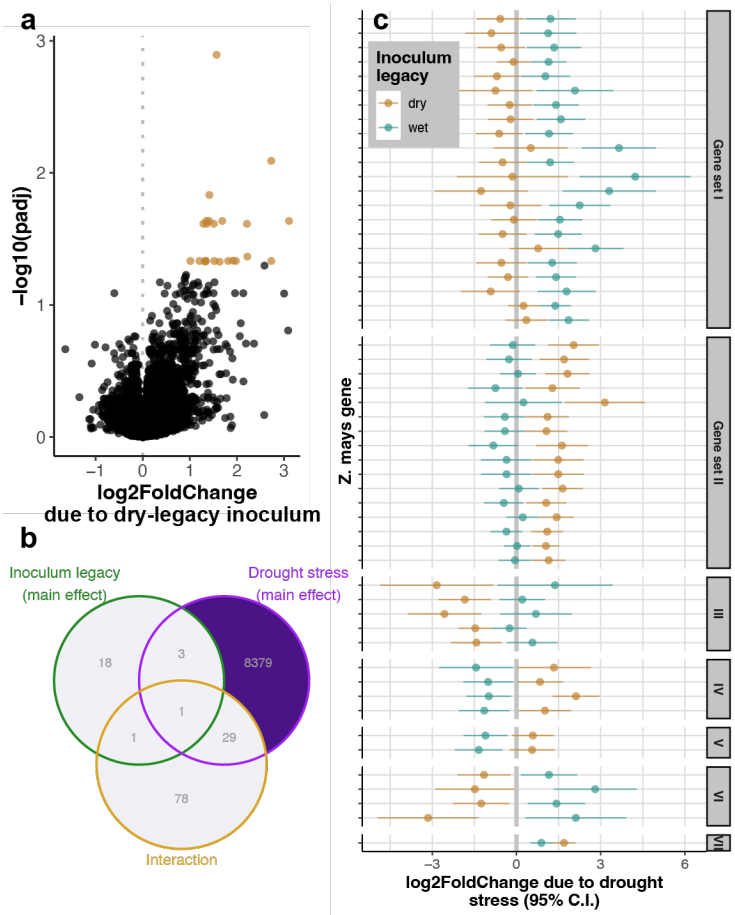

Extended Data Figure 14. Drought legacy of microbial inocula alters the transcriptional response to drought in the maize crown root. a. 23 genes were up-regulated in plants inoculated with microbiota from a low-precipitation region, relative to plants inoculated with microbiota from a high-precipitation region. **b.** The sets of genes that responded to the main effects of inoculum legacy and Test Phase drought stress had minimal overlap with each other or with the set of genes that were sensitive to the interaction between the two. **c.** In total, 109 maize genes responded to drought in a manner that was dependent on the drought legacy of the soil microbiota, regardless of the inoculum's treatment during the conditioning phase. For illustration purposes, only annotated genes with $|\log_2\text{FoldChange}| > 1$ in at least one microbial context are shown here; the full list is available in Supplementary Table S3. Each pair of points shows one gene; the relative position of the two points illustrates how the gene's expression changed in response to drought stress during the Test Phase, depending on whether the plant had been inoculated with microbiota derived from a low-precipitation or dry-precipitation environment. Genes are grouped into sets according to the pattern of how inoculum legacy altered their drought responses. Note: the names of these gene sets are not meant to correspond to the names of the *T. dactyloides* gene sets shown in Figure 4b; in each species, Gene set I contains the most genes, Gene set II contains the next most, and so on.

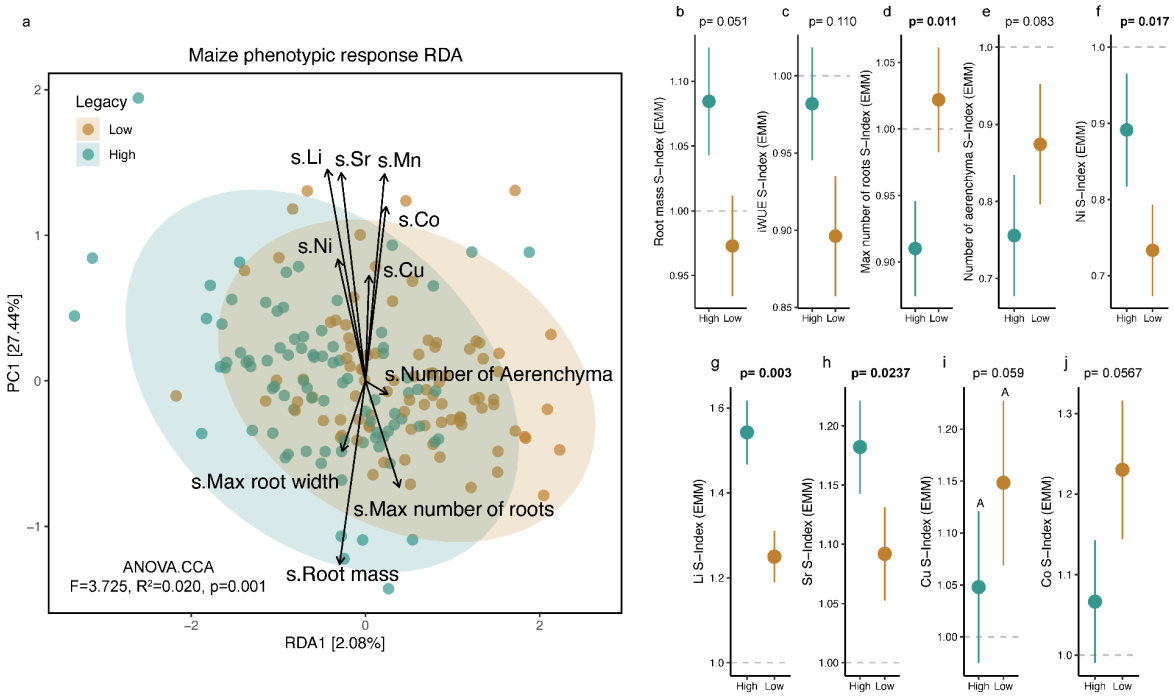

Extended Data Figure 15. Microbiome Legacy had minimal impact on maize phenotypic drought response. a. A constrained redundancy analysis on the top non-correlated traits found that legacy only explains 2.0% of maize phenotypic response to acute drought. **b-j.** Assessment of individual traits indicates that microbiome drought legacy did not significantly improve maize performance under drought, but did impact several mineral nutrient concentrations. Points are EMMs and error bars represent the standard error, and significant *p*-values (≤ 0.05) are bolded.

Supplementary Table Legends.

Supplementary Table S1. List of identified regions in the United States and Cabo Verde representing precipitation gradients. The soils used in this work were collected from these regions. The table also shows the coordinates associated with these regions, the state, municipalities, and country where these regions are located.

Supplementary Table S2. List of bacterial markers of soil water legacy identified in this work using soils from the two precipitation gradients from Kansas and Santiago. In addition to the bacterial taxa ID (taxID), the table also shows taxonomical attributes (Family, Genus, label Family, and Label genus) of the bacterial markers identified. The column F shows the direction of the marker enrichment: High to low is the marker is enriched in the soils with high precipitation levels as compared to soils with low precipitation levels and vice versa. The localization of the precipitation gradient is shown in column G.

Supplementary Table S3. Differentially expressed genes of test phase gamagrass and maize roots. Tab one provides information for interpreting the column names and four other tabs. Tab two lists gamagrass genes that are significantly up or down-regulated based on the main effects of microbial inoculum legacy. Tab three lists gamagrass genes that are significantly up or down-regulated based on the interaction of test phase water treatment and microbial inoculum legacy. Tab four lists maize genes that are significantly up or down-regulated based on the main effects of microbial inoculum legacy. Tab five lists maize genes that are significantly up or down-regulated based on the interaction of test phase water treatment and microbial inoculum legacy.

Supplementary Table S4. Test phase plant phenotypic data and microbiome metadata. Tab one provides information for interpreting the column names. Tab two provides the measurements for all plants used in the plant phenotypic analyses, including both Gamagrass and maize. Tab three provides the measurements for the plant samples used in the root bacterial microbiome data analyses, with sequencing data that passed all qualify checks and filtering.

Supplementary Table S5. Differentially abundant test phase gamagrass and maize root microbiome ASVs. Tab one provides information for interpreting the column names. Tab two lists the gamagrass root microbiome ASVs, including their full taxonomic assignment that where significantly differentially abundant based on legacy in the context of test phase water treatment. Tab three lists the maize root microbiome ASVs, including their full taxonomic assignment that where significantly differentially abundant based on legacy in the context of test phase water treatment.